

POLITECNICO DI TORINO

Collegio di Ingegneria Chimica e dei Materiali

Master of Science Course in Materials Engineering



Master's degree Thesis

Development of green flame-retardant bio composites based on nanocellulose and hexagonal boron nitride nanoparticles

Supervisor:

Prof. Federico Carosio

Co-supervisor:

Lengwan Li, PhD

Candidate:

Alessandro Cipriano

July 2023

Abstract

Bio based nanocomposites have become of significant interest in recent years because they might facilitate the transition from a linear economy based on the disposal of production waste to a circular economy that utilizes waste as a resource for producing new materials. They have been studied in various sectors for various reasons such as: sustainability, lightness and high mechanical resistance, improvement of barrier and thermal properties and functionalization. Among the prominent bio-based materials, nanocellulose CNF stands out for its unique properties such as non-toxicity, biodegradability, high aspect ratio, large surface area, and mechanical strength, making it highly researched for various applications. However, nanocellulose exhibits poor fire resistance, and the purpose of this thesis is to explore the use of nanocellulose in the development of flame-retardant nanocomposite.

The properties of nacre-inspired nanocomposite hybrids of TEMPO - oxidized cellulose nanofibers (TOCN) and h-BN nanoparticles are investigated in this thesis work, in order to produce a material with competitive properties compared to conventional materials and to analyze its fire retardancy behavior. TEMPO (2,2,6,6-tetramethylpiperidine-1-oxyl radical) oxidation is a process that can convert native wood cellulose into individual nanofibers, which are typically 3-4 nm wide and at least several microns long, with aspect ratios greater than 100. The TOCN was prepared by using pulp demineralization, TEMPO-mediated oxidation, and finally high pressure micro-fluidification. The produced TOCN – h-BN dispersions exhibited relatively good stability with some sedimentation after a few days. h-BN/CNF bio-nanocomposites with a wide range of compositions were prepared by vacuum-assisted filtration of TOCN reinforced by exfoliated h-BN nanoparticles.

The morphological analysis was carried out using scanning electron microscopy that shows good distribution and poorly dispersion of h-BN nanoparticles in all sample compositions. The mechanical characterization was carried out using tensile test. The samples exhibited reduced mechanical properties compared to neat TOCN samples due to poor nanoparticle dispersion. The films showed a maximum fracture strength of 62 MPa for the 60% boron nitride samples and a Young's modulus of approximately 4 GPa for all compositions, significantly lower than the 14 GPa of the neat TOCN films. Spectroscopy, thermal, and fire behaviour analyses were conducted, revealing that the 60% boron nitride samples performed the best in terms of mechanical properties and fire propagation, exhibiting a self-extinguishing behaviour. Further flame penetration tests demonstrated how the poor nanoparticle dispersion negatively impacted penetration resistance.

Keywords:

Cellulose nanofibrils, boron nitride, vacuum-assisted filtration, fire behaviour, mechanical properties, morphological analysis.

Contents

Summary	i
Lists of Abbreviations.....	xxix
1 Introduction.....	1
1.1 Bio-based materials overview	1
1.2 Cellulose.....	2
1.2.1 Structure and chemical properties of cellulose.....	3
1.3 Nanocellulose	4
1.3.1 Nanocellulose Production	5
1.3.2 Cellulose Nanofibers (CNF).....	7
1.4 Nanocomposites.....	8
1.5 Nanocellulose base composites and applications	9
1.6 Hexagonal-Boron Nitride	11
1.6.1 Properties	11
1.6.2 Synthesis	13
1.6.3 Applications	13
1.7 Hexagonal Boron Nitride polymer nanocomposites	14
1.7.1 h-BN nanocomposites preparation techniques	15
1.8 Water-based Composites.....	17
1.9 Research Aims and thesis structure	18
2 Materials and sample preparations	21
2.1 Materials.....	21
2.2 Samples and dispersions preparation	22
2.2.1 TEMPO-CNF production.....	22
2.3 h-BN/CNF films preparation.....	27
2.3.1 Preliminary calculations.....	28
2.3.2 Sonication.....	33
2.3.3 Centrifugation.....	34
2.3.4 Vacuum filtration.....	35

2.3.5 Drying	35
3 Samples characterization methods	39
3.1 Spectroscopy analysis	40
3.1.1 Fourier Transform Infrared Spectroscopy analysis (FTIR)	40
3.2 Morphological Analysis	41
3.2.1 Scanning electron microscopy (SEM) – Energy Dispersive X-ray Spectroscopy (EDS)	41
3.3 Thermal analysis	41
3.3.1 Thermogravimetric Analysis (TGA).....	41
3.4 Mechanical Analysis.....	42
3.4.1 Tensile test	42
3.5 Fire behavior analysis	43
3.5.1 UL-94 flammability test.....	43
3.5.2 Flame penetration test.....	44
4 Results and discussion	47
4.1 Characterization of h-BN/CNF nanocomposite films	47
4.1.1 Stability dispersions	47
4.1.2 Surface composition analysis	48
4.1.3 Morphological and chemical analysis.....	52
4.1.4 Thermal conductivity analysis.....	55
4.1.5 Thermal gravimetric analysis	55
4.1.6 Stress-strain behavior and mechanical properties.....	59
4.1.7 Flammability tests.....	61
4.1.8 Flame penetration analysis	63
4.2 Conclusions and future perspectives.....	64
References.....	67
Acknowledgements.....	75

Summary

This section summarizes the content of the thesis in Italian as required by Politecnico di Torino in its guidelines.

Introduzione

Materiali bio-based

I materiali bio-based sono materiali prodotti da fonti biologiche rinnovabili come piante, animali e microorganismi. Questi materiali sono spesso considerati una soluzione sostenibile e a basso impatto ambientale rispetto ai materiali tradizionali, prodotti da fonti non rinnovabili come il petrolio. Il settore dell'imballaggio rappresenta una delle principali aree di utilizzo per le plastiche tradizionali [1], portando ad un accumulo significativo di scarti e rifiuti. Negli ultimi decenni si è sentito il bisogno di effettuare una transizione da una economia lineare basata sullo smaltimento dei rifiuti di produzione ad una economia circolare che utilizza i rifiuti come risorsa per la produzione di nuovi materiali. I materiali biobased possono vantare benefici ambientali come la riduzione delle emissioni di CO₂ e la diminuzione del consumo di risorse non rinnovabili. Tuttavia, ci sono ancora alcune sfide da affrontare come la produzione su larga scala, i costi e la necessità di garantire la sostenibilità delle fonti biologiche utilizzate.

Tra i materiali biobased più comuni vi sono la cellulosa, l'amido, la gomma arabica, il bambù, la canapa, la lana e la pelle vegetale. Questi materiali possono essere utilizzati in diverse settori, tra cui edilizia, abbigliamento, automotive e imballaggi.

Cellulosa e nanocellulosa

La cellulosa è un materiale naturale e rappresenta una fonte primaria di materiali sostenibili in campo industriale. La maggior parte della cellulosa proviene dalla polpa di legno ed è principalmente utilizzata per la produzione di carta e cartone. Tuttavia, viene utilizzata anche per la produzione di derivati della cellulosa, che vengono impiegati in una vasta gamma di applicazioni come rivestimenti, laminati, pellicole ottiche e additivi per vari prodotti, tra cui materiali da costruzione, prodotti farmaceutici, alimentari e cosmetici [7].

La cellulosa è definita chimicamente come una catena lineare di polisaccaride composta da unità di β -D-glucopiranosio legate insieme da legami β -1,4-glicosidici (**Figura 1**). È composta principalmente da carbonio (44,44%), idrogeno (6,17%) e ossigeno (49,39%). La sua formula chimica è $(C_6H_{10}O_5)_n$, dove n è chiamato grado di polimerizzazione (DP) e rappresenta il numero di unità di glucosio, che va da decine di unità a decine di migliaia.

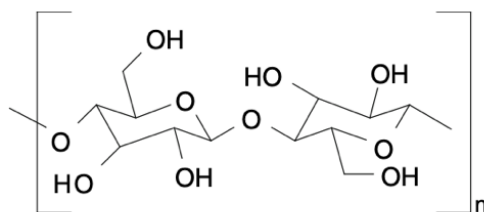


Figura 1.3 – *Struttura molecolare cellulosa*

La presenza di tre gruppi idrossile su ogni monomero nella cellulosa è significativa a causa della loro capacità di formare legami idrogeno. Questi legami svolgono un ruolo cruciale nel modo in cui la cellulosa si compatta in una struttura cristallina e ne governano le proprietà fisiche [9]. Le fibre di cellulosa si formano dall'unione di fibrille, che sono lunghi fasci filiformi di molecole stabilizzate lateralmente da legami idrogeno intermolecolari. Ogni fibrilla può essere considerata una serie di cristalli di cellulosa collegati lungo l'asse della fibrilla da domini amorfi disordinati. Con l'uso di opportuni metodi chimici, meccanici e/o enzimatici, la cellulosa può ridursi in dimensioni nanometriche [10]. In questo caso si fa riferimento alla nanocellulosa e alle nanofibre di cellulosa(CNF).

La nanocellulosa presenta ottime proprietà meccaniche grazie alla sua elevata area superficiale, capacità di trattenere acqua e alla presenza di gruppi OH reattivi sulla superficie, ai quali è possibile attaccare praticamente quasi tutti i gruppi funzionali [13]. La nanocellulosa, grazie alla sua elevata cristallinità, elevato rapporto di aspetto, ampia area superficiale specifica, elevata trasparenza, elevata idrofilicità, elevato modulo di Young e basso coefficiente di dilatazione termica, suscita un notevole interesse come supporto di template o unità di rinforzo nei materiali nanocompositi. Inoltre, queste fibre di nanocellulosa possono essere utilizzate come sostituto dei tradizionali riempitivi come il vetro nei compositi rinforzati, grazie alle loro proprietà desiderabili.

Le potenziali applicazioni delle nanofibre di cellulosa CNF includono: catalizzatori, film elettro-ottici, compositi rinforzati, microelettronica, film barriera ai gas, cosmetici e altri materiali ad alta tecnologia e prestazioni [30], [31]. Nel corso dell'ultimo decennio, sono state ampiamente utilizzate in prodotti di consumo come carta e tessuti, ma anche in materiali ad alta tecnologia come componenti di display a cristalli liquidi, fibre cave per la dialisi renale artificiale, componenti farmaceutici e additivi alimentari. Grazie ai numerosi gruppi reattivi sulla superficie, la nanocellulosa è un buon template biologico per la deposizione fisica di nanoparticelle. Le nanoparticelle inorganiche [37], come i metalli, i quantum dots, gli ossidi, i nitriti, garantiscono proprietà uniche e permettono la realizzazione di innovativi nanocompositi bio-based.

In questa tesi, viene indagato l'uso del nitrato di boro come riempitivo in nanocompositi polimerici a base TOCN (nanocellulosa ossidata TEMPO).

Nitruro di Boro esagonale

Il nitruro di boro esagonale (h-BN) è un materiale composto da atomi di Boro (B) e Azoto (N) disposti in un modello esagonale, senza legami liberi tra i suoi strati. I nanofogli di nitruro di boro (BNNS) sono sottili fogli esfoliati dal nitruro di boro esagonale (h-BN). Simile al grafene, il BNNS è un materiale bidimensionale che può essere utilizzato come riempitivo ideale per preparare nanocompositi termoconduttivi.

Il BNNS condivide una geometria simile, proprietà fisiche e termiche al grafene, che è il suo analogo completamente in carbonio. Nonostante abbia una struttura cristallina simile al grafene, dal punto di vista elettrico, il nitruro di boro è un isolante con una banda proibita indiretta di circa 6 eV [41]. Inoltre, l'h-BN appare di colore bianco invece del grafene che è di colore nero.

L'h-BN influenza positivamente la conducibilità termica sotto specifiche condizioni di dispersione [43]. Questa proprietà di solito aumenta all'aumentare della quantità e della dimensione delle particelle ceramiche. Utilizzando particelle ceramiche che hanno un alto rapporto d'aspetto, a forma di scaglie o fibre, viene creato un percorso più conduttivo grazie alla soglia percolativa inferiore rispetto alle particelle sferiche.

L'h-BN è inoltre altamente efficace nel migliorare il comportamento antincendio dei compositi. Quando un materiale viene sottoposto a combustione, viene creato un gradiente di temperatura che causa la migrazione delle BNNS dal bulk alla superficie a causa del consumo della matrice di nanocellulosa. Queste particelle si accumulano per formare uno strato superficiale termicamente isolante chiamato "char", che è uno strato ibrido composto da carbonio proveniente dal degrado del polimero e h-BN. Il char agisce come barriera al calore e all'ossigeno, proteggendo il materiale sottostante da ulteriori degradazioni. Il percorso tortuoso che si genera limita il trasferimento di massa tra le fasi gassose e condensate, riducendo anche l'apporto di ossigeno, proteggendo così la resina interna da ulteriori degradazioni e riducendo il tasso di rilascio di calore.

È di recente scoperta che l'h-BN ha proprietà piezoelettriche naturali, che offrono nuove proprietà ottiche ed elettromeccaniche, rendendolo un candidato promettente per hyper lenses [49], near-field imaging [50], emettitori deep-UV [51] e quantum optoelettronici.

Compositi a base d'acqua

Negli ultimi anni c'è stato un crescente interesse per i nanocompositi a base d'acqua come una nuova frontiera nel campo dei nanocompositi. L'ispirazione per la loro produzione deriva dalla struttura "brick and mortar" della madreperla [64]. In questa struttura particolare, vi è una struttura altamente orientata in cui le placche di aragonite sono tenute insieme da polimeri morbidi, con conseguenti proprietà meccaniche migliorate come maggiore rigidità e resistenza. Inoltre, garantiscono la conduzione del calore lungo gli strati dei nanofogli, risultando in una grande conducibilità termica nel piano (**Figura 2**).

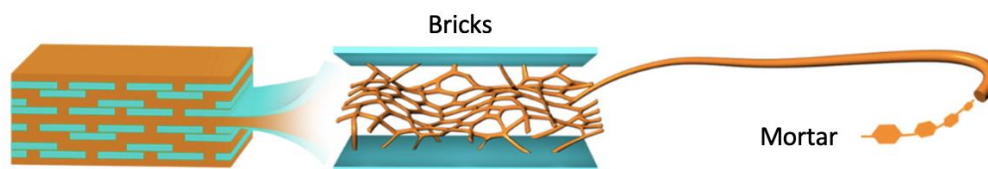


Figura 2 – Struttura biomimetica “Brick and mortar”

Questi compositi a base d'acqua sono ecologici e presentano una bassa tossicità rispetto ai compositi a base di solventi organici, una maggiore conducibilità elettrica e un miglioramento della resistenza al fuoco, rendendoli molto desiderabili per diverse applicazioni come film, vernici e adesivi. La solubilità o la dispersione della matrice polimerica in acqua è fondamentale per la produzione di nanocompositi a base d'acqua, infatti la cellulosa, un polimero naturale con elevata solubilità in acqua, viene spesso impiegata come matrice polimerica. Lo stesso concetto viene applicato alla creazione di un materiale bio in cui i nanofogli di h-BN fungono da "Brick" e un polimero fa da "mortar". Per produrre nanocompositi a base d'acqua, il polimero e l'h-BN vengono sospesi in acqua. La sospensione risultante può essere elaborata in due modi, filtrandola per ottenere sottili film o essiccandola per ottenere aerogel. Entrambi i tipi di materiali presentano proprietà meccaniche superiori e una maggiore resistenza al fuoco rispetto al polimero puro [65].

Struttura della tesi e scopi della ricerca

Gli obiettivi della presente tesi di ricerca sono la produzione e lo studio delle caratteristiche di nanocompositi a base biologica basati su nanofibrille di cellulosa (ottenute dal legno) e nitrato di boro esagonale, utilizzati per migliorare le proprietà ignifughe del materiale puro. La cellulosa è una nanoparticella organica che offre un'alternativa rinnovabile e naturale ai combustibili fossili. È ampiamente disponibile e considerata una fonte di materia prima pressoché illimitata per la crescente domanda di prodotti ecologici e biocompatibili. L'obiettivo è produrre un materiale con proprietà competitive rispetto ai materiali convenzionali e analizzarne il comportamento di ritardo alla fiamma, poiché questo aspetto viene raramente valutato in letteratura. La struttura della tesi è divisa in due fasi (**Figura 3**): la prima è relativa alla sezione sperimentale dell'attività di ricerca svolta presso il *KTH-Royal Institute of Technology* di Stoccolma e la seconda è relativa all'attività di ricerca svolta presso il Politecnico di Torino nel campus di Alessandria.

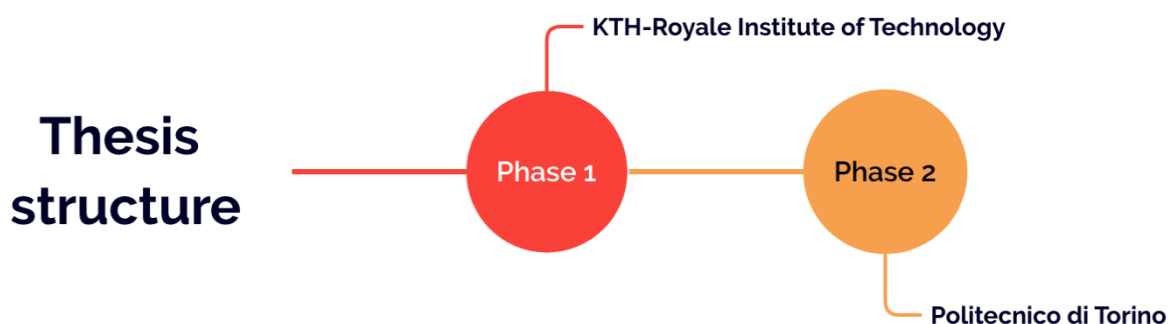


Figura 3 – Struttura tesi

Nella Fase 1 presso il *KTH-Royal Institute of Technology* di Stoccolma, con il gruppo di ricerca del *Wallenberg Wood Science Center* è stata effettuata la preparazione di TEMPO-CNF a partire dalla polpa di cellulosa. Una volta completate tutte le fasi preliminari di preparazione, è stata realizzata la preparazione dei nanocompositi h-BN/CNF, dopo una valutazione delle condizioni e dei processi da utilizzare per la corretta produzione di film con diverse concentrazioni di nitrato di boro, rispettivamente 20, 40, 60, 80% in peso.

La ricerca prosegue con la fase 2 nei laboratori del *Politecnico di Torino* nel campus di Alessandria, al fine di caratterizzare le proprietà meccaniche, la stabilità termica e la conducibilità termica, la morfologia e ritardo alla fiamma, correlando la struttura e le proprietà e confrontando il comportamento del materiale con e senza nitrato di boro.

La parte sperimentale della tesi è suddivisa come segue.

Il Capitolo 2 fornisce la prima parte della sezione sperimentale della tesi con la descrizione dell'attività di ricerca svolta presso il KTH di Stoccolma: preparazione di TEMPO-CNF e produzione di film nanocompositi h-BN/CNF. Inoltre, vengono illustrate in dettaglio anche le caratteristiche dei materiali utilizzati per la preparazione dei film a base di nanocellulosa e h-BN/CNF.

Il Capitolo 3 fornisce la seconda parte della sezione sperimentale della tesi con la descrizione dell'attività di ricerca svolta presso il *Politecnico di Torino* nel campus di Alessandria: caratterizzazione morfologica dei campioni utilizzando SEM, analisi spettroscopiche utilizzando FTIR, caratterizzazione chimica utilizzando l'analisi TGA, caratterizzazione meccanica utilizzando prove di trazione, infiammabilità e infine prove di penetrazione alla fiamma.

Il Capitolo 4 fornisce le conclusioni del lavoro di tesi con particolare attenzione ai risultati e alle discussioni: sviluppo del processo, proprietà colloidali, morfologia, composizione chimica, comportamento di ritardo alla fiamma, resistenza alla penetrazione della fiamma e conducibilità dei campioni. Inoltre, vengono spiegati anche i fattori e gli sviluppi che potrebbero essere attenzionati in futuro.

Materiali e metodi

La sospensione di CNF è stata preparata a partire dalle fibre di polpa di solfato di legno chiaro, fornite da Nordic Paper Seffle AB, Saffle, Svezia, con il 14% in peso di emicellulosa e meno dell'1% di lignina. Queste fibre possono essere disgregate in particelle idrocolloidali prima di essere sottoposte al processo di microfluidificazione ad alta pressione per ottenere TEMPO-CNF.

La polvere di nitrato di boro esagonale con purezza del 98% (GRAPHENE SUPERMARKET®) è stata utilizzata come dispersione per la preparazione dei film nanocompositi h-BN/CNF.

L'acido cloridrico al 37% ($\text{HCl}_{(\text{aq})}$) con peso molecolare di 36,46 è stato utilizzato per la preparazione di TEMPO-CNF per la demineralizzazione dell'acqua e per la dispersione di fibre di polpa. È stato fornito da Fisher Scientifics, Bishop Meadow Rd. Loughborough, Regno Unito.

TEMPO (98%), fornito da Sigma-Aldrich Co. LLC, St. Louis, Stati Uniti, è stato utilizzato per ossidare le nanofibre di cellulosa in acqua, specificamente per la conversione regioselettiva degli idrossili primari C6 in gruppi carbossilati. Il processo prevedeva l'incorporazione di quantità catalitiche di TEMPO e bromuro di sodio NaBr ($\geq 99\%$), fornito da Sigma-Aldrich Co. LLC, St. Louis, Stati Uniti, in soluzioni con pH 11. Infine, l'ossidazione veniva iniziata con ipoclorito di sodio al 14% (NaClO), fornito da VWR International, Milano, Italia, come ossidante primario. È stato inoltre aggiunto NaOH 2M (fornito da Sigma-Aldrich Co., St. Louis, Stati Uniti) per stabilizzare il pH.

Il buffer acetato viene utilizzato per mantenere il pH della soluzione in un intervallo stabile e tollerabile per le CNF durante il processo di ossidazione. In particolare, il buffer acetato viene utilizzato per mantenere il pH della soluzione intorno a 5, garantendo l'efficacia dell'ossidazione ma anche per proteggendo le CNF dalla degradazione. È stato preparato aggiungendo 18,3 mL di acido acetico ($\geq 99\%$) con formula chimica CH_3COOH e 27 g di acetato di sodio con formula chimica $\text{C}_2\text{H}_3\text{NaO}_2$ ($\geq 99\%$) (entrambi forniti da Sigma-Aldrich Co. LLC, St. Louis, Stati Uniti) in acqua deionizzata (2 L). La soluzione è stata agitata magneticamente (298 rpm) a pH 4,8 fino a scomparsa delle bolle.

Il clorito di sodio con formula chimica NaClO_2 (80%) è stato utilizzato come agente sbiancante nel trattamento col buffer acetato della dispersione di polpa di cellulosa. È stato anch'esso fornito da Sigma-Aldrich Co. LLC, St. Louis, Stati Uniti.

Preparazione dispersioni colloidali e campioni

CNF production

La dispersione di CNF è stata preparata secondo il lavoro di Lengwan Li et al [67]. Innanzitutto, la sospensione di CNF è stata preparata utilizzando l'ossidazione TEMPO sviluppata da Saito et al. Nella produzione di TEMPO-CNF, sono coinvolte diverse fasi: Demineralizzazione polpa e lavaggio, ossidazione mediata da TEMPO, trattamento con buffer acetato e micro-fluidificazione ad alta pressione.

Demineralizzazione e lavaggio della polpa

La polpa (20 g in peso secco) è stata demineralizzata mediante agitazione magnetica (marca Fisher - Isotemp®) in una soluzione diluita di HCl e acqua deionizzata a pH 2,5 per 2 ore a 25°C . Dopo questo trattamento, la dispersione è stata lavata tre volte con acqua

deionizzata mediante filtrazione sottovuoto con filtro in PTFE (come mostrato nella **Figura 4**). Successivamente, la sospensione è stata sospesa in 2000 mL di acqua deionizzata con una resistività di 18.2 M Ω , pronta per l'ossidazione mediata da TEMPO.

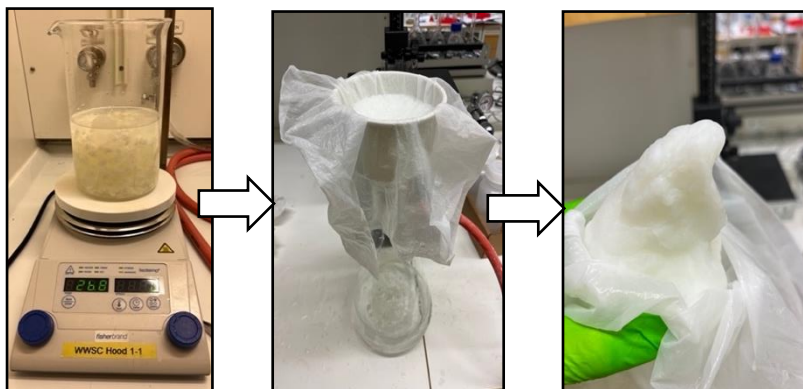


***Figura 4** – Demineralizzazione della polpa di cellulose con HCl e DI mediante magnetic stirring e lavaggio con acqua deionizzata*

Ossidazione mediata TEMPO

Per questa fase, quantità catalitiche di TEMPO (0,32 g) e NaBr (2g) sono state disciolte nella sospensione di CNF che è stata sottoposta ad agitazione meccanica, e l'ossidazione è stata avviata aggiungendo NaClO (60 mL) come agente ossidante.

Il processo di ossidazione può essere monitorato dal consumo di NaOH, che viene aggiunto continuamente alla miscela di reazione per mantenere il pH a 11 durante l'ossidazione. Dopo 1h, la soluzione è stata lavata sette volte con acqua deionizzata con una resistività di 18.2 M Ω mediante filtrazione sottovuoto con filtro in PTFE per rimuovere i residui di TEMPO.

Trattamento con buffer acetato

Dopo questo trattamento, la polpa ossidata è stata sospesa in acqua deionizzata con una resistività di 18.2 M Ω (fornita dal sistema Milli-Q di Millipore) e successivamente trattata in un buffer acetato a pH 4.8 per 24 ore con l'aggiunta del 1% di NaClO₂ (20 g) sotto agitazione meccanica (miscelatore a statore digitale IKA® EUROSTAR 20). Il becher è stato anche coperto con parafilm perché la soluzione è altamente volatile come mostrato nella **Figura 5**. Dopo questo trattamento, la soluzione è stata lavata sette volte con acqua deionizzata con una resistività di 18.2 M Ω utilizzando un filtro in PTFE.

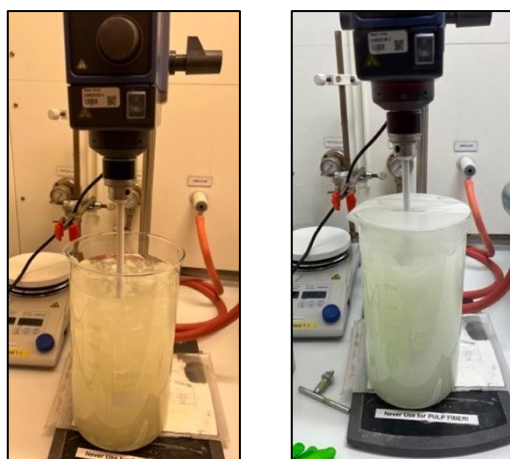


Figura 5 – Polpa ossidata trattata con buffer acetato e clorito di sodio per 24 h

Microfluidificazione ad alta pressione

Dopo il lavaggio, le fibre di polpa sono state sottoposte a un microfluidizzatore ad alta pressione (Microfluidics Corp, Newton, Massachusetts, USA). Prima di inserire la polpa nel microfluidizzatore, sono stati inseriti 5 litri di acqua deionizzata nella tramoggia per pulire i condotti. La polpa è stata sottoposta ad alta pressione (1600 bar), passando una volta attraverso canali da 400-200 μm e due volte attraverso canali da 200-100 μm per produrre un colloide trasparente di TEMPO-CNF. Per realizzare film nanocompositi di h-BN/TOCN, è stato necessario calcolare la concentrazione a secco di TEMPO-CNF ottenuta. È stato utilizzato un analizzatore elettrico (METTLER TOLEDO HB43-S Halogen). La concentrazione a secco calcolata di TEMPO-CNF è 0,75% in peso.

Preparazione film h-BN/CNF

Uno degli obiettivi preliminari delle attività svolte presso il KTH Royal Institute of Technology era trovare i parametri corretti per preparare i film nanocompositi di h-BN/CNF con uno spessore di 0,05 mm a diverse percentuali di h-BN: 20, 40, 60, 80% in peso (**Tabella 1**). Sono stati ottenuti almeno 3 campioni per ciascuna composizione.

Table 2.1 – Nomenclature used for h-bn/CNF nanocomposites films

Nomenclature	Concentrations [% wt]
20% h-BN/CNF	20 % wt h-BN
	80 % wt CNF
40% h-BN/CNF	40 % wt h-BN
	60 % wt CNF
60% h-BN/CNF	60 % wt h-BN
	40 % wt CNF
80% h-BN/CNF	80 % wt h-BN
	20 % wt CNF

Lo schema del processo di filtrazione dei film di h-BN/CNF, che sarà spiegato in dettaglio di seguito, è mostrato nella **Figura 6**.

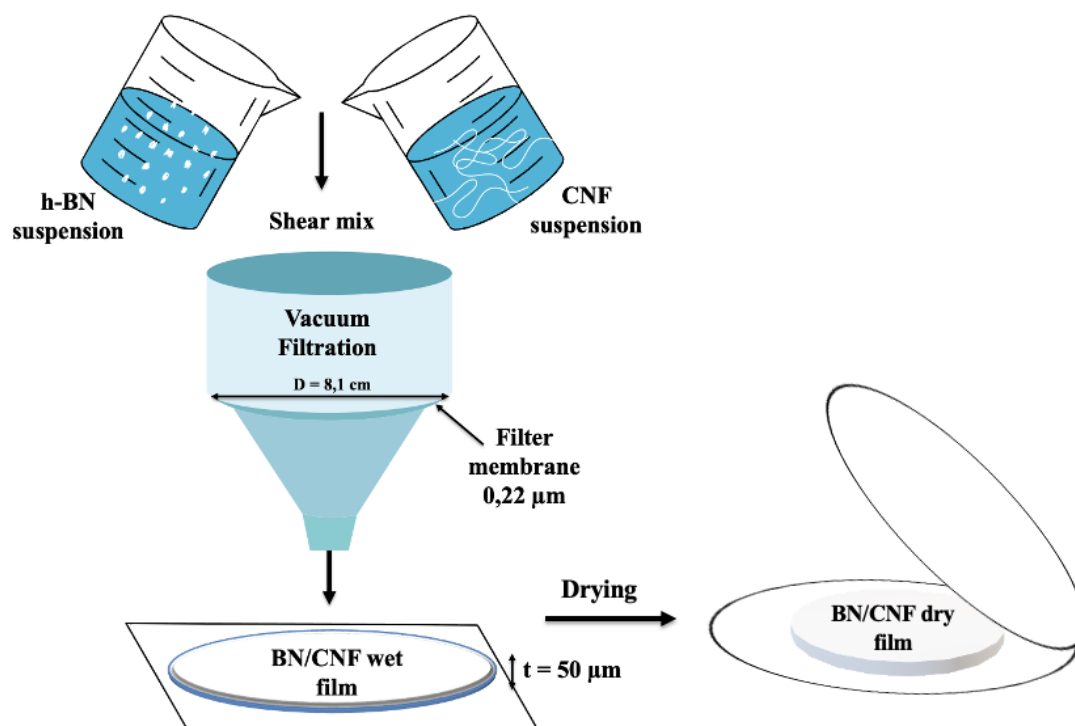


Figura 6 – Preparazione del processo per l'ottenimento di film h-BN/CNF

Una volta ottenuta la TEMPO-CNF, sono stati effettuati calcoli preliminari per determinare le giuste quantità di materiali da utilizzare a diverse percentuali di h-BN, considerando vincoli dimensionali e la concentrazione di TEMPO-CNF prodotta.

I risultati ottenuti sono riassunti nella tabella sottostante (**Tabella 2**).

Tabella 2 – Parametri utilizzati per i film nanocompositi h-BN/CNF

Parameters	20% BN/CNF	40% BN/CNF	60% BN/CNF	80% BN/CNF
$\rho_{TOT} \left[\frac{g}{cm^3} \right]$	1.69	1.8	1.9	2
$m_{TOT} [mg]$	435	463	489	515
$m_{BN} [mg]$	0.087	0.185	0.293	0.412
$m_{CNF(dry)} [mg]$	348	258	195.6	103
$m_{CNF} [mg]$	46.4	33.95	25.7	13.5
Water content [mL]	200	230	250	260

Dopo i calcoli preliminari, h-BN e CNF sono stati pesati con una bilancia analitica (METTLER Toledo AE-163). Successivamente, TEMPO-CNF e h-BN sono stati aggiunti separatamente all'acqua deionizzata con una resistività di 18.2 MΩ per ottenere due diverse dispersioni.

Sonicazione e centrifugazione

Le dispersioni sono state sottoposte a sonicazione con un omogeneizzatore ad ultrasuoni con sonda a punta piatta Vibracell VCX 750, per 2 minuti per ottenere dispersioni esfoliate di h-BN e CNF. Successivamente, sono state messe insieme in un becher per il passaggio successivo.

Dopo la sonicazione, la soluzione di h-BN/CNF è stata equamente divisa in provette per eseguire la centrifugazione. La centrifugazione assicura la separazione della fase surnatante dalla fase solida. La centrifuga da banco utilizzata per questa fase è la ROTINA 420 - Hettich®. È importante sottolineare che le provette sono state disposte in modo uguale per bilanciare il peso durante il processo di centrifugazione. Le sospensioni sono state trattate per 10 minuti a $T=35^{\circ}\text{C}$, 3000 rpm, con una scala di rampa da 9 a 5. Dopo la centrifugazione, la fase surnatante è stata separata dalla fase solida una provetta alla volta mediante pipetta graduata. Successivamente, la fase surnatante è stata conservata per il passaggio successivo della filtrazione, mentre la fase solida sul fondo della provetta è stata rimossa.

Filtrazione sottovuoto

Le co-dispersioni sono state quindi filtrate sotto vuoto utilizzando un setup di vetro poroso e una membrana filtrante idrofila in PVDF (filtri a membrana DURAPORE®) con una dimensione dei pori di 0,22 micron sulla base di supporto in vetro. Il tempo di filtrazione delle co-dispersioni di h-BN/TEMPO CNF è stato in media 12 ore, anche se il tempo di filtrazione variava con il contenuto di h-BN, dello spessore del nanofilm finale e della dispersione effettiva. Il campione dell'80% di h-BN ha il tempo di filtrazione più lungo (~16 ore). Dopo la filtrazione, i film umidi sono stati rimossi con cura dalla membrana di filtrazione. I campioni umidi ottenuti sono stati posizionati sotto un filtro in teflon e successivamente tra due fogli di copertura prima dell'essiccazione, per ottenere i campioni finali.

Per eseguire l'essiccazione del film è stato utilizzato un Sheet Former Rapid-Köthen (RL-ASF-A). Per trovare i giusti parametri di processo sono stati effettuati diversi test. In particolare, è risultato complesso definire il giusto compromesso tra tempo e pressione per i campioni al 60% e all'80% wt. La figura sottostante (**Figura 7**) mostra due campioni essiccati rispettivamente al 20% e al 60% in peso di h-BN.

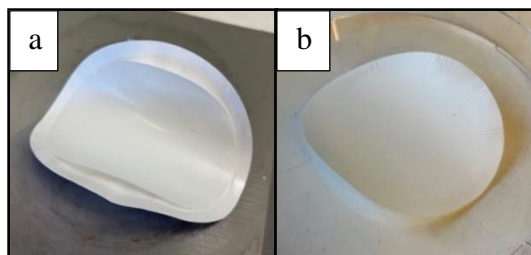


Figura 7 –BN/CNF 20% wt secco (a), BN/CNF 60% wt secco (b)

Le condizioni operative utilizzate per i film variano a seconda della quantità di nitrato di boro aggiunto, ad eccezione della temperatura, che è stata fissata a 93°C per tutti i campioni alle diverse percentuali in peso.

- Per i campioni al 20% di h-BN/CNF e al 40% di h-BN/CNF, è stata applicata una pressione di 0 bar per 25 minuti.
- Per i campioni al 60% di h-BN/CNF, è stata applicata una pressione di 0 bar per 5 minuti, quindi aumentata a 0.6 bar per altri 25 minuti.
- Per i campioni all'80% di h-BN/CNF, è stata applicata una pressione di 0 bar per 10 minuti, quindi aumentata a 0.4 bar per altri 25 minuti.

Metodi di caratterizzazione

Per caratterizzare i campioni ottenuti, sono state eseguite le seguenti analisi:

- Spettroscopia infrarossa (IR): fornisce informazioni legate ai legami chimici e alle modalità di vibrazione dei gruppi funzionali nelle molecole di un materiale. Lo spettrofotometro utilizzato per i film è lo spettrometro FTIR Frontier prodotto da Perkin Elmer. Questa tecnica è stata accoppiata alla tecnica di riflessione totale attenuata (ATR) sui campioni h-BN/CNF. In modalità ATR, il campione viene posto a contatto con un cristallo di diamante ad alto indice di rifrazione. Gli spettri sono stati registrati a temperatura ambiente nell'intervallo (4000-700) cm^{-1} con 16 scansioni (risoluzione 4 cm^{-1}).
- Caratterizzazione morfologica (SEM): analisi morfologica effettuata utilizzando un microscopio elettronico a scansione EVO 15 prodotto da Zeiss con una tensione del fascio di elettroni di 20 kV. Questa analisi è stata accoppiata alla spettroscopia a dispersione di energia dei raggi X (EDS). La microscopia SEM è stata fondamentale per valutare la distribuzione e la dispersione della carica all'interno della matrice CNF. La microsonda EDS utilizzata è la ULTIM MAX 40 EDS di OXFORD. Per i campioni h-BN/CNF, i rispettivi ingrandimenti utilizzati sono stati: 500X, 1,00KX, 2,50KX, 5,00KX, 10,00KX, 20,00KX, 50,00KX, 75,00KX.
- Analisi termogravimetrica (TGA): tecnica utilizzata per valutare la stabilità termica e la reattività dei materiali, misurando la variazione di massa che avviene durante il processo di

decomposizione e la velocità con cui questo processo si verifica. In questo studio è stato utilizzato il dispositivo Discovery TGA di TA Instrument per indagare come la preparazione dei film h-BN/CNF con diverse concentrazioni di h-BN possa influenzare il processo di decomposizione del materiale. Questa analisi ha anche permesso l'identificazione e la quantificazione della carica di h-BN presente, che è stata precedentemente analizzata qualitativamente utilizzando la tecnologia FTIR. In particolare, i campioni (circa 10 ± 1 mg) vengono posizionati in crogioli di allumina in atmosfera controllata e sottoposti a un riscaldamento con una rampa di $10^\circ\text{C}/\text{min}$ da 100°C fino a raggiungere 800°C , sia in atmosfera inerte (N_2) che ossidante (aria). Il test è stato eseguito su polveri di h-BN e su campioni netti di CNF, nonché su campioni h-BN/CNF con diverse percentuali di h-BN: 20, 40, 60, 80 % in peso in atmosfera di azoto o aria.

- Prova di trazione: Il dinamometro Instron 5966 è stato utilizzato per eseguire prove di trazione sui campioni h-BN/CNF. Sono stati ottenuti 4 campioni rettangolari per ogni composizione con lati di dimensioni 50×10 mm e uno spessore di 0,05 mm, a partire da un campione circolare nativo con un diametro iniziale di 81 mm mediante taglio manuale meccanico. La prova di trazione è infatti una prova distruttiva e i campioni non possono essere riutilizzati dopo l'esecuzione della prova. Le curve risultanti da questa analisi meccanica mostrano la relazione tra lo stress e la deformazione. Il software associato allo strumento fornisce le curve sforzo-deformazione dalle quali è possibile derivare il modulo elastico (E) in MPa, la deformazione di rottura (ϵ_r) in % e lo stress massimo a trazione (σ_{\max}) in MPa.
- UL-94: valuta il comportamento di infiammabilità del materiale, in particolare la capacità di resistere alla propagazione della fiamma, simulando le condizioni di un incendio iniziale, la velocità di propagazione delle fiamme e la presenza di afterglow dopo l'estinzione delle fiamme. Date le dimensioni ridotte dei campioni, è stato utilizzato una procedura modificata derivata dal test UL 94 in modalità di combustione orizzontale (HB) per indagare il comportamento di infiammabilità dei materiali. Pertanto, sono stati eseguiti solo determinati requisiti della norma ASTM D 5132, tra cui il condizionamento, il tipo e la durata dell'applicazione della fiamma. I campioni di h-BN/CNF (3 per ogni composizione) con lati di dimensioni 50×10 mm e uno spessore di 0,05 mm sono stati condizionati in una camera climatica per 48 ore a $23 \pm 2^\circ\text{C}$ e $50 \pm 1\%$ di umidità relativa. Il test consiste in un'applicazione singola di una fiamma di metano blu di 20 mm ad un angolo di 45° per una durata di 6 secondi. Questo test è meno severo della modalità di combustione verticale (VB). È stato effettuato un test di penetrazione delle fiamme su campioni di h-BN/CNF ($50 \times 50 \times 0,05$ mm³) per valutare la resistenza alla penetrazione di una piccola fiamma (150 W).
- Test di penetrazione alla fiamma (**Figura 8**): Utilizzando due termocoppie (tipo K rivestite in acciaio inossidabile; diametro 1 mm) poste a contatto con il campione e a una certa altezza, è possibile registrare i profili di temperatura sia del lato esposto alla fiamma che del lato posteriore non esposto del campione. Più bassa è la temperatura del lato esposto, maggiore è la resistenza alla fiamma. Il campione può bruciare e collassare immediatamente o formare uno strato carbonizzato che impedisce al calore di propagarsi sul lato posteriore. Il test viene eseguito fino alla completa perforazione del campione da un lato all'altro e viene registrato

il tempo impiegato. È stata utilizzata anche una termocamera, (BT-TC8), per valutare il comportamento del lato posteriore del campione dopo l'applicazione della fiamma. È stato utilizzato il software PicoLog per registrare la variazione di temperatura nel tempo. Come per i test di infiammabilità, i campioni sono stati condizionati per 48 ore in una camera di condizionamento a temperatura e umidità controllate. I campioni sono stati rimossi prima di iniziare il test.

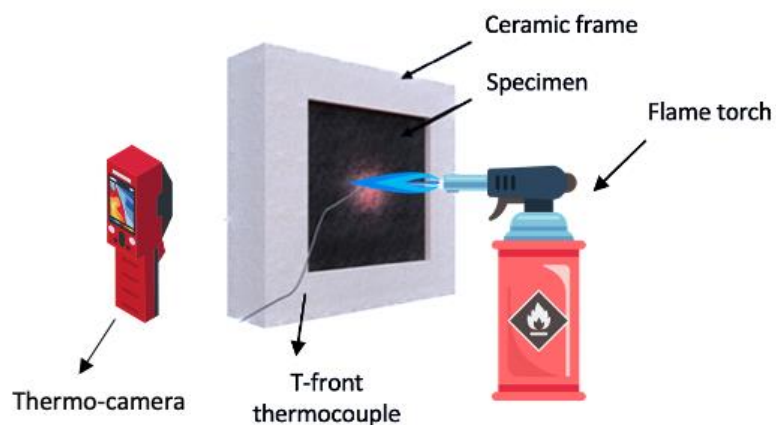


Figura 8 – *Setup sperimentale del test di penetrazione alla fiamma*

Risultati e discussioni

La produzione di film h-BN/TOCN è stata condotta variando la concentrazione di nitrato di boro. La superficie dell'h-BN è carica negativamente ed è dispersa in soluzione acquosa attraverso trattamenti di sonicazione. Questo processo mira a ottenere una dispersione uniforme delle nanoparticelle di h-BN. In ugual modo, il TOCN presenta una carica negativa superficiale, che aumenta la repulsione elettrostatica tra le nanoparticelle di h-BN esfoliate all'interno del colloide. Questa repulsione dovrebbe contribuire a migliorare la dispersione di h-BN all'interno della matrice di fibrille di cellulosa. I film di h-BN/CNF sono stati preparati sfruttando un processo di filtrazione su carta, come spiegato nel Capitolo 2 - Materiali e Preparazione dei Campioni e mostrato nella Figura 2.7. Le dispersioni di h-BN/CNF risultano di colore biancastro, a causa del colore bianco della polvere di nitrato di boro. Queste dispersioni hanno mostrato una buona stabilità, pur presentando una certa sedimentazione dopo 10 giorni.

Gli spettri normalizzati di TOCN e polveri di h-BN sono stati presi come riferimento, come mostrato rispettivamente nella **Figura 9** e nella **Figura 10**, al fine di valutare le modifiche della matrice di nanocellulosa quando viene aggiunto il riempitivo di h-BN. La **Tabella 3** presenta l'attribuzione dei picchi di segnale degli spettri di TOCN e h-BN e le relative descrizioni.

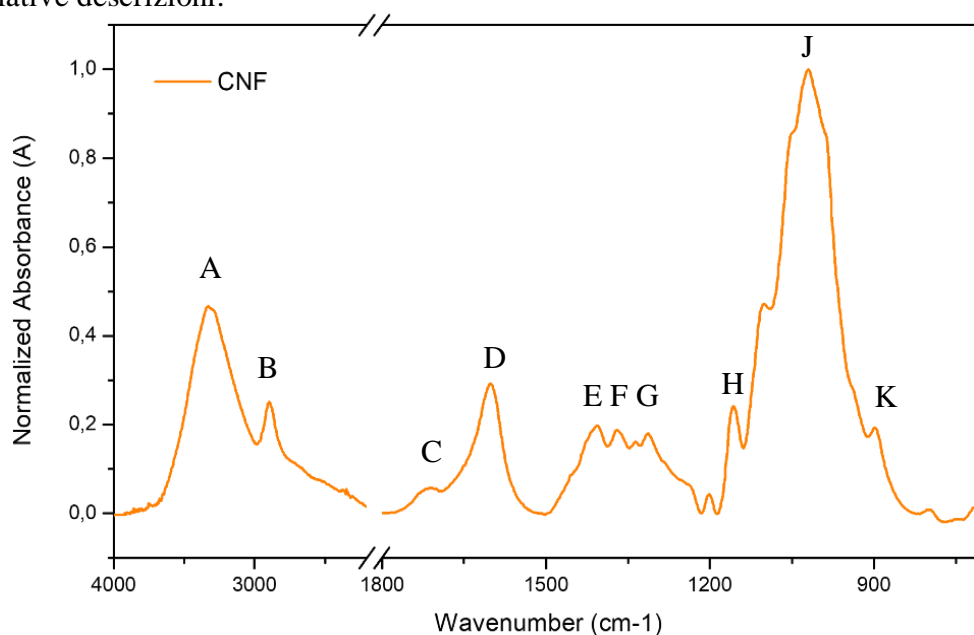


Figura 9 – Spettro normalizzato in IR-ATR di TEMPO-CNF

Lo spettro del CNF mostra una serie di picchi caratteristici della cellulosa [70]. Presenta una banda a 3335 cm^{-1} (A) che corrisponde all'allungamento dei gruppi ossidrilici O-H. A 2900 cm^{-1} (B) vi è un picco relativo all'allungamento dei gruppi C-H nelle unità glicosidiche, a 1709 cm^{-1} (C) una spalla attribuita al legame O-H dell'acqua assorbita. Secondo la letteratura [71], la CNF ossidata TEMPO mostra un picco prominente a 1602 cm^{-1} (D) che corrisponde ai gruppi carbonilici che lo differenziano dalla CNF non trattata. Altri picchi osservati nell'intervallo tra 1400 cm^{-1} e 1300 cm^{-1} possono essere attribuiti

all'allungamento dei legami C-H₂ e C-H [72]. In particolare, a 1410-1420 cm⁻¹ (E) si osservano i movimenti di oscillazione dei gruppi -CH₂ nella cellulosa, a 1369-1373 cm⁻¹ (F) la flessione dei gruppi C-H e ~ 1317 cm⁻¹ (G) il wagging del CH₂. I picchi nella regione di 1154-1159 cm⁻¹ (H) mostrano la banda di allungamento dell'anello C-C. Picchi a 1052 cm⁻¹ (J) mostrano la vibrazione del C-O-. Inoltre, a 900 cm⁻¹ (K) vi è un picco relativo ai legami β glucosidici.

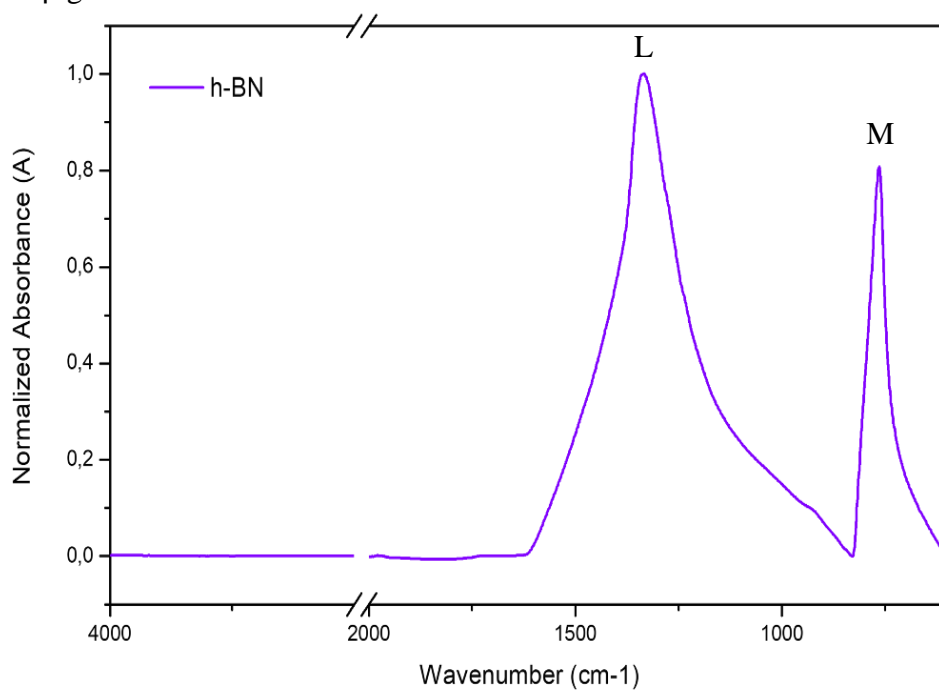


Figura 10 – Spettro normalizzato ATR-IR della polvere di h-BN

Tabella 3 – Descrizione delle bande di TOCN e polvere di h-BN

	Signal	Wavenumbers [cm ⁻¹]	Bands description
CNF	A	3335	(O-H) Stretching
	B	2900	(C-H) Stretching
	C	1709	(O-H) Absorbed water
	D	1602	(COO ⁻) of TOCN
	E	1410-1420	(-CH ₂) scissoring motion in cellulose
	F	1369-1373	(C-H) bending
	G	~ 1317	(CH ₂) wagging
	H	1154-1159	(C-C) ring stretching band
	J	1052	(C-O-C) skeletal vibrations
	K	900	β glycosidic linkage
h-BN	L	1335	(B-N) in-plane stretching vibration
	M	764	(B-N-N) out-of-plane bending vibration

Lo spettro FT-IR delle polveri di h-BN mostra i picchi caratteristici del nitrato di boro a 776 cm^{-1} (M) e 1335 cm^{-1} (L), corrispondenti alle vibrazioni del legame B-N. Più specificamente, l'ampia banda osservata a 1335 cm^{-1} è attribuita alla vibrazione di stretching in piano dei legami B-N, mentre la banda meno ampia a 764 cm^{-1} corrisponde alla vibrazione di flessione fuori piano di B-N-B, come indicato dai picchi caratteristici dell'h-BN presenti in letteratura [73][74].

Per comprendere come variano i legami chimici all'aumentare della percentuale di nitrato di boro sono stati ottenuti spettri FTIR ad ogni composizione (**Figura 11**), rispettivamente h-BN/CNF al 20%, 40%, 60% e 80% wt. Lo spettro della CNF è stato utilizzato come riferimento. Come si può osservare dagli spettri normalizzati, l'aggiunta di h-BN mostra l'insorgenza di nuovi picchi caratteristici del nitrato di boro alle lunghezze d'onda di 764 cm^{-1} (M) e 1335 cm^{-1} (L), indici di un mescolamento tra le nanofibre di cellulosa e il nitrato di boro.

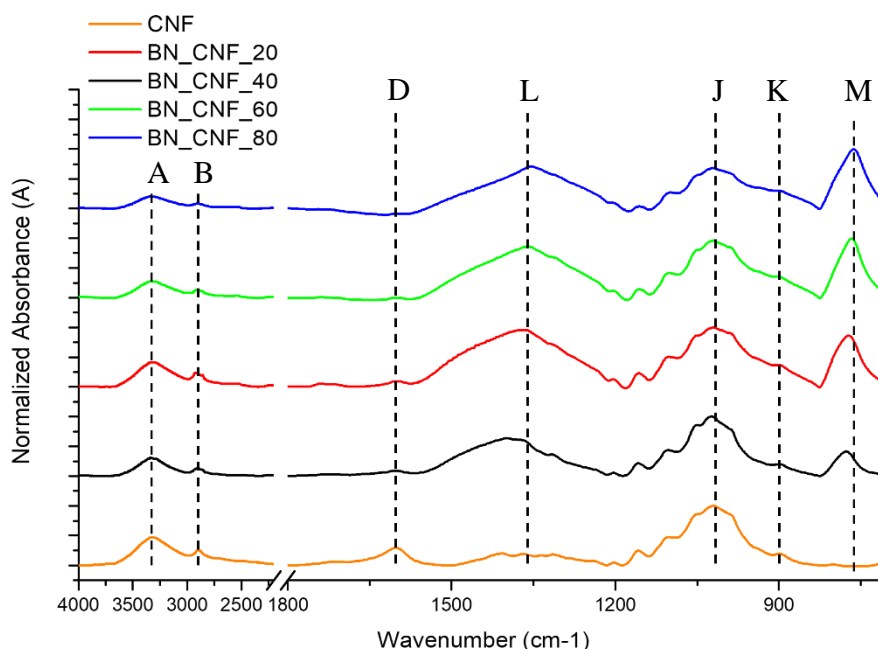


Figura 11 – Spettro normalizzato ATR-di film nanocompositi h-BN/CNF con spettro normalizzato di TOCN come riferimento

I picchi caratteristici della nanocellulosa TEMPO a 3335 cm^{-1} (A), 2900 cm^{-1} (B), 1602 cm^{-1} (D), $\sim 1317\text{ cm}^{-1}$ (G) e 900 cm^{-1} (K) rimangono pressoché inalterati. Tuttavia, si può osservare una riduzione del segnale del picco proporzionale all'aumento della concentrazione di nitrato di boro dal 20% all'80% in peso. D'altra parte, si nota un aumento dell'intensità dei picchi caratteristici dell'h-BN a 1335 cm^{-1} (L) e 764 cm^{-1} (M), anch'esso dovuto all'aumento della concentrazione di h-BN.

Le superfici dei campioni appaiono microscopicamente piatte a una scala di $40\text{ }\mu\text{m}$ e a un ingrandimento di 500X. Il campione con il 60% di h-BN sembra presentare una struttura laminata, che potrebbe essere attribuito a vari fattori come la preparazione del campione o

una regione più ricca di cellulosa che è stata investigata. Inoltre, si sono osservate significative inomogeneità nei campioni ad un ingrandimento maggiore, in particolare a 20.00 KX e 50.00 KX. Nella **Figura 12** sono riportate le microfotografie trasversali dei campioni di h-BN/CNF studiati, in cui in rosso sono raccolte immagini ingrandite in dettaglio a 300-400 nm dei film con diverse composizioni.

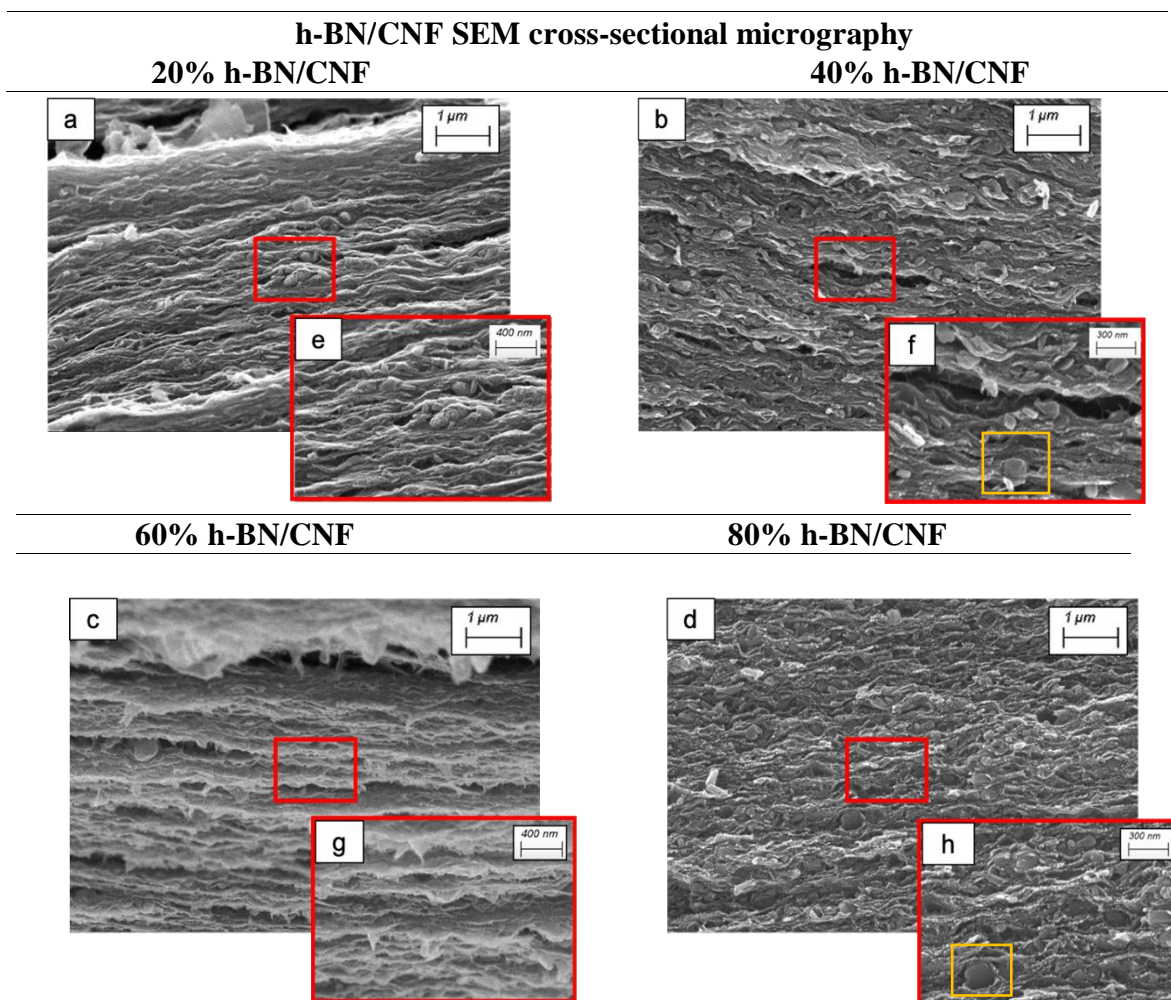


Figura 12 – Immagini SEM in cross-section mode di h-BN/CNF a differenti percentuali: 20% (a, e), 40% (b, f), 60% (c, g), 80% (d, h) ad alti ingrandimenti (20.00 – 50.00 KX)

Dopo la sonicazione le fibre di CNF si frammentano, come è possibile osservare a 1 μm e ancora meglio a una scala di 300/400 nm e per tale ragione risulta effettivamente difficile distinguere il nitrato di boro esagonale dalle fibre di nanocellulosa TEMPO. Come osservato dalle immagini SEM, vi è un allineamento lungo una direzione delle fibre di nanocellulosa lungo il piano, tipico dei film TOCN tal quali prodotti con questa procedura [75]. A una scala di 300 nm per il 40% di h-BN/CNF (**Figura 12 - b, f**) e l'80% di h-BN/CNF (**Figura 12 - d, h**), possiamo osservare probabilmente particelle circolari di h-BN all'interno della matrice di CNF (rettangolo giallo). Inoltre, come mostrato nel film 20% h-BN/CNF (**Figura 12 - a, e**), sono presenti fibre sottili che si intrecciano tra loro, formando una struttura fibrosa tridimensionale. Inoltre, come possiamo vedere nella **Figura 12 - c, g**,

è possibile osservare una superficie porosa con buchi di varie dimensioni, che possono essere visualizzati come punti scuri nella microscopia SEM, tipici della fuoriuscita di gruppi di cluster di TOCN [75]. Inoltre, i buchi che possono essere osservati, soprattutto nei campioni di h-BN/CNF, sono il risultato di fratture lungo piani diversi, che lasciano sporgenze sul lato opposto della frattura. Tutti i campioni di h-BN/CNF presentano una buona distribuzione di BNNS nel volume della matrice di CNF e non vi è presenza di stratificazione di h-BN. D'altra parte, come si può osservare più chiaramente nella **Figura 12 - a, e**, la dispersione delle nanoparticelle di nitrato di boro a tutte le diverse composizioni non è ottimale, in quanto sono state osservate agglomerazioni di particelle di dimensioni macrometriche. Ciò può essere attribuito alla scarsa affinità delle particelle di nitrato di boro con il solvente acquoso. Per approfondire ulteriormente la presenza di h-BN, è stata effettuata un'analisi qualitativa EDS (come mostrato nella **Figura 13**). Non è possibile effettuare stime esatte, ma è comunque utile per comprendere se, aumentando la concentrazione, vi sia un aumento qualitativo del contenuto effettivo di B e N. I segnali degli elementi B, N e C si sovrappongono a causa delle loro caratteristiche simili. I campioni al 20% e 40% mostrano qualitativamente la stessa composizione (come mostrato nella **Tabella 4**). I campioni all' 80% e 60% presentano la stessa quantità di azoto (N), mentre vi è un leggero aumento di boro (B) dal 40% all'80%. La concentrazione aumenta ma non è proporzionale alla concentrazione teorica poiché l'h-BN tende a precipitare sul fondo a causa della sua scarsa affinità con il solvente acquoso. La presenza di Na potrebbe essere attribuita al processo di ossidazione TEMPO della polpa di cellulosa.

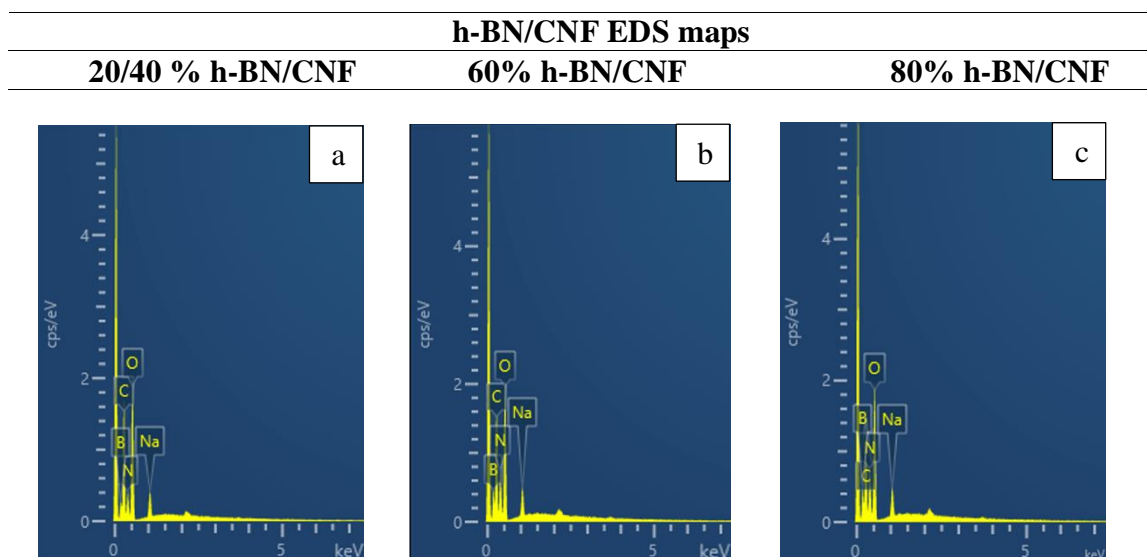


Figura 13 – Spettri EDS di film nanocomposite di h-BN/CNF a composizioni differenti: 20-40 % (a), 60% (b), 80 % (c)

Tabella 4– Analisi EDS di film nanocompositi h-BN/CNF alle diverse composizioni: 20-40 % (a), 60% (b), 80 % (c)

Samples	C [wt%]	O [wt%]	N [wt%]	B [wt%]	Na [wt%]
20% BN/CNF	35.7	32.1	16.5	14	1.7
40% BN/CNF	35.7	32.1	16.5	14	1.7
60% BN/CNF	31.1	27.4	22.4	17.8	1.4
80% BN/CNF	31.4	26.6	22.4	18.3	1.4

A causa della scarsa affinità dell'h-BN con l'acqua, è probabile che il nitrato di boro si sia agglomerato in microparticelle all'interno della matrice di TOCN a causa della presenza di interazioni deboli di van der Waals. Questo fenomeno ha comportato una scarsa conducibilità termica poiché le particelle non sono risultate abbastanza vicine da creare un percorso percolativo. I test preliminari sulla conducibilità termica non hanno fornito risultati conclusivi.

La stabilità termica dei film nanocompositi di h-BN/CNF è stata caratterizzata nelle stesse condizioni operative, sia in azoto che in aria, tra 100°C e 700°C , al fine di determinare il profilo di perdita di peso dei compositi h-BN/CNF. La stabilità termica delle polveri di h-BN e del film di TEMPO-CNF è rappresentata nella **Figura 14**.

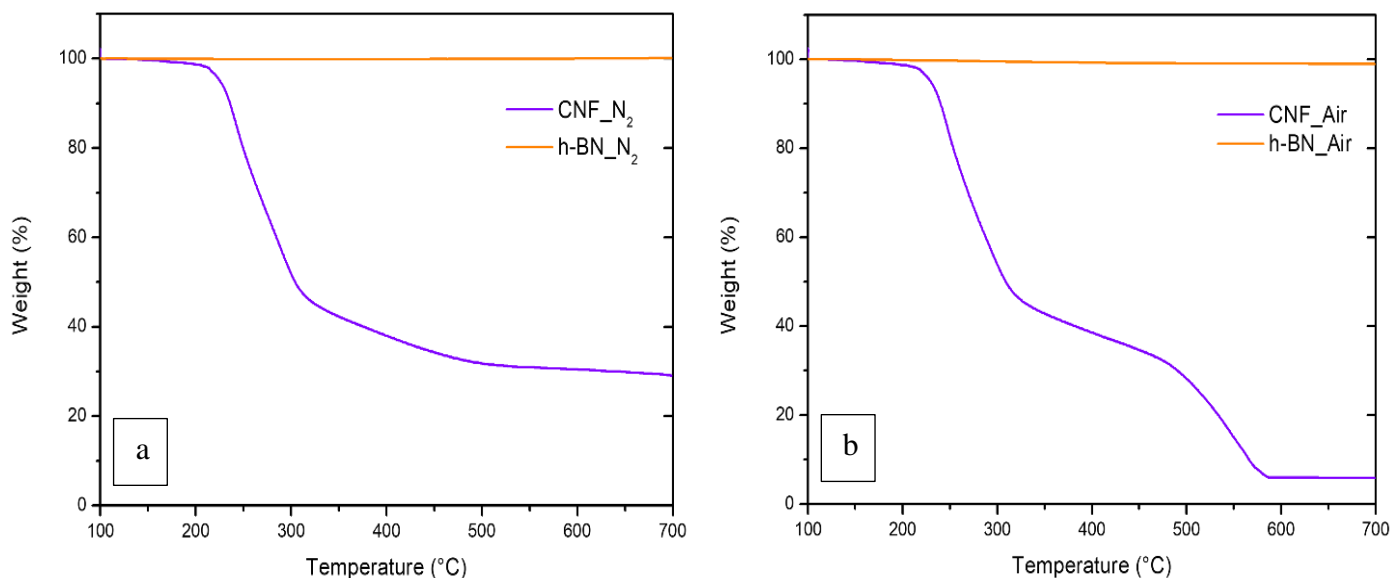


Figura 14 – Curve termogravimetriche dei film di TOCN e polvere h-BN in condizione di N₂ (a) e Aria (b)

Prima dei 100°C, si verifica l'evaporazione dell'acqua assorbita sia nella TEMPO-CNF che nell'h-BN in entrambe le condizioni ambientali. In atmosfera inerte (**Figura 14 - a**), è

stato osservato come il processo di decomposizione della TOCN avvenga in un unico step tra 200°C e 340°C, con una velocità massima di decomposizione intorno ai 300°C. Questa fase può essere attribuita a due processi competitivi [76]: depolimerizzazione e decomposizione delle unità glicosidiche. La depolimerizzazione avviene attraverso la rottura dei legami acetali tra le unità glicosidiche, con formazione di levoglucosano volatile. D'altra parte, la decomposizione avviene mediante eliminazione intramolecolare ed intermolecolare di acqua, portando alla formazione di una struttura alifatica termicamente stabile, che viene successivamente convertita in carbonio aromatico, rilasciando CO₂, CO, H₂O e CH₄ oltre i 350°C. I film di CNF hanno prodotto un residuo carbonioso del 29,12% a una temperatura di 700°C. Nella stessa atmosfera, la massa di h-BN rimane quasi stabile all'aumentare della temperatura nell'intervallo misurato fino a 700°C. In aria (**Figura 14 - b**), il processo di decomposizione della TOCN avviene in due step. La prima fase di decomposizione avviene intorno ai 300°C e comporta una perdita di peso del 60%, che rappresenta una stabilità termica relativamente bassa. Questo fenomeno è attribuito alla decomposizione dei composti glicosidici. La seconda fase, causata dalla decomposizione delle strutture piraniche, inizia intorno ai 450°C e porta a una perdita di peso complessiva del 90%. La massa residua del CNF in presenza di aria è del 5,84%. Anche in questo caso, la massa del nitrato di boro rimane costante nell'intervallo studiato di 100-700°C. Secondo la letteratura [77], la resistenza all'ossidazione dell'h-BN sembra essere correlata al grado di cristallinità e all'area superficiale specifica del BN. Una elevata cristallinità, combinata con una piccola area superficiale specifica, comporta meno siti reattivi per l'ossidazione e, di conseguenza, una ridotta perdita di massa. L'h-BN inizia ad ossidarsi a una temperatura più elevata (1200°C). A questa temperatura, avviene l'ossidazione del nitrato di boro in B₂O₃, con rilascio di N₂. Inoltre, a questa temperatura si osserva un aumento di massa dovuto alla formazione di ossido di boro sulla superficie. Le curve termogravimetriche dei film h-BN/CNF alle diverse composizioni e condizioni atmosferiche sono mostrate in **Figura 15**.

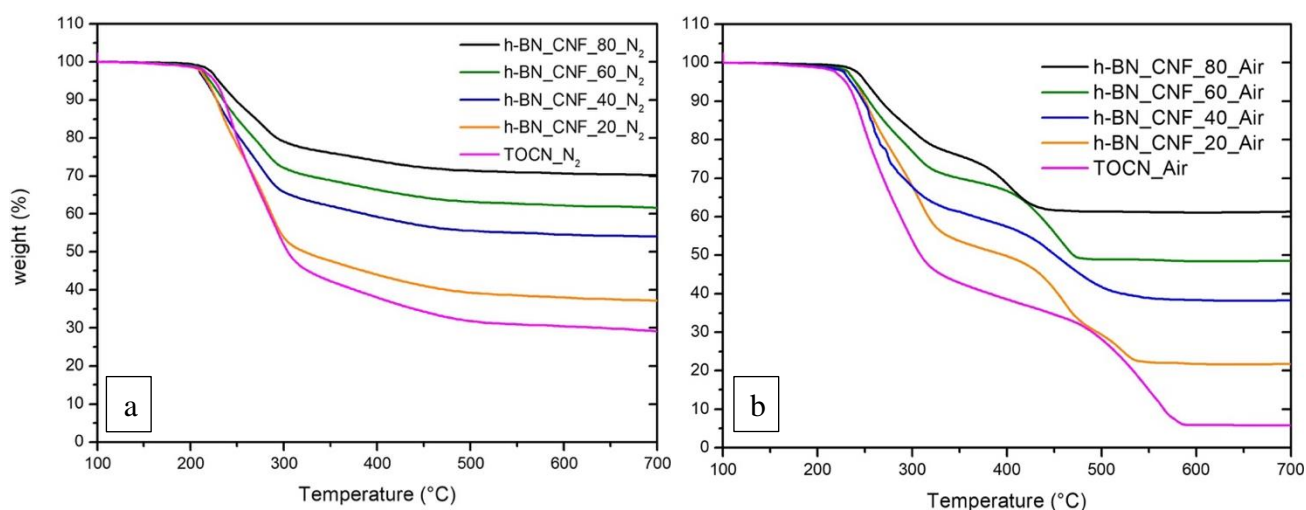


Figure 15 – Curve termogravimetriche dei film h-BN/CNF a differenti composizioni in N₂ (a) and Air (b)

L'h-BN non modifica il comportamento di decomposizione del TOCN in atmosfera inerte poiché avviene in un unico step (Figura 15 - a). La produzione di carbone residuo può essere utilizzata come indicatore di un buon comportamento di reazione al fuoco. In accordo con quantitativo teorico di h-BN aggiunto, in entrambe le condizioni si ha un aumento di residuo all'aumentare della % di h-BN. La massa residua dei campioni è determinata dalla somma del contributo di h-BN aggiunto e dal residuo di char della TOCN. Il residuo è attribuibile principalmente al nitrato di boro. In ambiente ossidativo (**Figura 15 - b**), il comportamento di decomposizione di questi nanocompositi avviene in due fasi perché le polveri di h-BN non sono in grado di sopprimere la seconda fase di perdita di peso e di formare una barriera alla diffusione dell'ossigeno. La ragione è probabilmente riconducibile all'aspect ratio più basso e la scarsa dispersione dell'h-BN all'interno della matrice. La matrice di nanocellulosa in azoto ha già una buona capacità di produrre carbone come mostrato in figura. In aria, il residuo a 700°C è sostanzialmente dovuto all'h-BN. Rispetto al quantitativo teoricamente aggiunto, dopo il 40% non si riesce ad ottenere il quantitativo target del 60% e dell'80%, come è possibile vedere in figura. La **Tabella 5** mostra i residui dei film di TOCN, h-BN e h-BN/CNF a diverse composizioni e in diverse atmosfere.

Tabella 5 – Residui dei film di nanocomposito h-BN/CNF a composizioni differenti e in condizioni ambientali differenti

Samples	N ₂ Residue [% wt]	Air Residue [% wt]
Net TOCN	29.12	5.84
h-BN	99.7	98.83
20% h-BN/CNF	36.5	21.70
40% h-BN/CNF	53.6	38.22
60% h-BN/CNF	60.9	48.52
80% h-BN/CNF	69.2	61.23

Eseguendo dei test di trazione è stato possibile ottenere curve sforzo-deformazione e, di conseguenza, raccogliere informazioni sulle proprietà meccaniche dei film nanocompositi h-BN/CNF. Le curve sforzo-deformazione ottenute sono mostrate nella **Figura 16** e le proprietà meccaniche sono riassunte nella **Tabella 6**.

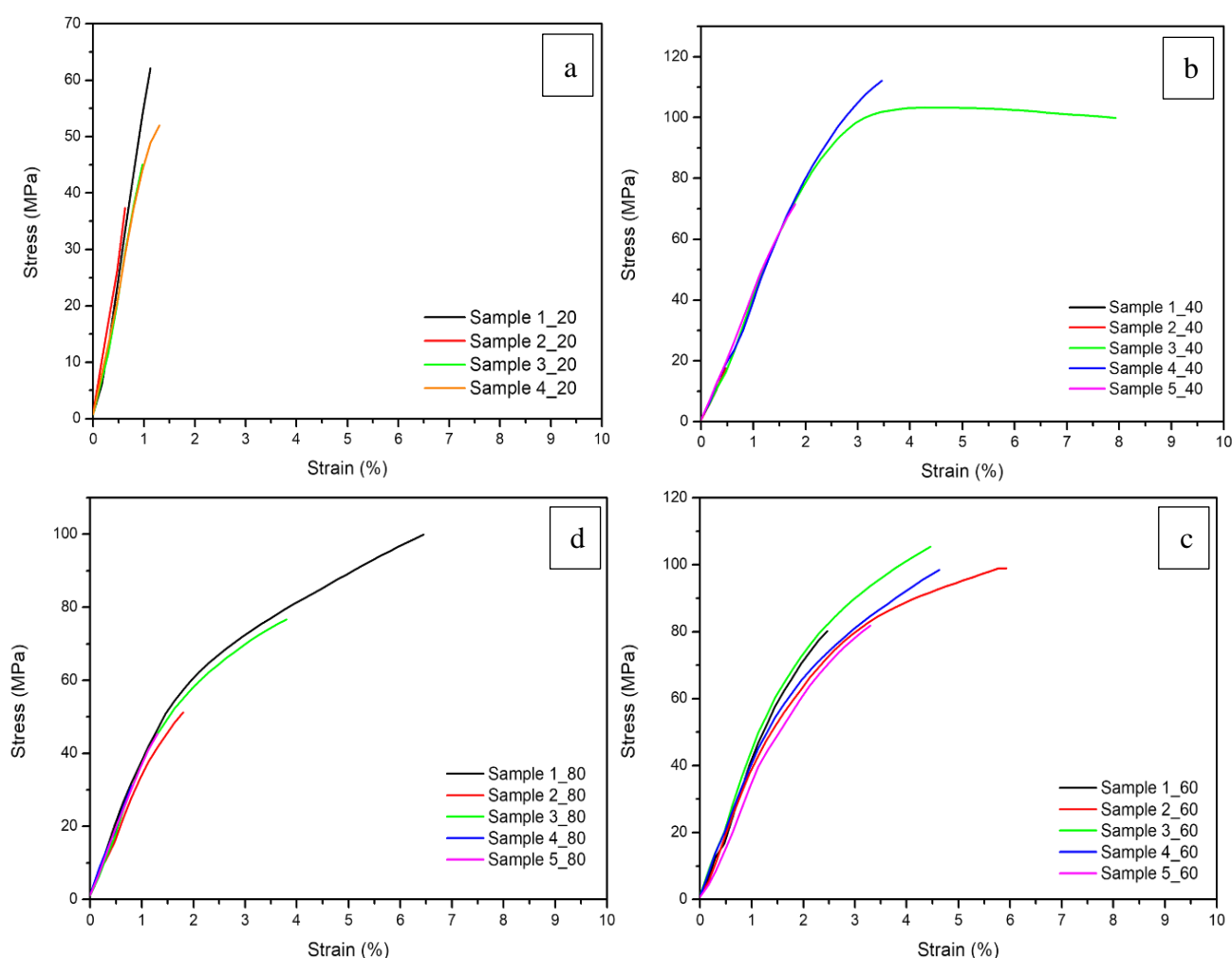


Figure 16 – Curve sforzo-deformazione di film h-BN/CNF alle differenti composizioni studiate: 20% h-BN (a), 40% h-BN (b), 60% h-BN (c), 80% h-BN(d)

Secondo la letteratura [68], i film TOCN prodotti con lo stesso processo di produzione mostrano proprietà significativamente superiori rispetto ai nanocompositi h-BN/CNF. Il modulo di Young dei film TOCN è di circa 14 GPa e lo stress a rottura è intorno ai 310 MPa. Inoltre, si osserva un comportamento plastico seguito da incrudimento lineare ed infine frattura. Questo è principalmente attribuito alle orientazioni casuali delle nanofibre nel piano del film e alla presenza minima di porosità. D'altra parte, i film h-BN/CNF, a causa della scarsa dispersione delle nanoparticelle nella matrice TOCN, si verifica una riduzione drastica delle proprietà meccaniche risultando in un comportamento fragile (**Tabella 5**). Il modulo di Young non supera i 4 GPa e lo stress a rottura non supera i 93

MPa. Questi campioni subiscono principalmente frattura fragile. La deviazione standard è molto alta a causa della scarsa dispersione delle particelle. La presenza di aggregati di dimensioni variabili influisce negativamente sul modulo elastico. Quando la percentuale di h-BN è al 20% in peso, i nanocompositi h-BN/CNF mostrano un modulo di Young medio più alto (4124.4 ± 1070 MPa), probabilmente perché la matrice TOCN prevale sull'h-BN, mostrando un comportamento più simile a quello dei film TOCN puri. Con un alto contenuto di h-BN (40% in peso), si osserva un aumento della resistenza media a rottura (σ_{mb}), ad eccezione del campione con un contenuto di h-BN dell'80% in peso. I campioni con un contenuto di h-BN del 60% in peso mostrano resistenza media e deformazione a rottura più elevate ($2,8 \pm 3.1$ % e 93 ± 11 MPa, rispettivamente). Ciò potrebbe essere dovuto al miglioramento del livello di dispersione ottenuto per i campioni con il 60% di h-BN. Inoltre, si riscontra un aumento della duttilità evidenziato dall'aumento di ϵ_{mb} , probabilmente dovuto alle proprietà lubrificanti dell'h-BN che migliorano lo scorrimento tra le fibrille di cellulosa. Infine, si osserva una riduzione non lineare del modulo di Young medio all'aumentare del contenuto di h-BN, probabilmente correlata alla nanostruttura agglomerata che riduce gli effetti di rinforzo e il trasferimento dello stress. Risultati differenti dal nitrato di boro sono stati riportati in letteratura [68], in cui sono state utilizzate diverse composizioni di nano-argilla a diversi aspect ratio (montmorillonite (MTM), mica e saponite (SPN)). MTM/CNF ha raggiunto il più alto modulo di Young, raggiungendo 30-40 GPa con una percentuale di argilla dell'80%. Ad alto contenuto di argilla, i campioni SPN/CNF hanno mostrato anche una transizione da un comportamento fragile a uno duttile, superando i 250 MPa con il 40% in volume di argilla. Ciò è stato attribuito al fatto che la SPN ha un rapporto di aspetto più basso e una buona dispersione delle lamine di argilla rispetto alle polveri di h-BN.

Table 4.3 – *Properties of h-BN/CNF nanocomposite films at different compositions*

Samples	Properties		
	E_m [MPa]	ϵ_{mb} [%]	σ_{mb} [MPa]
CNF [68]	≈ 14000	/	≈ 310
20% BN/CNF	4124 ± 1070	1.0 ± 0.3	49 ± 10
40% BN/CNF	3450 ± 332	2.8 ± 3.1	62 ± 46
60% BN/CNF	3521 ± 1005	4.2 ± 1.3	93 ± 11
80% BN/CNF	3727 ± 437	2.8 ± 2.3	61 ± 27

Sono stati condotti test di infiammabilità orizzontale utilizzando una procedura derivata del test UL-94 per determinare la propensione all'innesco dei nanocompositi h-BN/CNF quando esposti ad una fiamma di metano blu. Come riportato nella letteratura [68], il TOCN puro mostra un innesco alla fiamma molto rapido, seguita da un comportamento di autoestinzione e un fenomeno di incandescenza (ossidazione in assenza di fiamma) fino al completo consumo del campione. D'altra parte, i compositi h-BN/CNF hanno mostrato eccellenti proprietà ritardanti di fiamma, garantendo quindi un elevato livello di sicurezza antincendio. Durante il test, una volta rimossa la fiamma, i campioni analizzati mostrano un comportamento di autoestinzione (come mostrato nella **Figura 17**). Durante l'esposizione alla fiamma, i composti rilasciati dalla decomposizione del TOCN vengono intrappolati all'interno delle particelle di nitruro di boro creando un ostacolo alla diffusione dell'ossigeno e riducendo la velocità di ossidazione, promuovendo l'autoestinzione. Queste particelle formano uno strato ibrido composto da carbonio proveniente dalla degradazione del TOCN e dell'h-BN. Le proprietà ritardanti di fiamma aumentano con il contenuto di h-BN, fatta eccezione per il film all'80% wt. Infatti, come si può vedere nei campioni a fine test nella **Figura 17**, ci sono diverse lunghezze di campione bruciato. Il campione 80% h-BN/CNF mostra una sezione bruciata più pronunciata (e quindi una lunghezza residua più breve). Questo è dovuto alla scarsa dispersione delle nanoparticelle di nitruro di boro. Infatti, con un'alta percentuale, si formano molti aggregati sub micrometrici, che aumentano significativamente la propagazione della fiamma.

Nei campioni analizzati è stato osservato il fenomeno di afterglow (persistenza del calore dopo l'applicazione della fiamma), mostrando diversi tempi di incandescenza. In particolare, i campioni con 40% di h-BN/CNF mostrano il tempo di incandescenza più lungo di tutti (9.3 secondi). D'altra parte, i campioni con 60% di h-BN/CNF dimostrano la migliore performance, presentando il tempo di incandescenza più breve di tutti (4 secondi) e la lunghezza residua più ampia. Il test è stato superato con successo da tutti i campioni con diverse percentuali di h-BN, in quanto hanno mostrato un comportamento di autoestinzione prima di raggiungere 1/5 della lunghezza utile dei campioni.

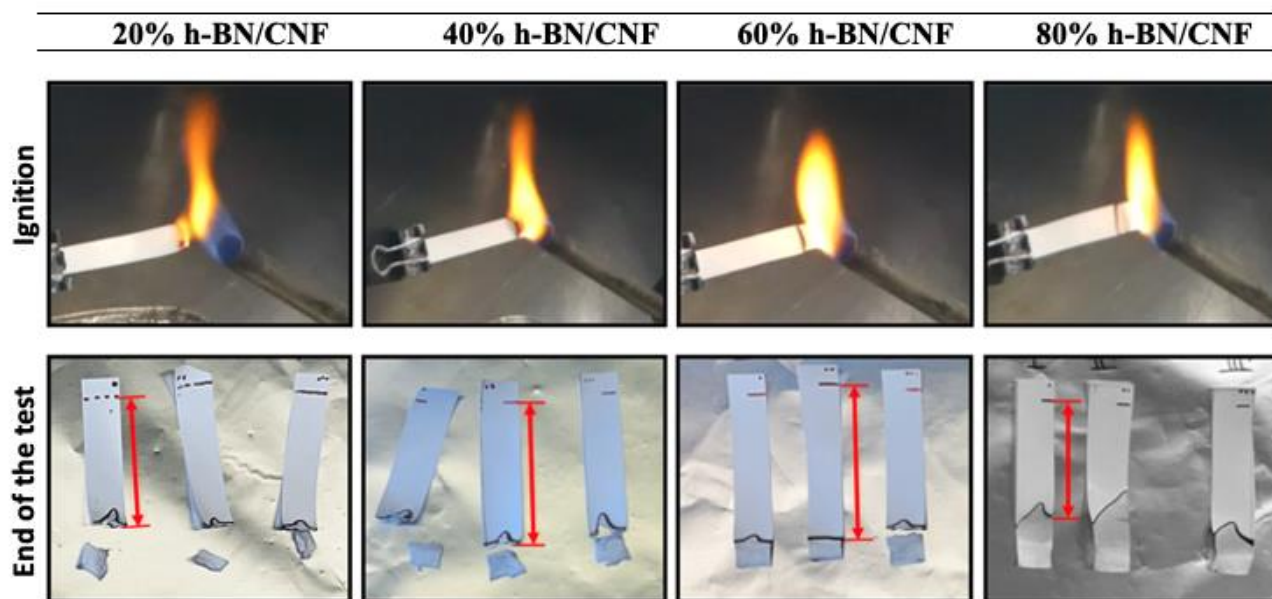


Figura 17 – UL-94 test sui film h-BN/CNF alle diverse composizioni

La **Figura 18** riporta il flame penetration test eseguito sui campioni alle diverse composizioni, mostrando il profilo di temperatura registrato nel tempo. L'applicazione di una fiamma diretta sulla superficie del campione è stata sufficiente per penetrare e distruggere immediatamente tutti i campioni di h-BN/CNF. Le ragioni possono sempre essere attribuite alla scarsa distribuzione del nitrato di boro.

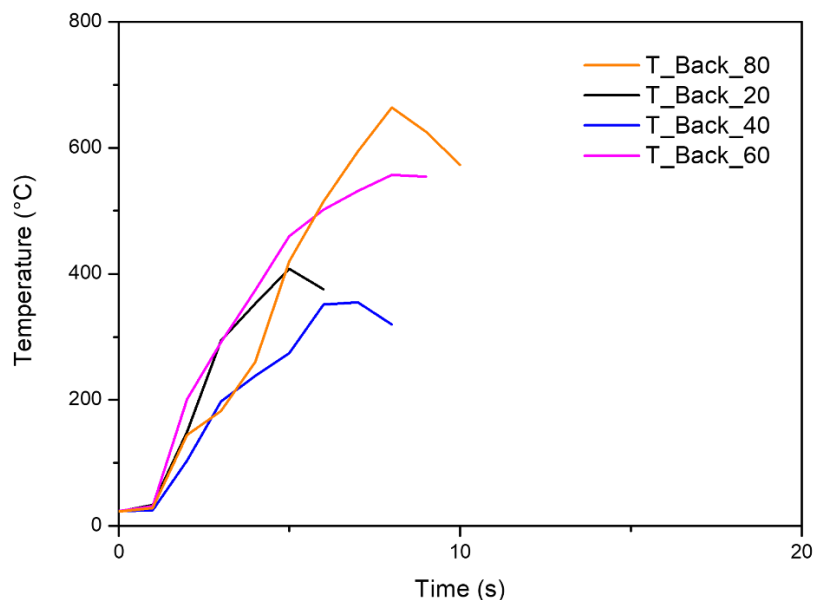


Figure 18 – Flame penetration tests: Temperatura frontale e posteriore dei campioni in funzione del tempo alle diverse percentuali: 20% h-BN (T_{Back_20}), 40% h-BN (T_{Back_40}), 60% h-BN (T_{Back_60}), 80% h-BN (T_{Back_80})

Per comprendere meglio il comportamento dei nanocompositi, è stata utilizzata una termocamera come supporto all'analisi. Le immagini termografiche dei test di penetrazione sono mostrate nella **Figura 19**.

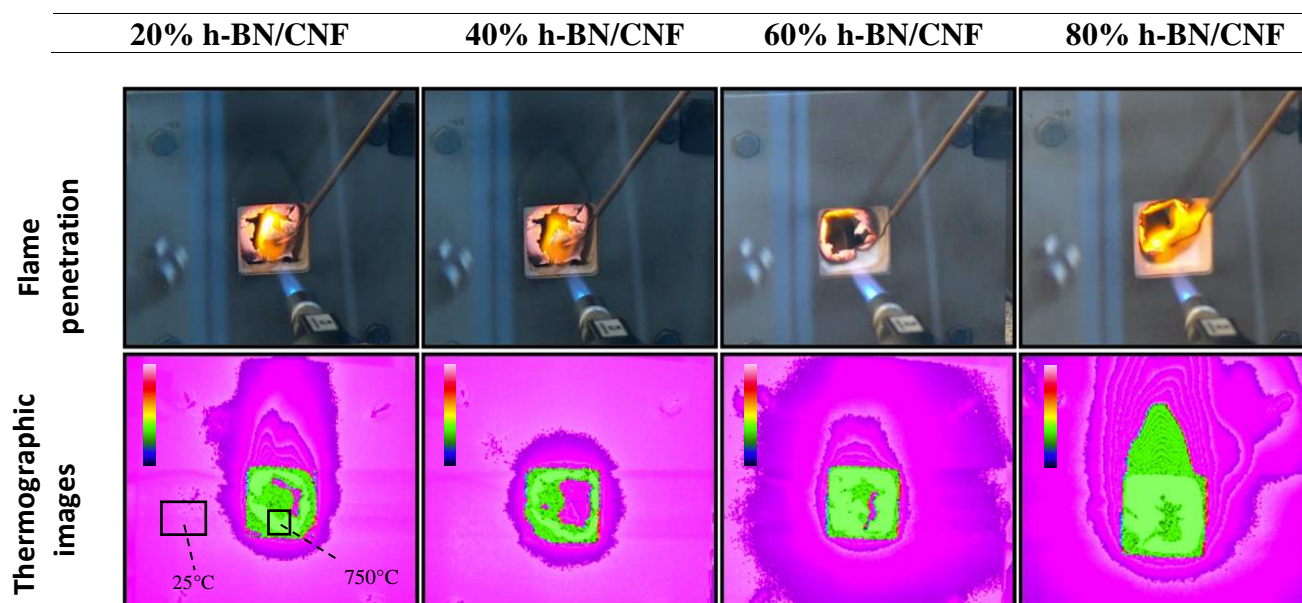


Figura 19 – Test di penetrazione alla fiamma: frame della superficie frontale dei film h-BN/CNF durante il test e immagini termografiche della superficie posteriore dei campioni

Conclusioni e prospettive future

L'obiettivo principale di questa tesi è stato quello di investigare se la presenza di nitrato di boro esagonale (h-BN) all'interno di nanocompositi a base di nanocellulosa potesse migliorare le proprietà del composito, in particolare le proprietà di ritardo alla fiamma rispetto alla nanocellulosa pura. Per questo motivo, sono stati prodotti film di h-BN/CNF con uno spessore di circa 50 micrometri utilizzando la filtrazione assistita da vuoto, a partire dalla produzione di TOCN dalla polpa di cellulosa. Si è osservato che i film prodotti utilizzando questa tecnica non presentavano una buona dispersione delle particelle di nitrato di boro all'interno della matrice di nanocellulosa a causa della scarsa affinità dell'h-BN con l'acqua. Tuttavia, mostrano una distribuzione casuale delle particelle all'interno della struttura che determina la produzione di un microcomposito. Grazie alla presenza di nitrato di boro, questi compositi mostrano migliori proprietà antincendio. Bruciando la matrice di CNF, lo strato di carbone formato dalla nanocellulosa con h-BN tende a raggiungere la superficie, creando una debole nano-barriera al calore e all'ossigeno, proteggendo il materiale dalla degradazione indotta dalla fiamma e riducendo il tasso di rilascio di calore. Tale barriera però, non è in grado di prevenire il fenomeno di afterglow facendo passare l'ossigeno, probabilmente per la presenza di aggregati di h-BN. Questa analisi è stata ulteriormente supportata dall'analisi TGA, che ha mostrato un aumento proporzionale del residuo con l'aumento della concentrazione di nitrato di boro aggiunto sia in aria che in azoto. Rispetto al quantitativo teoricamente aggiunto, dopo il 40% non si riesce ad ottenere il quantitativo target del 60% e dell'80%. I compositi con il 60% in peso di h-BN hanno dimostrato il miglior compromesso tra distribuzione e dispersione, risultando la composizione più performante.

D'altra parte, la scarsa dispersione delle nanoparticelle ha causato diversi problemi per i campioni realizzati. In particolare, ha portato a una scarsa resistenza alla penetrazione della fiamma, poiché i campioni di tutte le composizioni si sono perforati nel giro di pochi secondi. Inoltre, è stata osservata una bassa conducibilità termica a causa della scarsa dispersione, che non ha creato un percorso percolativo. La scarsa dispersione ha anche determinato una drastica riduzione delle proprietà meccaniche rispetto ai film di nanocellulosa pura, con una perdita di quasi il 75% nel modulo elastico e nella resistenza a trazione per il film di 60% h-BN/CNF.

In conclusione, l'obiettivo della tesi è stato parzialmente raggiunto considerando il miglioramento del comportamento di infiammabilità. Sviluppi futuri potrebbero riguardare l'utilizzo di tecniche alternative di preparazione per questo tipo di film, al fine di migliorare la dispersione delle particelle. Ciò potrebbe portare a un miglioramento di ritardo alla fiamma mantenendo eccellenti proprietà meccaniche e di conducibilità termica.

Lists of Abbreviations

ANC	Amorphous nanocellulose
ATR	Attenuated total reflection
BNNS	Boron nitride nano-sheets
CMF	Cellulose microfibrils
CNF	Cellulose nanofibrils
DI	Deionized water
EDS	Energy dispersive X-ray Spectroscopy
FTIR	Fourier Transform Infrared Spectroscopy
HB	Horizontal Burning
h-BN	hexagonal – Boron Nitride
MCC	Microcrystalline cellulose
NCC	Nanocrystals of cellulose
PFI	Pulverized fibre instrument
SCB	Sugarcane cellulose bagasse
SEM	Scanning Electron Microscopy
TGA	Thermogravimetric Analysis
TOCN	TEMPO-oxidized cellulose nanofibers
VB	Vertical burning

1 Introduction

1.1 Bio-based materials overview

Bio-based materials are materials produced from renewable biological sources such as plants, animals, and microorganisms. These materials are often considered a sustainable and low environmental impact solution compared to traditional materials, produced from non-renewable sources such as petroleum. Plastic-based packaging is an area of concerns where biobased materials might find suitable applications. Indeed, short-life applications in the packaging sector represent one of the primary usage areas for plastics with a long lifespan [1], leading to a significant accumulation of waste. As a result, there is a pressing need for optimized a “circular economy” pathway that can retain the value of plastics within the economy by preventing their disposal.

Among the most common bio-based materials are cellulose, starch, gum arabic, bamboo, hemp, wool, and vegetable leather. These materials can be used in various industries, including construction, apparel, automotive, packaging, and consumer products.

Bio-based materials can have environmental benefits such as reducing CO₂ emissions and decreasing the consumption of non-renewable resources. However, there are also some challenges such as large-scale production, cost and the need to ensure the sustainability of the biological sources used.

The term "bio-based material" has different meanings depending on the context. The Sustainable Biomaterials Collaborative (SBC) defined a bio-based plastic such as made entirely from agricultural resources and sustainable forestry, such as corn starch, and cellulose. However, the American Society for Testing and Materials International (ASTM) defines a bio-based plastic as an organic material that derives its carbon from a renewable resource through biological processes[2]. The latter definition seems more suitable for the bio-based material examined in this project, as it contains some non-renewable chemicals during production. Nevertheless, it is a valuable material even if it is not entirely bio-based, as it can replace non-renewable fossil resources.

Bio-based polymer are generally classified into two main categories known as "Old economy" and "New economy." The "Old economy" bioplastics were utilized before the discovery of petrochemicals, and they are derived from modified natural compounds like rubber, gelatin, or cellulose. The "New economy" bioplastics are those plastics that are developed as a natural and renewable alternative to petrochemical materials, such as Cellulose fibers[3]. The term "bioplastics" can be divided into two main groups depending on their chemical composition.

The first group is called “drop-ins” and refer to plastic materials that are designed to directly replace traditional petroleum-based polymers such as polyethylene (PE), polypropylene (PP), or polyethylene terephthalate (PET). These materials are made using

biological sources such as biomass or vegetable oils, but their chemical structure and properties are similar to those of conventional plastics. The second group is “Chemical Novel” that refer to completely new plastic materials developed using innovative chemical processes. These materials can have a unique chemical structure or different properties compared to traditional plastics (es. PLA)[4].

These examples are shown in the European Bioplastics Association graph [5] in **Figure 1.1**.

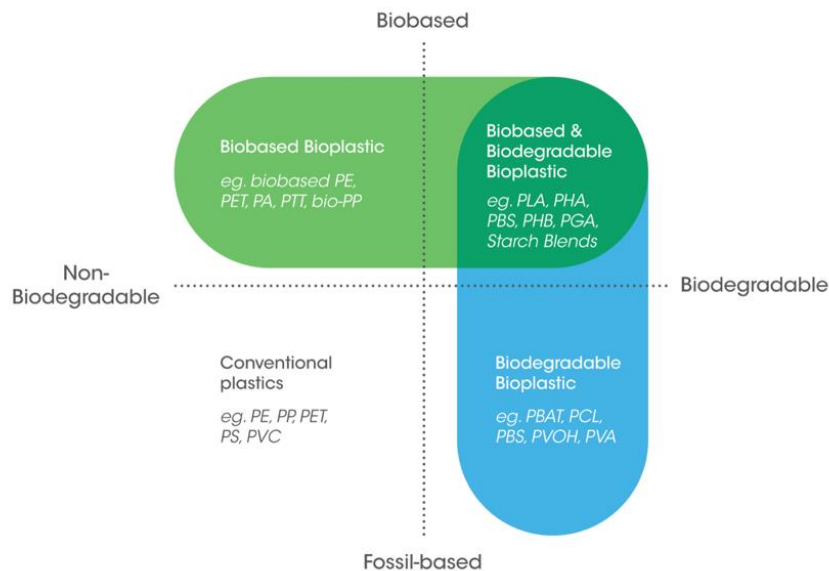


Figure 2.1 – European Bioplastics Association graph

In summary, bio-based materials represent an interesting alternative to traditional materials and can help reduce the environmental impact of many industrial sectors. However, it is important to carefully evaluate their properties, sources of production, and long-term sustainability before using them extensively.

1.2 Cellulose

Cellulose is a crucial natural polymer and an essential source of sustainable materials in industry. It has been used for thousands of years in the form of plant fibers and wood for various purposes such as energy, construction, and clothing. Apart from plants, cellulose is also produced by fungi and bacteria as an extracellular polymer that is chemically pure and has a molecular structure identical to that of cellulose found in plants [6]. In 1838, Anselme Payen, a French chemist, discovered a fibrous solid left after the treatment of plant tissues with acids and ammonia, which he identified as cellulose. He determined its molecular formula $C_6H_{10}O_5$ and observed isomerism with starch. Nowadays, cellulose is a widely used organic polymer and an almost limitless source of raw material for environmentally friendly and biocompatible products. Most of the cellulose processing comes from wood pulp and

is primarily used for paper and paperboard production. However, it is also utilized for the production of cellulose derivatives, which are used in a wide range of applications such as coatings, laminates, optical films, and additives for various products including building materials, pharmaceuticals, foods, and cosmetics[7].

There are numerous available sources that can be broadly categorized as Agricultural-waste and Plant-source (as shown in **Figure 1.2**) [8]. The processes involved in obtaining these sources typically include various chemical procedures such as alkaline extraction, bleaching, acid hydrolysis, and chlorination.

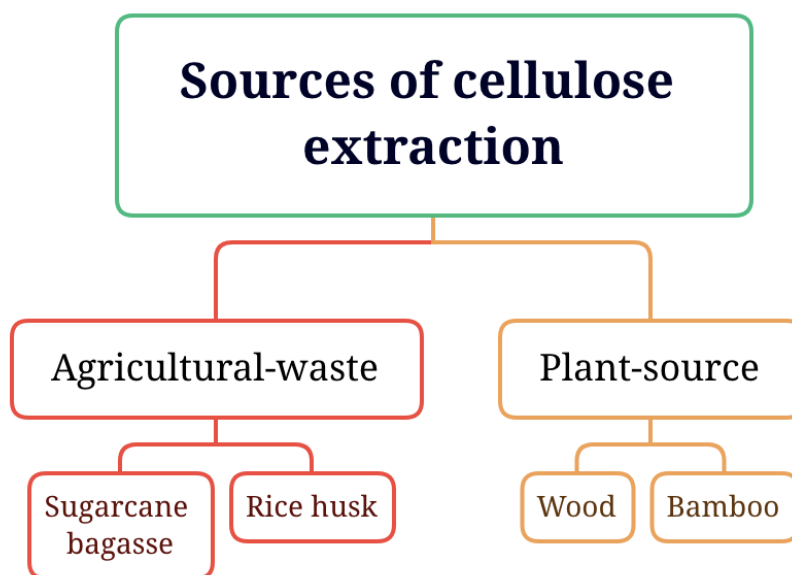


Figure 3.2 – Different sources of cellulose extraction

The extraction of cellulose from sugarcane bagasse (SCB) using environmentally friendly pre-treatment methods such as steam explosion and xylanase treatment. The aim was to reduce the reliance on chemical bleaching and investigate the properties of cellulose derived from SCB. Sugarcane bagasse is an agricultural residue with low economic value, and it contains approximately 40-50% cellulose, which is a glucose polymer.

Rice husk, being the most widely cultivated cereal crop globally. Utilizing rice husk as a primary source for the production of cellulose fibres and nanocrystals proves to be efficient. The approach involves extracting cellulose fibres from rice husk through alkali and bleaching treatments [8].

1.2.1 Structure and chemical properties of cellulose

Cellulose is chemically defined as a linear chain of polysaccharide composed of β -D-glucopyranose units linked together by β -1-4-glycosidic bonds. It consists mainly of carbon

(44.44%), hydrogen (6.17%) and oxygen (49.39%). Its chemical formula is $(C_6H_{10}O_5)_n$ shown in **Figure 1.3**, where n is called the degree of polymerization (DP) and represents the number of glucose units, ranging from tens of units to tens of thousands.

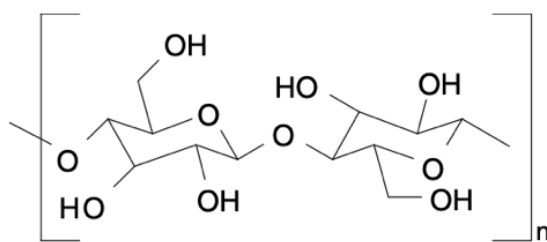


Figure 4.3 – Molecular structure of cellulose
(n = degree of polymerization)

The presence of three hydroxyl groups on each monomer in cellulose is significant due to their ability to form hydrogen bonds. These bonds play a crucial role in how cellulose packs together in a crystalline structure and govern its physical properties[9]. Cellulose fibres are formed by the union of fibrils, which are long filiform bundles of molecules stabilized laterally by intermolecular hydrogen bonds. Each fibril can be thought of as a series of cellulose crystals linked along the fibril axis by disordered amorphous domains. The main chain of cellulose consists of crystallites with intercalated amorphous regions, called native cellulose or cellulose I. There are also other types of amorphous cellulose: cellulose II, which is the most stable, cellulose III and cellulose IV.

With the use of appropriate chemical, mechanical and/or enzymatic methods, cellulose can reduce its size in diameter or both in diameter and length to the nanoscale [10]. In this case we refer to nanocellulose.

1.3 Nanocellulose

The term nanocellulose generally refers to cellulose materials that have at least one dimension in the nanometre range. The three main types of nanocellulose are cellulose nanofibers (CNF), cellulose nanocrystals (NCC), and bacterial cellulose (BC), which differ in size, function, and preparation methods[11].

Recently, the Technical Association of the Pulp and Paper Industry (TAPPI) presented a rigorous classification of cellulose crystal structures based on their size and shape [12], subdividing them into:

- MCC or microcrystalline cellulose, consisting of spherical particles or rods ranging in size from 10 to 200 microns;
- CMF (cellulose microfibrils) with width from 20 to 100 nm and length from 500 to 2000 nm;

- CNF (cellulose nanofibrils) consisting of aggregated elemental fibres, with widths of 20 to 50 nm and lengths of 500 to 2000 nm, usually including amorphous portions;
- NCC (nanocrystals of cellulose) also known as cellulose nanorods, with diameters between 5 and 50 nm and lengths between 100 and 500 nm, usually corresponding to the elemental fibres from which the amorphous portion has been removed and therefore highly crystalline; This type of cellulose is prepared from natural cellulose by acid hydrolysis.
- ANC (amorphous nanocellulose), spheres between 50 and 200nm in diameter;
- CNY (nanowires of cellulose) obtainable by electrospinning with diameters between 600 and 800nm. Of these only the first four types come from direct digestion of crystalline cellulose, the last two types from manipulations of amorphous cellulose.

Nanocelluloses exhibit improved mechanical properties due to their high surface area, large water-holding capacity and reactive OH side group surface, where almost any desired functional group can be attached[13].

Based on the literature, the term micro-fibrillated cellulose, microfibers and microfibrils (MFC) is generally used to describe a cellulose structure with 210 nm of thickness and with microns of length [14]. The terms nano fibrillated cellulose, nanofibrillar cellulose, nanofibrils, cellulose nanofibrils, and CNF are also used as synonyms for MFC.

When exposed to acid hydrolysis, CNFs suffer transverse cleavage along their amorphous regions. Additionally, the use of sonication creates a stick-shaped material that has a relatively low aspect ratio and is known as cellulose whisker [15]. The hydrogen bonding between individual cellulose crystals encourages re-aggregation [16] resulting in the formation of a different cellulose structure called microcrystalline cellulose (MCC).

Due to these excellent properties, nanocellulose has found applications in various fields, such as nanocomposite reinforcement[17], biomedicine[18], conductive devices[19], battery membranes[20], food packaging [21], environmental applications [22] or sensors [23]. However, each application requires specific properties of the materials used, so only one or a few nanocelluloses (CNF, NCC, BC) may be the most suitable depending on the final application. In addition, because of the high surface reactivity, nanocellulose is often modified and combined with other compounds to achieve synergistic effects to meet the requirements of specific applications.

1.3.1 Nanocellulose Production

Nanocellulose can be obtained from a wide variety of cellulose sources, including wood, seed fibers (cotton, coconut, etc.), flax, hemp, jute, kenaf, ramie, grasses (bagasse, bamboo, etc.), marine animals (tunicates), algae, fungi, invertebrates, and bacteria.

Wood is currently the most widely used source of cellulose [24]. In addition to cellulose (45%), wood contains hemicellulose (30%), lignin (23%) and relatively small amounts of inorganic extracts and salts. Therefore, wood must be treated mechanically and chemically to remove non-cellulosic substances before it can be used for nanocellulose production. Wood can be divided into “hardwood” and “softwood” based on its anatomical characteristics. Hardwood fibers are 34 times shorter than softwood fibers and have a higher Rankel factor (cell wall thickness divided by light radius), which results in a stiffer structure[25] (**Figure 1.4**). In addition, hardwoods have a more complex and heterogeneous structure than softwoods and require more rigid processing to induce an equivalent level of fibrillation[26].

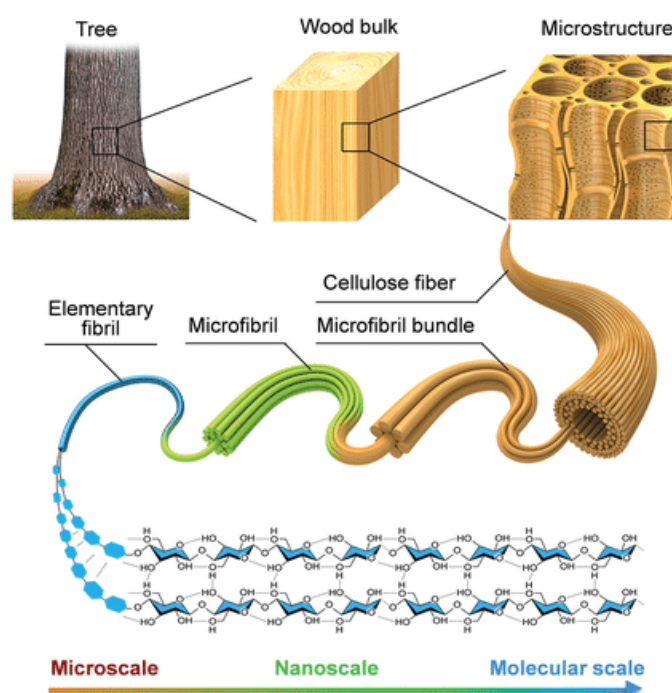


Figure 5.4 – Hierarchical structure of wood biomass and the characteristics of cellulose microfibrils [68]

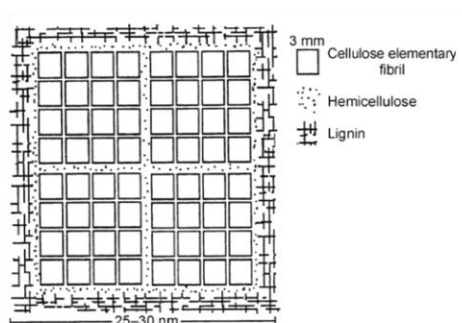


Figure 6.5 – Cross section of structural organization of cell-wall components in wood that shows different layers [77]

Figure 1.5 shows the elementary fibrils that are created through extrusion from rosette complexes during cellulose biosynthesis. Instead, microfibrils are formed by the aggregation of elementary fibrils after biosynthesis. The secondary cell wall of wood is composed of several layers, including the outer S1 layer and the central S2 layer. These layers differ in terms of their cellulose content and the orientation of their cellulose fibrils.

The production of CNF and CNC from cellulose sources such as annual plants, agroforestry residues, aquatic plants and grasses is a developing trend and represents a high demand by the pulp and paper industry. Compared with wood, non-woody plants and crops have environmental advantages and consume less energy as an insulator for cellulose particles. This thesis paper will illustrate the preparation of CNF in the experimental section.

1.3.2 Cellulose Nanofibers (CNF)

The first producers of CNF were Turbak et al. and Herrick et al. [27], refining a wood pulp to 2 wt% water in a PFI mill (pulverized fibre instrument) up to 10.000 rpm and passing it through a Manton-Gaulin homogenizer at 550 bar. The result was obtaining individualized CNFs with a diameter of less than 100 nm.

This type of nanocellulose was created and used for this thesis work to be able to realize h-BN/CNF bio-based nanocomposites for applications such as flame retardants, as will be shown later on.

There are several mechanical processes that can be used to produce CNFs, including high-pressure homogenization, microfluidization, refining, and grinding [28]. Other less commonly used mechanical treatments include electrospinning, ultrasonic treatment, cryocryption, and vapor explosion. However, a significant disadvantage of these mechanical processes is the high energy required. To address this issue, various chemical or enzymatic pre-treatments of pulp have been employed, such as cationization, hydrolysis, TEMPO (2,2,6,6-tetramethylpiperidine-1-oxyl) oxidation, acetylation, and silylation. These treatments aim to facilitate mechanical treatment, reduce energy consumption, and achieve the desired surface chemistry of the resulting product.

TEMPO (2,2,6,6-tetramethylpiperidine-1-oxyl radical) oxidation is a process that can convert native wood cellulose into individual nanofibers, which are typically 3-4 nm wide and at least several microns long, with aspect ratios greater than 100. The original crystalline structure of the native cellulose remains unchanged during this process. Soft mechanical disintegration of TEMPO-oxidized wood cellulose fibres leads to the creation of TOCNs (TEMPO-oxidized cellulose nanofibers) that can be dispersed in water. The formation of these nanofibers is due to electrostatic repulsion and/or osmotic effects acting between the anionically charged cellulose microfibrils. The resulting films made of TOCNs are flexible and transparent, exhibiting high tensile strengths of 200-300 MPa and an elastic modulus of 6-7 GPa [29].

Potential applications of nanofibers include efficient catalysts, electro-optic films, nanofiber-reinforced composites, microelectronics, gas barrier films, cosmetics, flame-resistant materials, and other high-tech and high-performance materials [30], [31]. In the past decade, they have been widely used in commodities such as paper and textiles, but also in high-tech materials such as components of liquid crystal displays, hollow fibres for artificial kidney dialysis, drug components, and food additives.

1.4 Nanocomposites

A nanocomposite is a material composed of two phases, where one phase has a dimension in the nanometer range [32]. Toyota researchers developed the first nanocomposite in 1985, which was a belt cover for cars made of Nylon-Montmorillonite nanocomposites, also known as "hybrids". Since then, research in this area has gained significant importance due to the exceptional properties exhibited by nanocomposites. Having nanometer-scale dimensions results in a higher surface-to-volume ratio for the reinforcing phase, leading to enhanced matrix properties, such as increased tensile strength and modulus, improved thermal stability, reduced gas permeability, and improved flame retardancy. These advantages make nanocomposites ideal for a wide range of applications, including energy conversion devices, sensors, structural materials, coatings, optical, magnetic, mechanical, electronic and catalysts.

Nanocomposites typically consist of a matrix that can be made of polymeric, ceramic or metal materials. Polymer materials being the most commonly used. Among polymeric matrices, epoxy resin represents the majority[33].

Polymer-inorganic hybrid composites are commonly used in industry. For instance, researchers at Toyota[34] have developed melt-processable polymer-clay nanocomposites for use in the automotive industry. These nanocomposites have improved mechanical, thermal, and gas barrier properties at low clay contents[35], which are typically below 10 wt %. The improved properties can be attributed to the nanoscale dimension of the silicate platelets, which have a large aspect ratio, high intrinsic platelet modulus and strength, and low thermal expansion. Moreover, the nanoscale silicates can strongly influence the structure and molecular mobility of the polymer matrix itself.

Regarding the fillers used in nanocomposites, there are three essential characteristics that they must possess to fulfill their function. Firstly, they must have good mechanical properties, such as a high Young's modulus. Secondly, the fillers must have a high aspect ratio and surface area to facilitate interaction with the polymer matrix. Finally, the fillers must be well-dispersed to prevent agglomerations. The combination of these three factors results in a material that is superior to the neat polymer. Good dispersion of nanofillers leads to better load distribution between the polymer and the filler, while the increased interfacial area due to the nano size results in improved strength.

According to **Figure 1.6**, there are four types of nanofillers categorized based on their dimensions at the nanoscale[36]:

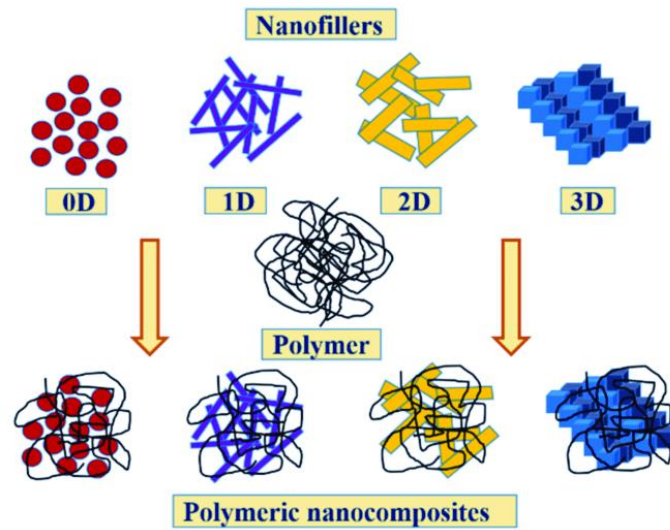


Figure 1.6 – Types of nanofillers based of their

- 0D nanofillers that have all dimensions under 100 nm. These nanofillers may be amorphous, crystalline, amorphous, metallic or polymeric nanoparticles;
- 1D nanofillers that have one dimensions up to 100 nm. These materials include nanorods, nanotubes and nanowires, which includes phyllosilicates, phosphates, graphene, and clay;
- 2D nanofillers that have two dimensions up to 100 nm. They include nanosheets, nanofilms, nanowalls, nanofibers and nanowhiskers. Significant examples are montmorillonite and carbon nanotubes;
- 3D nanofillers that have three dimensions up to 100 nm, but the size of the structural units is on the nanometric scale. These materials include nanoclays and nanogranules. Significant examples are zeolites or silica.

Glass fibres, clay carbon black, metal powders are the most used as nanofillers. Today it is increasingly frequent the use of Boron Nitride such as nanofiller.

1.5 Nanocellulose base composites and applications

Nanocellulose due to its high crystallinity, high aspect ratio, large specific surface area, high transparency, high hydrophilicity, high young's modulus and low thermal expansion coefficient is attracting significant interest as template support or reinforcement unit in nanocomposite materials. In addition, these nanocellulose fibres can be utilized as a substitute filler for traditional fibres like glass in reinforced composites, due to their desirable properties.

Due to many reactive groups on the surface, nanocellulose is a good biological template for nanoparticles physical deposition. Inorganic nanoparticles [37] such as metals, quantum dots, oxides, nitrides, guarantee unique properties and innovative green based nanocomposites.

In summary, these nanocellulose base composites have become of great interest and study in various sectors for various reasons such as: sustainability, lightness and high resistance, improvement of barrier and thermal properties and functionalization. They therefore represent an interesting sustainable alternative to conventional materials, with potential applications in numerous industrial sectors.

Following a series of main applications for nanocellulose base composites.

- Biomedical and antibacterial materials

Nanocellulose matrix can incorporate antibacterial nanoparticles such as Ag, TiO₂, ZnO to create antibacterial materials with good mechanical and thermal properties of the matrix improved due to nanocellulose. These materials are usually used into skin repair and would healing because there is a combination of antibacterial activity, water absorption ability and biocompatibility. The high aspect ratio of CNF improved the formation of entanglement networks, which increase the conductivity for the loading of antibacterial nanoparticles. An example of these materials is AgNPs/CNF composite. Another example is Montmorillonite (MMT)/CNF composite films that containing metal ions with mechanical strength and disinfecting activity (es. against *Staphylococcus aureus*);

- Optical and electronic materials

Native nanocellulose don't have luminescent or conductive properties. When is loaded with specific nanoparticles shows photothermal and photoelectrical properties. In this way nanocellulose base composites can be used in photothermal fillers, battery, fluorescent probes (es. AuNPs-7CNF);

- DNA and Protein immobilization

Nanocellulose base composites can be used for DNA and protein immobilization due to high reactive surface groups and high specific area. An example is to use magnetic Fe₃O₄ nanoparticles with CNF to immobilization of papain [38];

- Sensors

Adding plasmonic or photoluminescent nanoparticles with nanocellulose substrate create excellent type of sensors used for chemical detection. This type of nanocellulose composites can detect target analytes via fluorescence, colorimetric assay, SERS and electrochemical signal. For example, AgNPs/BNC composite was used as a chemical probe for detecting cyanide ions in water samples;

- Reinforcement and Flame retardancy

Nanocellulose composites can also be used as reinforcement and flame-retardant material. An example of these composites is TEMPO-CNF with montmorillonite (MTM) nanoparticles. This material shows enhanced oxygen barrier, ultra-high tensile strength and high Young's modulus with 5 wt% of MTM;

1.6 Hexagonal-Boron Nitride

This paragraph focuses on the description of Hexagonal Boron Nitride as nanofiller that has been used for this thesis project. It shows interesting properties, including an atomically flat surface, lack of dangling bonds and charged impurities, high chemical stability, superior elastic modulus, great mechanical flexibility, and high thermal conductivity [39][40].

1.6.1 Properties

Hexagonal boron nitride (h-BN) is a material that consists of B and N atoms arranged in a hexagonal pattern, with no dangling bonds between its layers (**Figure 1.7**).

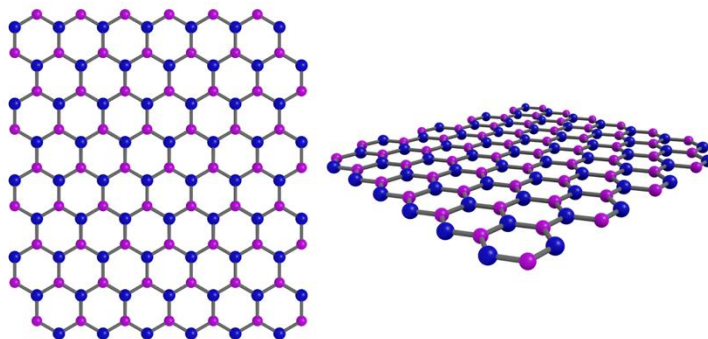


Figure 1.7 – Crystal structure of single-layer hexagonal boron nitride (h-BN)

Boron Nitride nano-sheets (BNNS) are thin sheets that are exfoliated from hexagonal Boron Nitride (h-BN). Similar to graphene, BNNS is a two-dimensional material that can be used as an ideal filler to prepare thermal conductive nanocomposites.

BNNS share a similar geometry, physical, and thermal properties as graphene, which is its all-carbon analog. Despite having a similar crystal structure to graphene, from an electrical standpoint, boron nitride is an insulator with an indirect bandgap of around 6 eV[41]. Therefore, h-BN appears white in color instead of graphene that shows black color.

The incorporation of BN as fillers into polymer matrices has been shown to enhance various properties. The subsequent paragraphs provide examples of the significant improvements observed in bio-based h-BN nanocomposites. The effects on mechanical, thermal, and barrier properties are dependent on the h-BN content and its dispersion into the polymer matrix.

For instance, an epoxy-h-BN nanocomposite study showed an overall enhancement in mechanical properties, where higher concentrations of BN led to higher modulus. This enhancement is closely related to the dispersion rate of the BN particles. Furthermore, the study results indicate that the filler particles can absorb impact force more effectively than the polymer matrix, leading to increased impact strength in composites with higher filler content. Optimal dispersion results in an increased interfacial contact area between BN and the matrix, leading to higher modulus and better mechanical behavior under load [42].

h-BN positively influences thermal conductivity, [43]. This property usually increases as the amount and size of the ceramic particles increases. When using ceramic particles that have a high aspect ratio, such as flake or fiber-shaped particles, they create a more conductive path due to their lower percolation threshold compared to spherical particles. However, using high aspect ratio particles leads to lower packing densities because they create more porosity[44]. According to K. C. Yung and H. Liem, as they wrote in their journal article [45], mixing ceramic particles of different sizes would increase the thermal conductivity of the composite because the packing density would be higher than those with single-sized particles.

In addition to the improvements observed in mechanical and thermal properties, h-BN is highly effective in enhancing the fire behavior of composites. For example, a study on an epoxy-h-BN nanocomposite demonstrated an overall improvement in fire retardancy, as reported in a research article[46]. When a material undergoes combustion, a temperature gradient is created that causes the migration of BNNS from the bulk to the surface due to their lower surface free energy. These particles accumulate to form a thermally insulative surface layer called "char", which is a hybrid layer made up of carbon from the polymer degradation and BN. The char acts as a barrier to heat and oxygen, protecting the underlying material from further degradation. **Figure 1.8** schematically represents this mechanism, where BNNS create a high-efficiency nano-barrier network that forms a "tortuous path." This path limits mass transfer between the gas and condensed phases while also reducing the supply of oxygen, thereby protecting the internal resin from further degradation and reducing the heat-release rate.

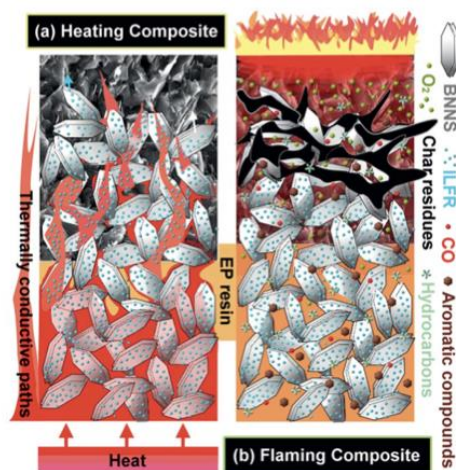


Figure 1.8 – Schematic illustration of (a) thermal conduction and (b) flame retardation mechanisms of EP/ILFR-fBNNS nanocomposites [46]

1.6.2 Synthesis

There are several techniques for synthesizing h-BN[47], including:

- Synthesis from boron and nitrogen: Synthesizing h-BN from boron and nitrogen is one of the most common techniques. In this technique, a mixture of boron and ammonium nitride is heated to high temperatures in a nitrogen pressure.
- Thermal conversion of BN precursors: In this technique, BN precursors such as borazole are subjected to high-temperature thermal conversion to produce h-BN.
- Liquid-phase condensation synthesis: In this technique, a solution of boron and ammonium nitride is heated to high temperatures to produce h-BN.
- Chemical vapor deposition (CVD) synthesis: In this technique, a BN precursor is deposited onto a substrate at high temperatures using reactive gases.
- Solution exfoliation synthesis: In this technique, h-BN is exfoliated in a solvent solution using mechanical or chemical energy to produce h-BN nanospheres.

Each technique has advantages and limitations depending on the intended applications. For example, CVD synthesis is often used for producing thin films of h-BN, while solution exfoliation synthesis is useful for producing h-BN nanoparticle for use in nanocomposites[48].

1.6.3 Applications

h-BN has shown great promise in a variety of applications (**Figure 1.9**). It has been indeed employed as passivation layer, a gate dielectric, a tunneling barrier, an electrical and thermal contact interface, and in van der Waals electronics.

Recently, h-BN has been discovered to have natural hyperbolic and piezoelectric properties, which offer novel optical and electromechanical properties, making it a promising candidate for hyper lenses[49], near-field imaging[50], deep-UV emitters[51], and detectors[52], quantum optoelectronics[53], nonlinear and stretchable optics[54].

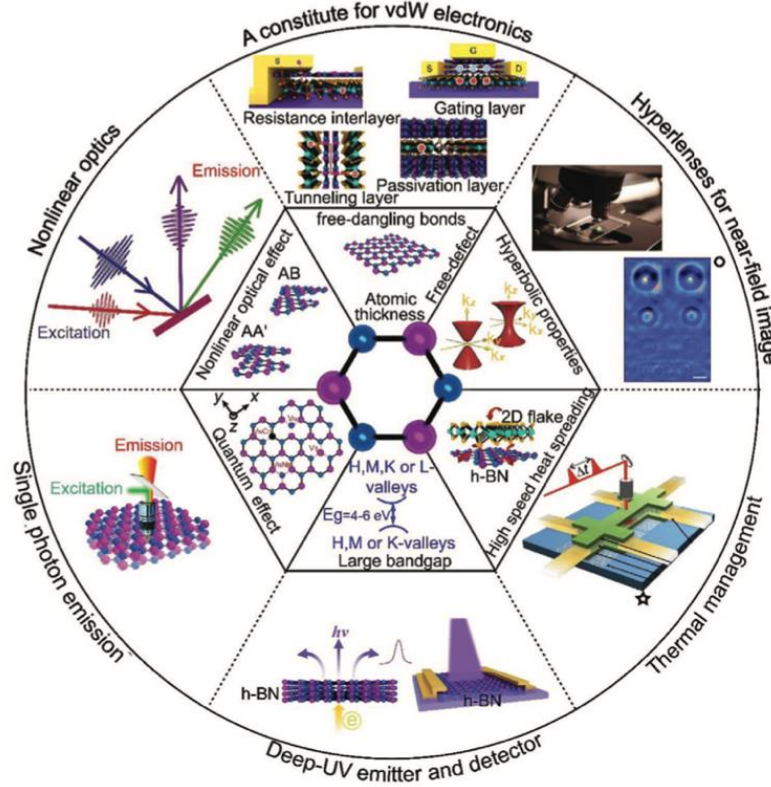


Figure 1.9– Properties of h-BN and its typical applications

In this thesis, among all the matrices, the use of boron nitride as a filler in polymer nanocomposites is investigated.

1.7 Hexagonal Boron Nitride polymer nanocomposites

The effectiveness of this type of filler is dependent on its interaction with the polymer matrix. Due to the hydrophilic nature of BN and the hydrophobic nature of the polymer, the BNNS (Boron Nitride Nanosheets) may clump together in the matrix. Based on the level of interaction between the polymer and h-BN, there are three distinct composite structures, which are illustrated in **Figure 1.10**.

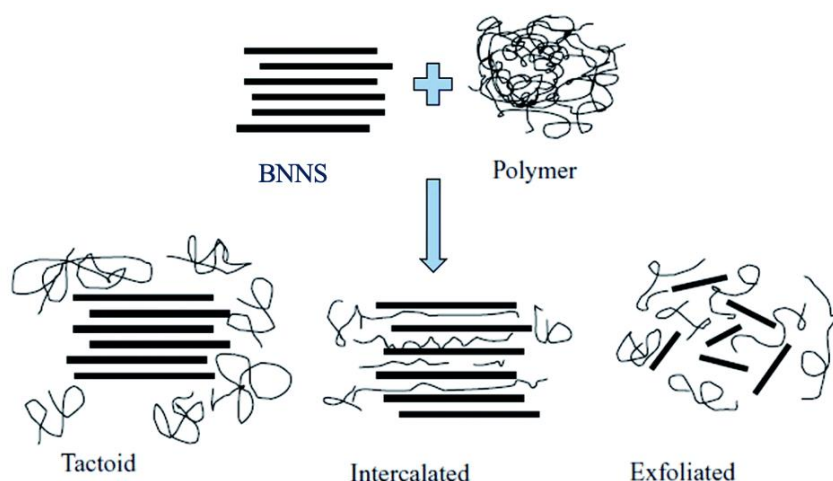


Figure 1.10 – Possible composite structures of h-BN/Polymer

The first structure is a Tactoid nanocomposite or micro-composite, which has weak interaction and compatibility between the two components, making it difficult for the polymer to intercalate within the h-BN layers. The second structure is an intercalated-nanocomposite, where the polymer chains are partially intercalated between the h-BN layers, creating an ordered stacking pattern of alternating polymer and h-BN. Finally, the third structure is an exfoliated-nanocomposite, where the h-BN layers are fully exfoliated, resulting in a homogeneous dispersion of h-BN within the polymer matrix[55]. The type of composite structure formed can have a significant impact on the properties of the resulting material, including mechanical strength and thermal conductivity.

Using the Tactoid structure would be inconvenient as it would result in suboptimal distribution, thereby compromising the properties, which could potentially be worse than those of the neat polymer. On the other hand, the Exfoliated structure is the desired one, but achieving such a high level of dispersion is extremely challenging.

h-BN/polymer nanocomposites are advanced materials that combine the thermal, mechanical and dielectric properties of hexagonal boron nitride (h-BN) with the elastic and processability properties of polymers. The preparation of these nanocomposites can be done through several techniques showed in the following subparagraph.

1.7.1 h-BN nanocomposites preparation techniques

There are several preparation techniques for h-BN nanocomposites such as:

- Single or double screw extrusion: this technique consists of melting the polymer and h-BN particles and then extruding the molten material through a screw. This

process improves particle dispersion and allows to obtain nanocomposites with a uniform distribution of h-BN particles [56].

- Melt compounding: This method involves mixing polymer and h-BN particles inside an extruder. The process takes place in two stages: the first stage is hot mixing, during which the polymer is dissolved and particle dispersion is improved. In the second stage, the molten material is extruded and the nanocomposite is produced[57].
- In situ polymerization: in this process, h-BN particles are synthesized within the polymeric matrix. This occurs through the addition of a polymer precursor and an h-BN precursor within the matrix and the subsequent polymerization and synthesis of the h-BN[58].
- Dispersion Methods: In this process, h-BN particles are dispersed within a polymer matrix using techniques such as mechanical mixing or ultrasound. This process requires the choice of suitable solvents and the use of surfactants to improve particle dispersion[59].
- Solvent intercalation: In this technique, the polymer is intercalated between the h-BN sheets via a solution. The polymer solution is made to penetrate the layers of h-BN, where it intercalates between the sheets of the hexagonal boron nitride. This process improves the dispersion of the polymer within the h-BN matrix and achieves a uniform distribution of the h-BN particles within the nanocomposite[60]. The intercalation process can be carried out in several stages. For example, the polymer can be intercalated within the h-BN layers before its polymerization, during the synthesis of the polymer itself, or after the polymerization of the polymer, by means of solutions or dispersions in suitable solvents.
- Intercalation of polymer from solution with h-BN can be used to prepare nanocomposites with a wide range of polymers, such as polystyrene, polypropylene, polyamide, polyurethane, rubber and others. The properties of the nanocomposite can be modified by selecting the appropriate polymer and intercalation conditions. For example, the presence of h-BN can increase the stiffness, tensile strength, wear resistance and thermal stability of the nanocomposite[61].
- Exfoliation of polymer from solution: This is another technique used to prepare h-BN/polymer nanocomposites. In this technique, h-BN powder is dispersed in a polymer solution and then exfoliated using mechanical or chemical methods. The polymer intercalates between the h-BN layers during exfoliation, forming an h-BN/polymer nanocomposite [62]. The properties of the nanocomposite can be modified by varying the exfoliation conditions, such as exfoliation time, temperature, stirring speed, and polymer/h-BN ratio. Exfoliation of polymer with

h-BN can also be used to prepare nanocomposites with high thermal properties, for instance, by using thermosetting polymers such as polyurethanes and polyamides [63].

In general, the choice of the preparation technique depends on the required properties of the final material and on the characteristics of the h-BN particles used and the most employed solvent is water because of economic and safety reasons.

The last technique will be explored in this thesis work as it has been used for the preparation of CNF/h-BN nanocomposites.

1.8 Water-based Composites

In recent years, there has been a growing interest in water-based nanocomposites as a new frontier in the field of nanocomposites. The inspiration for their production comes from the brick-and-mortar structure of natural nacre [64]. This is a layered composite biomaterial, consists of 95% CaCO_3 microplatelets and 5% biopolymers. In this peculiar structure there is highly oriented structure in which the aragonite platelets are held together by soft polymers, resulting in improved mechanical properties such as higher stiffness and strength. Also guarantee heat conduction along the nanosheet layers, resulting in large in-plane thermal conductivity (**Figure 1.11**).

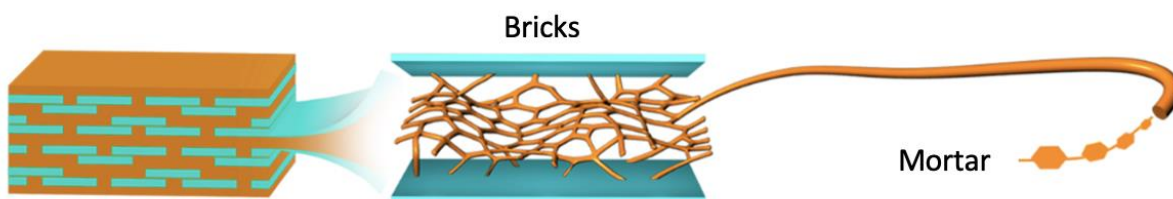


Figure 1.11 – Biomimetic Brick and Mortar Structure

These water-based composites are eco-friendly and have low toxicity compared to organic solvent-based composites, enhanced electrical conductivity and improved flame retardancy, making them highly desirable for various applications such as films, paints, and adhesives. The solubility or dispersibility of the polymer matrix in water is critical for the production of water-based nanocomposites, indeed cellulose, a natural polymer with high solubility in water, is frequently employed as the polymer matrix. The same concept is applied to creating a bio-inspired material where the h-BN nanosheets serve as the "bricks," and a polymer serves as the "mortar".

To produce water-based nanocomposites, polymer and h-BN is suspended in water. The resulting suspension can be processed in two ways, either by filtering it to produce thin films, or by freeze-drying it to obtain aerogels. Both types of materials exhibit superior mechanical properties and fire retardancy compared to the pure polymer [65].

In the journal article by Zeng X, et al. [66] is shown in detail a vacuum-filtration-induced self-assembly technique to produce thin BNNS/PVA water-based composite films. Hexagonal-Boron Nitride powders in water solution undergoes a sonication process to obtain BNNS. A polymer is dissolved in deionized water and then dropped into BNNS suspension. The mixture is sonicated and then filtered through a vacuum system equipped. The obtained wet paper is then dried at specific temperature.

Given the numerous advantages offered by this material, there is a desire to create a new composite that combines the best characteristics of its individual components. The aim of this thesis project is to design a process for producing thin films made from CNF and h-BN. This bio-based nanocomposite is composed entirely of natural and renewable resources, and it utilizes the presence of h-BN in CNF to enhance its mechanical properties and fire retardancy.

1.9 Research Aims and thesis structure

The present project of thesis aims to produce and study the characteristics of bio-based nanocomposites based on cellulose nanofibrils (obtained from wood) and hexagonal Boron Nitride, used to improve the fire-retardant properties of the neat material. Cellulose is an organic polymer that offers a renewable and natural alternative to fossil fuels. It is widely available and considered an almost limitless source of raw material for the increasing demand of environmentally friendly and biocompatible products. The objective is to produce a material with competitive properties compared to conventional materials and to analyze its fire retardancy behavior, since this aspect is seldom evaluated in literature.

The structure of the thesis is divided into two phases (**Figure 1.12**): the first one is related to experimental section of the research activity carried out at *KTH-Royal Institute of Technology* in Stockholm and the second one is related to research activity carried out at *Politecnico di Torino* in Alessandria campus.

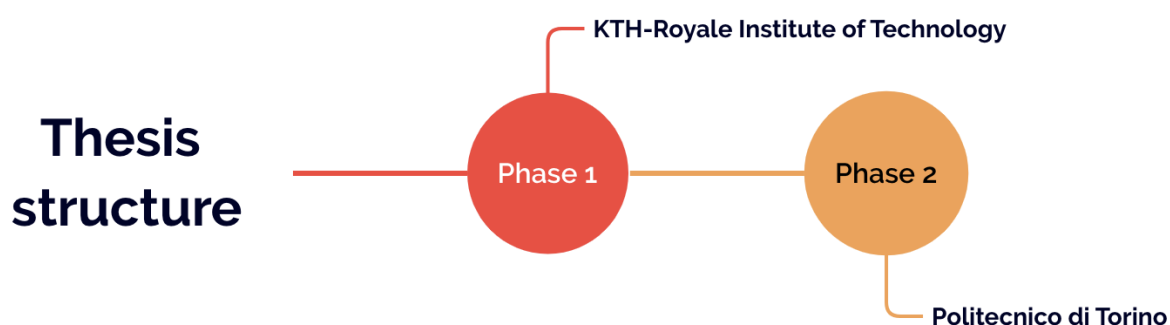


Figure 1.12 – Thesis Structure

This thesis project started with phase 1 at *KTH-Royal Institute of Technology* in Stockholm, with the research group of the *Wallenberg Wood Science Center*, where the preparation of TEMPO-CNF was carried out starting from cellulose pulp. Once all the preliminary preparation steps were completed, the preparation of h-BN/CNF nanocomposites was carried out, after an assessment of the conditions and process to be used for the correct production of films with different concentrations of boron nitride, respectively 20, 40, 60, 80% wt.

This thesis project continues with phase 2 in the laboratories of *Politecnico di Torino* in Alessandria, in order to characterize the mechanical, thermal stability and thermal conductivity, morphological and fire retardancy properties, correlating structure and property and compare the behavior of the material with and without Boron Nitride.

The experimental part of the thesis is divided as follows.

Chapter 2 provides the first part of experimental section of the thesis with the description of the research activity carried out at KTH in Stockholm: preparation of TEMPO-CNF and h-BN/CNF nanocomposites films production. Furthermore, the materials used in detail for the preparation of nanocellulose and h-BN/CNF-based films were also illustrated.

Chapter 3 provides the second part of experimental section of the thesis with the description of the research activity carried out at *Politecnico di Torino* in Alessandria campus: morphological characterization of the samples using SEM, spectroscopic analysis using FTIR, chemical characterization using TGA analysis, mechanical characterization using tensile tests, flammability and finally flame penetration tests.

Chapter 4 provides the conclusion of the thesis work with particular focus on results and discussions: process development, colloidal properties, morphology, chemical composition, flame retardancy behavior, flame penetration resistance and conductivity of samples. Furthermore, in addition, factors that may need attention in the future and future developments were also explained.

2 Materials and sample preparations

This chapter deals with all the experimental part carried out at the *KTH-Royal Institute of Technology* in Stockholm, with the research group of the Wallenberg Wood Science Center. It includes the synthesis of TEMPO-CNF, starting from cellulose pulp, followed by a series of steps such as pulp demineralization, washing, addition of TEMPO, addition of NaBr-based catalyst and NaClO-based oxidizing agent, subsequent treatment of the pulp with an acetate buffer and further washing. The process was completed with high-pressure micro fluidization to obtain TEMPO-CNF.

The preparation of h-BN/CNF nanocomposites films of 50-micron thickness is also discussed. Preliminary calculations were carried out to determine the right weight amounts of materials to be used at different percentages of h-BN, considering dimensional constraints and the concentration of TEMPO-CNF produced. Then, the actual preparation started with weighing the components, sonication of the solutions, centrifugation of the h-BN/CNF solutions, separation of the supernatant phase from the solid phase of higher density, vacuum filtration, and finally drying of the wet samples to obtain the final film.

2.1 Materials

The CNF suspension was prepared starting from bleached softwood sulfite pulp fibers, provided by Nordic Paper Seffle AB, Saffle, Sweden with 14 wt% hemicellulose and <1% lignin. These fibers can be disintegrated into hydrocolloidal particles, as will be shown in the following paragraph before undergoing the high pressure micro fluidification process to obtain TEMPO - CNF.

Commercial hexagonal Boron Nitride powder with purity of 98% was used as dispersion for the preparation of h-BN/CNF film nanocomposites. It was purchased from GRAPHENE SUPERMARKET®. It is an excellent brick in bio-based nanocomposites, due to the peculiarities discussed in previous paragraphs.

Hydrochloric acid 37% ($\text{HCl}_{(\text{aq})}$) with molecular weight of 36,46 was used for the preparation of TEMPO-CNF to do the demineralization of water and pulp fibers dispersion, as well will be showed in the following paragraph. It was provided by Fisher Scientifics, Bishop Meadow Rd. Loughborough, UK.

TEMPO (98%), provided by Sigma-Aldrich Co. LLC, St. Luis, United States, was used to oxidize cellulose nanofibers in water, specifically for regioselective conversion of C6 primary hydroxyls to carboxylate groups.

The process involved incorporating catalytic amounts of TEMPO and sodium bromide NaBr ($\geq 99\%$), provided by Sigma-Aldrich Co. LLC., St. Luis, United States), into solutions with pH 11, and then initiating oxidation with sodium hypochlorite 14% (NaClO), provided

by VWR International, Milano, Italy, as the primary oxidant. NaOH 2M (provided by Sigma-Aldrich Co., St. Luis, United States) was also added to stabilize the pH.

The Acetate buffer is used to maintain the pH of the solution in a stable and tolerable range for CNFs during the oxidation process. In particular, the acetate buffer is used to keep the pH of the solution around 5, to guarantee the efficacy of the oxidation but also to protect the CNFs from degradation. It was made by adding 18.3 mL of Acetic acid ($\geq 99\%$) with the chemical formula CH_3COOH and 27 g of Sodium acetate with chemical formula $\text{C}_2\text{H}_3\text{NaO}_2$ ($\geq 99\%$) (both provided by Sigma-Aldrich Co. LLC, St. Luis, United States) in Deionized Water (2 L). The solution was stirred magnetically (298 rpm) at pH 4.8 until the bubbles disappeared.

Sodium chlorite with chemical formula NaClO_2 (80%) has been used when cellulose pulp is treated with acetate buffer as a bleaching agent. It was provided by Sigma-Aldrich Co. LLC, St. Luis, United States.

2.2 Samples and dispersions preparation

2.2.1 TEMPO-CNF production

CNF dispersion was prepared according to the work by Lengwan Li et al [67]. First of all, CNF suspension was prepared by using TEMPO-oxidation developed by Saito et al. In the TEMPO-CNF production, several steps are involved, which are listed below in **Figure 2.1** and will be explained in detail:

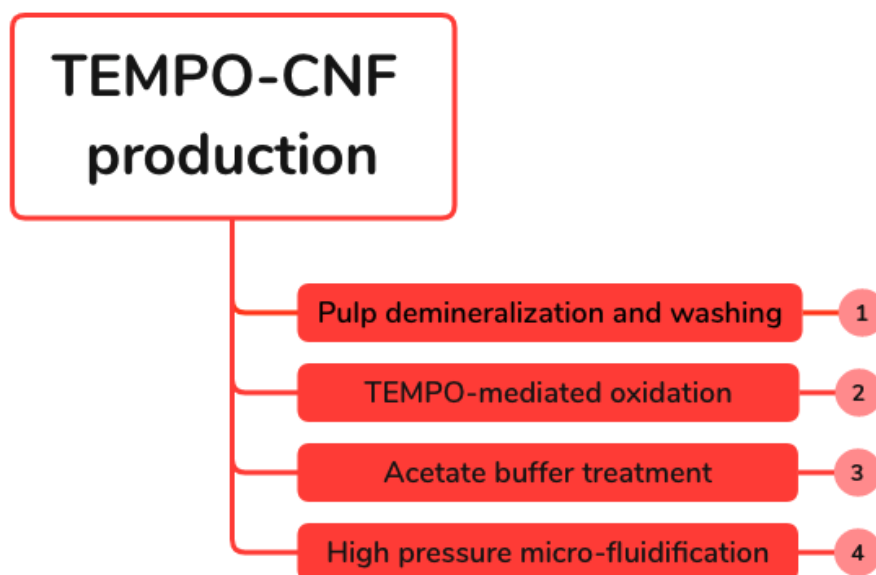


Figure 2.1 – TEMPO-CNF production steps

2.2.1.1 Pulp demineralization and washing

The pulp (20g by dry weight) was demineralized by magnetic stirring (Magnetic stirrers – fisher brand – Isotemp®) in a diluted HCl and DI solution at pH 2.5 for 2 h at 25°C.

After this treatment, the dispersion was three times washed with deionized water by vacuum filtration with PTFE filter (as shown in **Figure 2.2**). Then, the suspension was suspended in 2000 mL of deionized water 18.2 MΩ, ready for TEMPO-mediated oxidation.

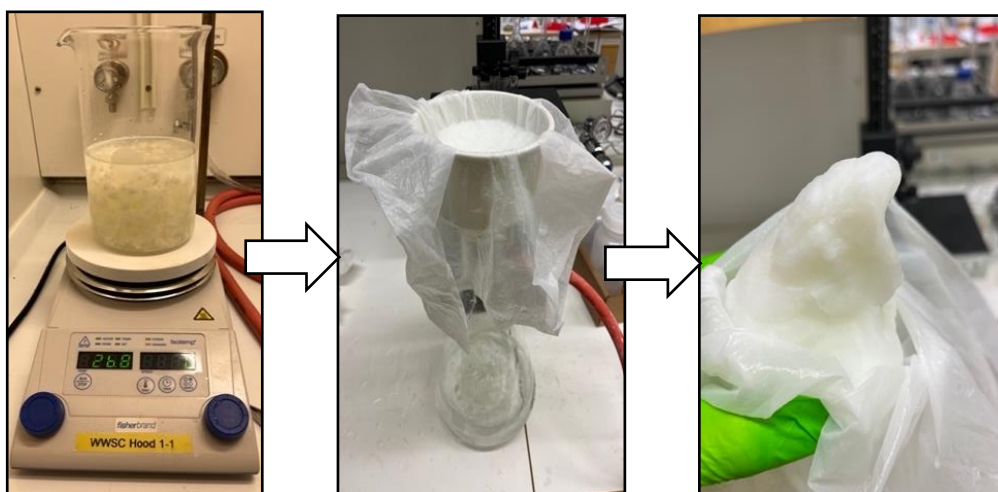


Figure 2.2 – Demineralization of cellulose pulp with a diluted HCl and DI solution by magnetic stirring (on the left) and DI washing of pulp after treatment (on the right).

2.2.1.2 TEMPO-mediated oxidation

For this step, catalytic amounts of TEMPO (0.32 g) and NaBr (2 g) were dissolved in CNF suspension that was subjected to mechanical agitation (as shown in **Figure 2.3**), and oxidation was started by the addition of NaClO (60 mL) as oxidant agent.



Figure 2.3 – TEMPO-mediated oxidation with pH monitoring

According to the scheme shown in **Figure 2.4** [69], the C6 primary hydroxyls of cellulose will be oxidized to C6 carboxylate groups by TEMPO/NaBr/NaClO oxidation in water at pH 11. The oxidation process can be monitored from NaOH consumption, which is added continuously to the reaction mixture to maintain the pH at 11 during the oxidation. After 1h, the solution was seven times washed with deionized water 18.2 M Ω by vacuum filtration with PTFE filter to remove TEMPO residue.

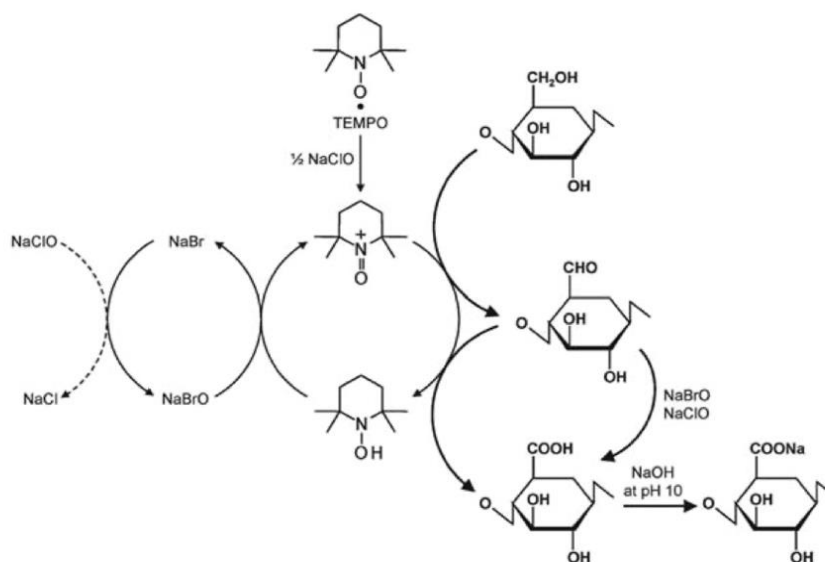
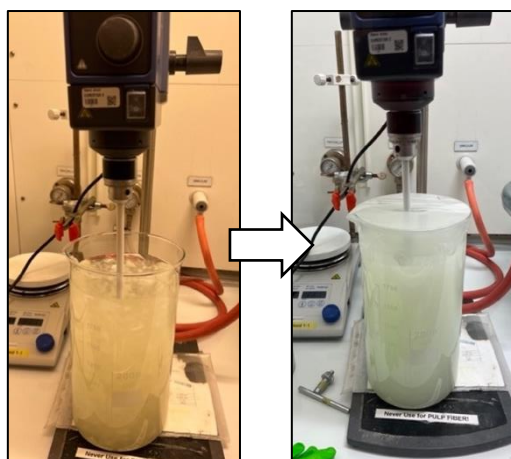


Figure 2.4 – Regioselective oxidation of C6 primary hydroxyls of cellulose to C6 carboxylate groups by TEMPO/NaBr/NaClO oxidation in water at pH 10–11.

2.2.1.3 Acetate buffer treatment

After this treatment, the oxidated pulp was suspended in deionized water 18.2 M Ω (provided by Milli - Q, Millipore system). and further treated in an acetate buffer at pH 4.8 for 24 h with 1 % of NaClO_2 (20 g) under mechanical stirring (IKA® EUROSTAR 20 digital stand mixer). The becher was also covered with parafilm because the solution is highly volatile as shown in **Figure 2.5**. After this treatment, the solution was washed seven times with deionized water 18.2 M Ω with PTFE filter.



***Figure 2.5** – Oxidated pulp treated with acetate buffer and Sodium chlorite for 24 h*

2.2.1.4 High pressure micro-fluidification

After washing, the pulp fibers were subjected to a high-pressure microfluidizer (Microfluidics Corp, Newton, Massachusetts, USA) (as shown in **Figure 2.6**).

Before inserting the pulp inside the microfluidizer, 5 liters of deionized water was inserted inside the hopper to clean the ducts. The pulp was subjected to high pressure (1600 bar) passing once through 400-200 μm channels and twice through 200-100 μm channels to produce a transparent TEMPO-CNF colloid (as shown in **Figure 2.7**).



Figure 2.6 – Microfluidics Corp, Newton, Massachusetts, USA

The transition from two channels of different diameters is used to switch from macro to micro fluidification.



Figure 2.7 – TEMPO-CNF

To realized TEMPO-CNF/h-BN nanocomposites films it was necessary to calculate the dry concentration of the TEMPO-CNF achieved. It was used an electric analyzer (METTLER TOLEDO HB43-S Halogen). The calculated dry concentration of TEMPO-CNF was 0.75 wt%.

2.3 h-BN/CNF films preparation

The goal of the activities part did at KTH Royal Institute of Technology was to find correct parameters to prepare h-BN/CNF nanocomposite films with a thickness of 0.05 mm at different percentage of h-BN: 20, 40, 60, 80 % wt (**Table 2.1**). At least 3 samples of each composition were obtained.

Table 2.1 – Nomenclature used for h-bn/CNF nanocomposites films

Nomenclature	Concentrations [% wt]
20% h-BN/CNF	20 % wt h-BN 80 % wt CNF
40% h-BN/CNF	40 % wt h-BN 60 % wt CNF
60% h-BN/CNF	60 % wt h-BN 40 % wt CNF
80% h-BN/CNF	80 % wt h-BN 20 % wt CNF

The sketch of paper-related filtration process of h-BN/CNF films, which will be explained in detail below, as shown in **Figure 2.8**.

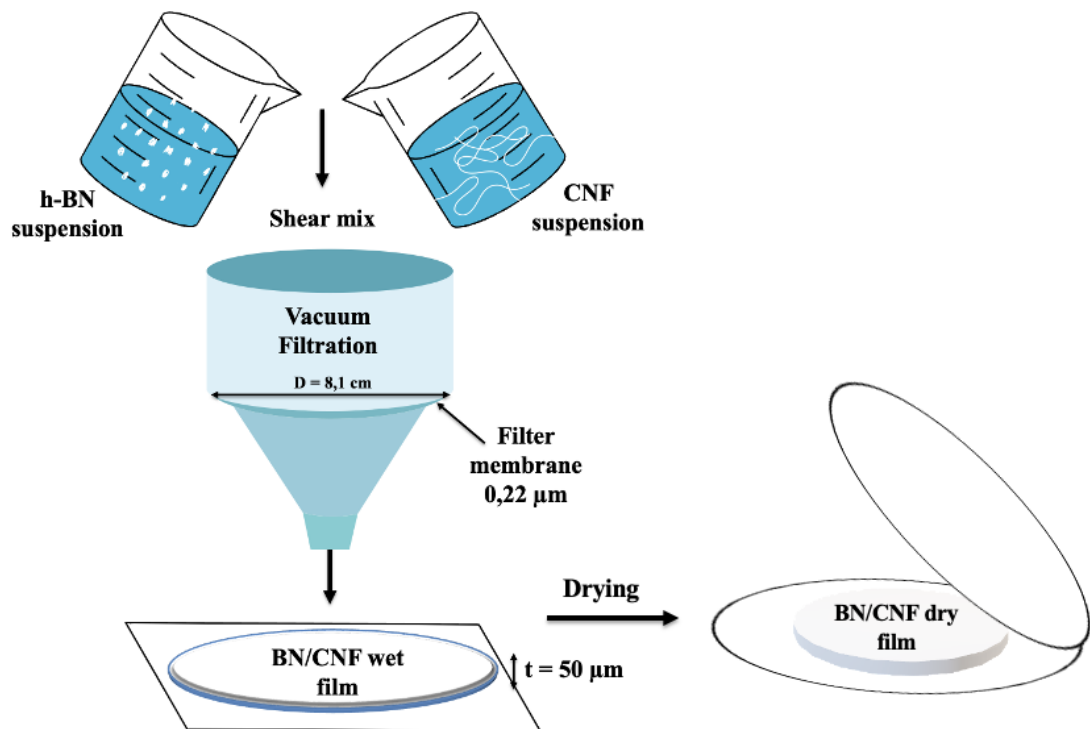


Figure 2.8 – Preparation process of h-BN/CNF films

2.3.1 Preliminary calculations

Once the TEMPO-CNF was made, preliminary calculations were carried out to determine the right weight amounts of materials to be used at different percentages of h-BN, considering dimensional constraints and the concentration of TEMPO-CNF produced multiple times.

Considering the h-BN density:

$$\rho_{\text{BN}} = 2.1 \frac{\text{g}}{\text{cm}^3} \quad (2,1)$$

the CNF density:

$$\rho_{\text{CNF}} = 1.6 \frac{\text{g}}{\text{cm}^3} \quad (2,2)$$

the film thickness chosen:

$$t = 50 \mu\text{m} \quad (2,3)$$

the setup diameter used:

$$d = 8.1 \text{ cm} \quad (2,4)$$

and the total volume V_{TOT} :

$$V_{\text{TOT}} = \pi r^2 \cdot h = \pi(4.05)^2 \cdot (50 \cdot 10^{-4}) = 0.26 \text{ cm}^3 \quad (2,5)$$

calculations were performed for all the different percentages:

- 20% h-BN

Considering the % of the components and their densities, the total density ρ_{TOT} has been calculated:

$$\begin{aligned}\rho_{TOT} &= (\rho_{CNF} \cdot \%_{CNF}) + (\rho_{BN} \cdot \%_{BN}) = \\ &= \left(1.6 \frac{\text{g}}{\text{cm}^3} \cdot 0.8\right) + \left(2.1 \frac{\text{g}}{\text{cm}^3} \cdot 0.2\right) = 1.69 \frac{\text{g}}{\text{cm}^3}\end{aligned}\quad (2,6)$$

Considering the total volume and the total density of the film, the total mass has been calculated:

$$m_{TOT} = \rho_{TOT} \cdot V_{TOT} = 1.69 \frac{\text{g}}{\text{cm}^3} \cdot 0.26 \text{ cm}^3 = 0.435 \text{ g} = 435 \text{ mg} \quad (2,7)$$

Consequently, m_{BN} and m_{CNF} (dry content) has been calculated:

$$m_{BN} = m_{TOT} \cdot \%_{BN} = 0.435 \text{ g} \cdot 0.2 = 0.087 \text{ g} \quad (2,8)$$

$$m_{CNF(dry)} = m_{TOT} \cdot \%_{CNF} = 0.435 \text{ g} \cdot 0.8 = 0.348 \text{ g} = 348 \text{ mg} \quad (2,9)$$

Finally, considering the TEMPO/CNF concentration and the dry CNF mass, the wet CNF mass has been calculated:

$$m_{CNF} = \frac{m_{TOT}}{C_{CNF}} = \frac{348 \text{ mg}}{0.75\%} = 46400 \text{ mg} = 46.4 \text{ g} \quad (2,10)$$

Considering the total mass, the amount of water to be used was calculated:

$$\text{Water content} = 200 \text{ mL} \quad (2,11)$$

- 40% h-BN

Considering the % of the components and their densities, the total density ρ_{TOT} has been calculated:

$$\rho_{TOT} = (\rho_{CNF} \cdot \%_{CNF}) + (\rho_{BN} \cdot \%_{BN}) =$$

$$= \left(1.6 \frac{\text{g}}{\text{cm}^3} \cdot 0.6 \right) + \left(2.1 \frac{\text{g}}{\text{cm}^3} \cdot 0.4 \right) = 1.8 \frac{\text{g}}{\text{cm}^3} \quad (2,12)$$

Considering the total volume and the total density of the film, the total mass has been calculated:

$$m_{\text{TOT}} = \rho_{\text{TOT}} \cdot V_{\text{TOT}} = 1.8 \frac{\text{g}}{\text{cm}^3} \cdot 0.26 \text{ cm}^3 = 0.463 \text{ g} = 463 \text{ mg} \quad (2,13)$$

Consequently, m_{BN} and m_{CNF} (dry content) has been calculated:

$$m_{\text{BN}} = m_{\text{TOT}} \cdot \%_{\text{BN}} = 0.463 \text{ g} \cdot 0.4 = 0.185 \text{ g} \quad (2,14)$$

$$m_{\text{CNF(dry)}} = m_{\text{TOT}} \cdot \%_{\text{CNF}} = 0.463 \text{ g} \cdot 0.6 = 0.258 \text{ g} = 258 \text{ mg} \quad (2,15)$$

Finally, considering the TEMPO/CNF concentration and the dry CNF mass, the wet CNF mass has been calculated:

$$m_{\text{CNF}} = \frac{m_{\text{TOT}}}{C_{\text{CNF}}} = \frac{258 \text{ mg}}{0.75\%} = 33947.4 \text{ mg} = 33.95 \text{ g} \quad (2,16)$$

Considering the total mass, the amount of water to be used was calculated:

$$\text{Water content} = 230 \text{ mL} \quad (2,17)$$

- 60% h-BN

Considering the % of the components and their densities, the total density ρ_{TOT} has been calculated:

$$\rho_{\text{TOT}} = (\rho_{\text{CNF}} \cdot \%_{\text{CNF}}) + (\rho_{\text{BN}} \cdot \%_{\text{BN}}) =$$

$$= \left(1.6 \frac{\text{g}}{\text{cm}^3} \cdot 0.4 \right) + \left(2.1 \frac{\text{g}}{\text{cm}^3} \cdot 0.6 \right) = 1.9 \frac{\text{g}}{\text{cm}^3} \quad (2,18)$$

Considering the total volume and the total density of the film, the total mass has been calculated:

$$m_{\text{TOT}} = \rho_{\text{TOT}} \cdot V_{\text{TOT}} = 1.9 \frac{\text{g}}{\text{cm}^3} \cdot 0.26 \text{ cm}^3 = 0.489 \text{ g} = 489 \text{ mg} \quad (2,19)$$

Consequently, m_{BN} and m_{CNF} (dry content) has been calculated:

$$m_{\text{BN}} = m_{\text{TOT}} \cdot \%_{\text{BN}} = 0.489 \text{ g} \cdot 0.6 = 0.293 \text{ g} \quad (2,20)$$

$$m_{\text{CNF(dry)}} = m_{\text{TOT}} \cdot \%_{\text{CNF}} = 0.489 \text{ g} \cdot 0.4 = 0.1956 \text{ g} = 195.6 \text{ mg} \quad (2,21)$$

Finally, considering the TEMPO/CNF concentration and the dry CNF mass, the wet CNF mass has been calculated:

$$m_{\text{CNF}} = \frac{m_{\text{TOT}}}{C_{\text{CNF}}} = \frac{195.6 \text{ mg}}{0.75\%} = 25736.8 \text{ mg} = 25.7 \text{ g} \quad (2,22)$$

Considering the total mass, the amount of water to be used was calculated:

$$\text{Water content} = 250 \text{ mL} \quad (2,23)$$

- 80% h-BN

Considering the % of the components and their densities, the total density ρ_{TOT} has been calculated:

$$\rho_{\text{TOT}} = (\rho_{\text{CNF}} \cdot \%_{\text{CNF}}) + (\rho_{\text{BN}} \cdot \%_{\text{BN}}) =$$

$$= \left(1.6 \frac{\text{g}}{\text{cm}^3} \cdot 0.2 \right) + \left(2.1 \frac{\text{g}}{\text{cm}^3} \cdot 0.8 \right) = 2 \frac{\text{g}}{\text{cm}^3} \quad (2,24)$$

Considering the total volume and the total density of the film, the total mass has been calculated:

$$m_{\text{TOT}} = \rho_{\text{TOT}} \cdot V_{\text{TOT}} = 2 \frac{\text{g}}{\text{cm}^3} \cdot 0.26 \text{ cm}^3 = 0.515 \text{ g} = 515 \text{ mg} \quad (2,25)$$

Consequently, m_{BN} and m_{CNF} (dry content) has been calculated:

$$m_{\text{BN}} = m_{\text{TOT}} \cdot \%_{\text{BN}} = 0.515 \text{ g} \cdot 0.8 = 0.412 \text{ g} \quad (2,26)$$

$$m_{\text{CNF(dry)}} = m_{\text{TOT}} \cdot \%_{\text{CNF}} = 0.515 \text{ g} \cdot 0.2 = 0.103 \text{ g} = 103 \text{ mg} \quad (2,27)$$

Finally, considering the TEMPO/CNF concentration and the dry CNF mass, the wet CNF mass has been calculated:

$$m_{\text{CNF}} = \frac{m_{\text{TOT}}}{C_{\text{CNF}}} = \frac{103 \text{ mg}}{0.75\%} = 13552.6 \text{ mg} = 13.5 \text{ g} \quad (2,28)$$

Considering the total mass, the amount of water to be used was calculated:

$$\text{Water content} = 260 \text{ mL} \quad (2,29)$$

The results obtained are summarized in the table below (**Table 2.2**).

Table 2.2 – Parameters used for BN/CNF nanocomposites films

Parameters	20% BN/CNF	40% BN/CNF	60% BN/CNF	80% BN/CNF
$\rho_{TOT} \left[\frac{g}{cm^3} \right]$	1.69	1.8	1.9	2
$m_{TOT} [mg]$	435	463	489	515
$m_{BN} [mg]$	0.087	0.185	0.293	0.412
$m_{CNF(dry)} [mg]$	348	258	195.6	103
$m_{CNF} [mg]$	46.4	33.95	25.7	13.5
Water content [mL]	200	230	250	260

After preliminary calculations the amount of h-BN powders, CNF and water has been weighted with analytical balance (METTLER Toledo AE-163). Then, TEMPO – CNF and h-BN was added into deionized water 18.2 M Ω separately to have two different dispersions.

2.3.2 Sonication

The dispersions were sonicated (as shown in **Figure 2.9**) with Ultrasonic homogenizer Vibracell VCX 750 with flat tip probe 2 minutes for solution, to obtained h-BN and CNF exfoliated solutions. Sequentially they are put together inside a becher for the next step.



Figure 2.9 – Sonication of h-BN and CNF solutions

2.3.3 Centrifugation

After sonication the h-BN/CNF solution was equally divided into test tubes to perform the centrifugation. Centrifugation ensures the separation of supernatant phase from solid phase. The bench centrifuge used for this step was ROTINA 420 – Hettich ® (as shown in **Figure 2.10**). It is worth emphasizing that test tubes were arranged equally to balance the weight during centrifugation process. Suspensions were treated 10 minutes at $T=35^{\circ}\text{C}$, 3000 rpm, 9 to 5 of ramp scale.



Figure 2.10 – ROTINA 420 centrifuge

After centrifugation a supernatant phase has been separated from solid phase one tube test a time with graduated pipette. Then, the supernatant phase was kept for the next step of filtration, while the aggregation in the bottom of the test tube was removed.

2.3.4 Vacuum filtration

The co-dispersions were then vacuum filtered by using a fritted glass setup (as shown in **Figure 2.11**) and PVDF hydrophilic filter membrane (DURAPORE® membrane filters) with pore size of 0.22 micron on the glass support base.



Figure 2.11 –Vacuum filtration with fritted glass setup

The time of filtration of h-BN/TEMPO CNF co-dispersions was about 12 h but filtration time increases with h-BN content. The 80% of h-BN sample has the longest filtration time (~ 16 h) depending on the thickness of the final nanofilm, to the effective dispersion, and content of h-BN in the sample. After filtration, the wet films were carefully peeled off from the filtration membrane.

2.3.5 Drying

The obtained wet samples were put under a Teflon filter and then, the samples were put between two cover sheets before drying, to obtain dry final samples.

To perform a drying film was used a Sheet Former Rapid-Köthen (RL-ASF-A) as shown in **Figure 2.12**.



Figure 2.12 – Sheet Former Rapid-Köthen (RL-ASF-A)

This machine allows to reach very low pressures thanks to the vacuum pumps present. The pumps of the machine working to reach a vacuum pressure desired.

A temperature of 93 °C has been set. The other process parameters, such as pressure and time, were influenced by the % of boron nitride added to the sample, as shown in the table (**Table 2.3**). For the 20% h-BN samples and 40% h-BN samples, a pressure of 0 bar was used for 25 minutes. Instead, for the 60% h-BN samples, a pressure of 0 bar was used for 5 minutes, then increased to 0,6 for another 25 minutes. Also, for the 80% h-BN samples, a pressure of 0 bar was used for 10 minutes, then increased to 0,4 for another 25 minutes.

Table 2.3 – Operative parameters used to dry samples

Samples	1st Time [s]	2nd Pressure [bar]	2nd Time [s]
20% BN/CNF	25	/	/
40% BN/CNF	25	/	/
60% BN/CNF	5	0,6	25
80% BN/CNF	10	0,4	25

To find the right process parameters several tests were carried out. In particular, it was difficult to find the right compromise between time and pressure for the 60 and 80% samples.

As reported in **Figure 2.13** below, using the same operating parameters of the other samples at 20% and 40% of h-BN, it led to breakage.



Figure 2.13 –BN/CNF 80% broken dry sample

To measure the right thickness of the samples was used a digital gauge ABS AOS – Mitutoyo.

The figure below (**Figure 2.14**) shows two dry samples respectively at 20 and 60% wt of h-BN.

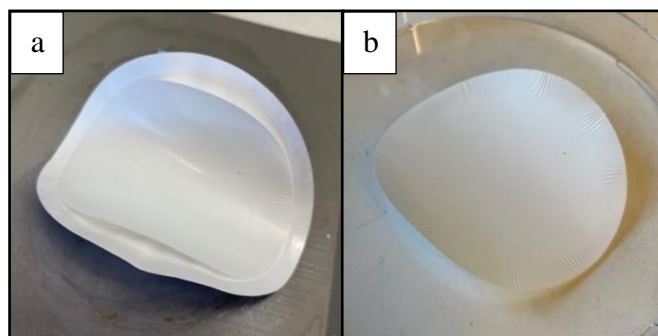


Figure 2.14 –BN/CNF 20% dry sample (a), BN/CNF 60% dry sample (b)

The 80% sample immediately showed a less transparent and more rigid appearance.

2.3.5.1 Operating conditions

In summary, the main production conditions selected for the films vary depending on the amount of added boron nitride, except for the temperature, which was set at 93°C for all sample types.

- For the 20% h-BN/CNF and 40% h-BN/CNF samples, a pressure of 0 bar was applied for 25 minutes.

- For the 60% h-BN/CNF samples, a pressure of 0 bar was applied for 5 minutes, then increased to 0.6 bar for an additional 25 minutes.

- For the 80% h-BN/CNF samples, a pressure of 0 bar was applied for 10 minutes, then increased to 0.4 bar for an additional 25 minutes.

3 Samples characterization methods

This chapter deals with all the experimental part carried out at *Politecnico di Torino* in Alessandria campus.

To characterize the obtained samples, the following analyses showed in the graph (**Figure 3.1**) were performed:

- Morphological analysis: SEM with EDS, to do superficial morphological analysis of h-BN/CNF nanocomposites;
- Thermal analysis: TGA, to do chemical characterization according to mass change profiles and to study the thermal stability and behavior of nanocomposites obtained during temperature increase;
- Spectroscopy analysis: Fourier Transform Infrared in ATR mode (FTIR-ATR) to analyze the chemical and molecular characteristics of h-BN/CNF nanocomposite films;
- Mechanical analysis: tensile tests to verify the tensile behavior of the nanocomposite films;
- Fire behavior analysis: UL-94 in vertical configuration for flammability tests and flame penetration tests with the aid of a thermal camera;

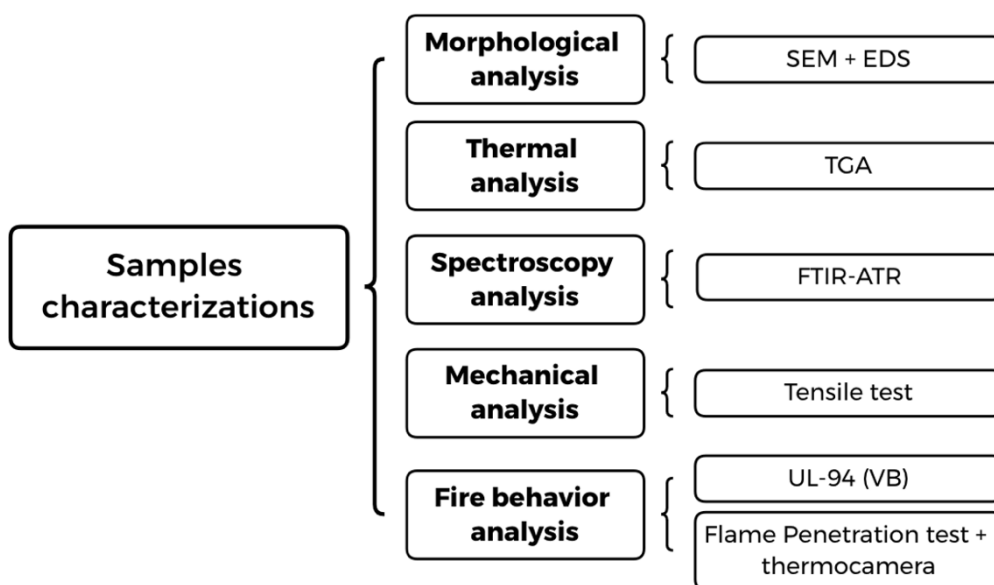


Figure 3.1—Samples characterization used in the thesis work

3.1 Spectroscopy analysis

3.1.1 Fourier Transform Infrared Spectroscopy analysis (FTIR)

Infrared spectroscopy (IR) is an absorption spectroscopic technique that provides information about the chemical bonds and the vibrational modes of the functional groups in the molecules of material. The spectrophotometer used for the h-BN/CNF nanocomposite films produced at the KTH Royal Institute of Technology is the FTIR Spectrometer Frontier produced by Perkin Elmer (as shown in **Figure 3.2**).



Figure 3.2 – FTIR Spectrometer Frontier in ATR mode

From this spectroscopic analysis, an infrared spectrum is obtained where the x-axis represents frequencies expressed in wavenumber, which is the number of wave cycles per centimeter. The y-axis represents the percentage of transmittance or absorbance.

In this thesis work, the Attenuated Total Reflectance (ATR) technique was employed on the h-BN/CNF samples. In ATR mode, the sample has been brought into contact with a high refractive index diamond crystal.

The spectra were recorded at ambient temperature in the range of $(4000-700) \text{ cm}^{-1}$ with 16 scans (resolution 4 cm^{-1}).

3.2 Morphological Analysis

3.2.1 Scanning electron microscopy (SEM) – Energy Dispersive X-ray Spectroscopy (EDS)

The surface morphological characterization of h-BN/CNF nanocomposite films was performed using an EVO 15 Scanning Electron Microscope produced by Zeiss with an electron beam voltage of 20 kV. This analysis was coupled with energy-dispersive X-ray spectroscopy (EDS), that utilizes X-rays emitted from the surface when it is struck by an electron beam, to obtaining compositional information. SEM microscopy was crucial for evaluating the distribution and dispersion of the charge within the CNF matrix. The EDS microprobe used for this thesis work is the ULTIM MAX 40 EDS microprobe by OXFORD. Before conducting the analysis, it is necessary to prepare the samples placing it on the pin stub using double-sided carbon tape. When dealing with non-conductive fibers, prior to analysis, it is necessary to proceed with metallization, whereby the samples are coated with a thin layer of gold.

For the h-BN/CNF samples, the respective magnifications used were: 500X, 1.00KX, 2.50KX, 5.00KX, 10.00KX, 20.00KX, 50.00KX, 75.00KX.

3.3 Thermal analysis

3.3.1 Thermogravimetric Analysis (TGA)

TGA (Thermogravimetric Analysis) is a technique used to evaluate the thermal stability and the reactivity of materials measuring mass undergoing degradation and the profile of weight loss.

The result of the analysis is expressed through a thermogram, where the temperature or time is plotted on the x-axis, and the percentage or absolute value of mass change is plotted on the y-axis.

In this study, the Discovery TGA by TA Instrument was used to investigate how the preparation for h-BN/CNF films at different h-BN concentrations can influence the material's degradation process. This analysis also allowed for the identification and quantification of the h-BN charge present, which was qualitatively analyzed using FTIR technology.

Specifically, the samples (approximately 10 ± 1 mg) are placed in an alumina crucible under a controlled atmosphere and subjected to a heating ramp of $10^\circ\text{C}/\text{min}$ from 100°C until reaching 800°C , in both inert (N_2) and oxidative atmospheres (Air). During the test, a highly sensitive balance measures the weight changes and generates the test output, which is a curve of weight loss [%] versus temperature [$^\circ\text{C}$]. From this curve, the residual value at the end of the test can be evaluated.

The test was performed on h-BN powders and net CNF sample and also on h-BN/CNF samples with different percentage of h-BN: 20, 40, 60, 80 % wt under either nitrogen or air conditions.

3.4 Mechanical Analysis

3.4.1 Tensile test

The Instron 5966 dynamometer (**Figure 3.3**) was used to perform tensile tests on the h-BN/CNF samples produced at the KTH Royal Institute of Technology. 4 rectangular specimens for each composition with sides measuring 50x10 mm, and a thickness of 0,05 mm, were obtained from the native circular sample with an initial diameter of 81 mm by mechanical manual cutting. Tensile test is indeed a destructive test, and the samples cannot be reused after the test is conducted.



Figure 3.3 – Instron 5966 dynamometer

This instrument consists of an upper movable crosshead and a lower fixed crosshead. The curves resulting from this mechanical analysis show the relationship between stress and strain. The software associated with the instrument provides output of stress-strain curves from which it is possible to derive elastic modulus (E) in MPa, fracture strain (ϵ_f) in %, and maximum tensile stress (σ_{max}) in MPa.

Before performing the test, the faces of the specimens were cleaned with ethanol to prevent them from slipping in the clamps and compromising the test. In order to determine the optimal process parameters, preliminary tests were conducted. The speed of the movable crosshead was set to 1mm/min for obtaining the most accurate elastic modulus. Initially, a clamping pressure of 3 bar was set, but it was later reduced to 1 bar as the sample fractures were occurring within the clamps, which invalidated the test.

Once the sample was positioned in the two clamps, before starting the test, a preload step was set to ensure that the specimen was properly aligned and positioned for testing. This preload step allowed the sample to settle into the optimal configuration.

The process parameters are summarized in **Table 3.1**.

***Table 3.1** – Process parameters of tensile test with dynamometer*

Parameters	Value
Preload [N]	0.2
Velocity ramp [mm/min]	1
Usable range [mm]	30
Clamping pressure [bar]	1

3.5 Fire behavior analysis

3.5.1 UL-94 flammability test

The UL-94 test evaluates the ability to resist flame propagation, simulating conditions of an initial fire, and allows for the evaluation of ignition time, flame propagation velocity, and the presence of glowing droplets after flame extinction.

Given the small size of the samples, a modified procedure derived from the UL 94 test in horizontal burning mode (HB) was used to investigate the fire behavior of the materials. Therefore, only certain requirements of the ASTM D 5132 standard were followed, including preconditioning, type, and duration of flame application.

h-BN/CNF specimens (3 for each composition) with sides measuring 50x10 mm, and a thickness of 0,05 mm were preconditioned in a climatic chamber for 48 h at $23\pm2^{\circ}\text{C}$ and $50\pm1\%$ relative humidity. The test consists in a single application of a 20 mm blue methane flame at 45° angle for a duration of 6 seconds. The specimen is also rotated 45° about its axis relative to the horizontal plane.

This test is less severe than the vertical burning (VB) mode. The used parameters are listed in **Table 3.2** and the experimental setup is shown in **Figure 3.4**.

Table 3.2 – *Used parameters for UL-94 flammability test*

Parameters	Value
Flame type	Blue methane
Flame length [mm]	20
Application time [s]	6
Preconditioned time [h]	48
Preconditioned temperature [°C]	23±2
Preconditioned relative humidity [%]	50±1



Figure 3.4 – *Experimental setup of UL-94 flammability test*

3.5.2 Flame penetration test

A flame penetration test was performed on a h-BN/CNF samples (50 x 50 x 0,05 mm³) to assess the resistance to penetration of a small flame (150W).

The test involves applying a high-powered butane flame torch at a distance from the surface of 100 mm with a flame pointed at the center of the specimen. It allows for a constant flame temperature of around 750 °C and direct contact with the surface of the sample. The flame length was 25 mm.

The setup involves placing the sample between two steel frames. They are inserted into a refractory cement frame, inside of which there is a layer of glass wool (thermal insulator), in order to isolate the sample from the metal frame.

By using two thermocouples (Stainless steel sheathed K-type; 1 mm diameter) placed into contact with the sample and at a certain height, it is possible to register the temperature profiles of both sides of our sample: the side exposed to the flame and the unexposed backside. The lower the temperature of the exposed side, the higher the fire resistance. It is a highly demanding test for the material, as the sample can either burn and immediately collapse or form a layer of char that prevents heat from propagating to the backside.

The test is carried out until complete perforation of the sample from one side to other, and the time was recorded. A schematic diagram of the experimental setup for flame penetration is shown in the **Figure 3.5**.

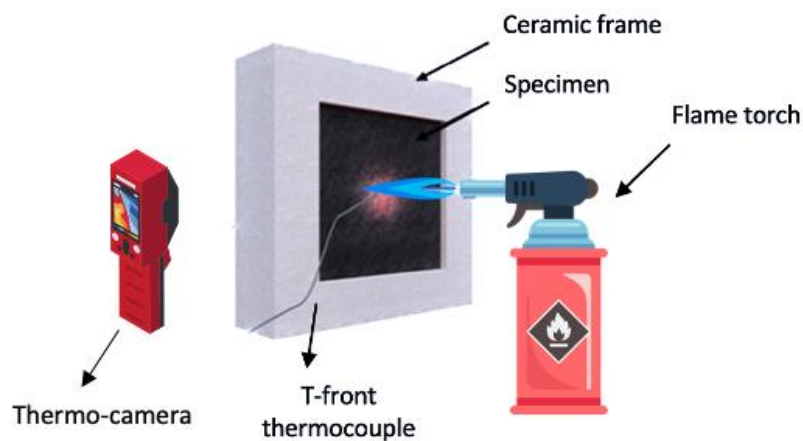


Figure 3.5 – Experimental setup of Flame penetration test

A thermal camera, specifically the BT-TC8 device, was also used to evaluate the behavior of the backside of the sample after the flame application.

The PicoLog software was used to record the temperature variation over time.

As flammability test, the samples were preconditioned for 48 hours in a conditioning chamber at a controlled temperature and humidity. The samples were removed prior to starting the test.

4 Results and discussion

4.1 Characterization of h-BN/CNF nanocomposite films

In this chapter, the experimental results obtained from laboratory tests on h-BN/CNF nano-composite films are presented and discussed. The purpose of this section is to compare the properties of the net TEMPO-CNF film with the h-BN/CNF film at various percentages, aiming to understand which formulation is optimal in terms of colloidal, chemical, morphological, mechanical, thermal and conductivity properties and flame retardancy behavior. In particular, the flammability behavior of CNF is evaluated as the percentage of h-BN added varies, in order to clarify whether the presence of boron nitride enhances flame retardant properties or not.

4.1.1 Stability dispersions

The production of h-BN/TOCN films was made varying the concentration of boron nitride. The surface of h-BN is negatively charged and is dispersed in water solution through sonication treatment. This process aims to achieve a uniform dispersion of h-BN nanoparticles. Similarly, the TOCN also has a negative charge, which enhances electrostatic repulsion between the exfoliated h-BN nanoparticles within the colloid. This repulsion should help in improving the dispersion of h-BN within the cellulose fibril matrix.

The h-BN/CNF films were prepared using a paper-filtration process, as explained in Chapter 2 - Materials and Sample Preparations and showed in **Figure 2.7**. The dispersions of h-BN/CNF appeared whitish in color, due to the boron nitride powder. These dispersions exhibited relatively good stability (**Figure 4.1**), although some sedimentation occurred after 10 days.

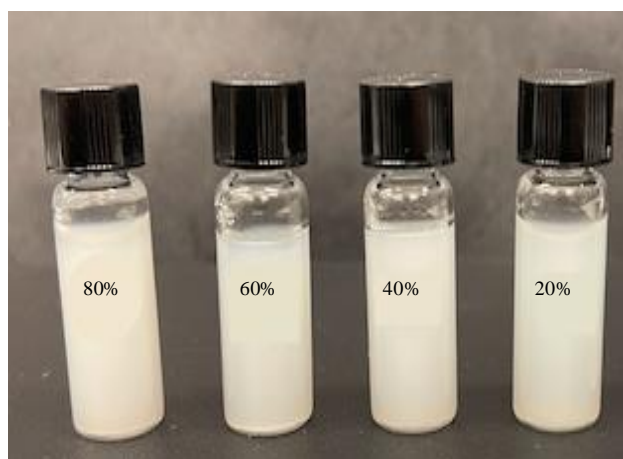


Figure 4.1 – Stability dispersions of h-BN/CNF after 10 days

4.1.2 Surface composition analysis

IR spectroscopy in ATR (Attenuated Total Reflection) configuration was used to evaluate the TOCN matrix changes following the charge deposition, providing information about the functional groups and molecular vibrations present in the material. The normalized spectra of TOCN and h-BN powders were evaluated as reference in **Figure 4.2** and in **Figure 4.3** respectively, in order to assess the changes of nanocellulose when h-BN filler is added.

Table 4.1 presents the main peaks and their signal attributions of the TOCN and the h-BN spectra and their corresponding descriptions.

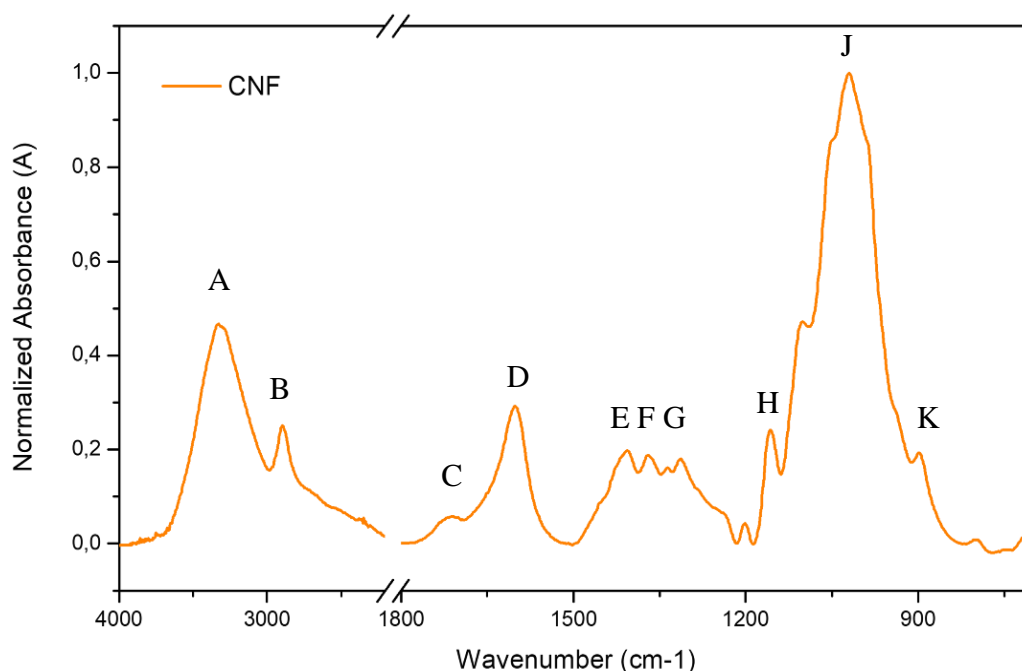


Figure 4.2 – ATR-IR normalized spectrum of TEMPO-CNF

The CNF spectrum shows a number of typical cellulose peaks [70]. It shows a band at 3335 cm^{-1} (A) that corresponds to hydroxyl groups O-H stretching, the peak at 2900 cm^{-1} (B) refers to the stretching of C-H groups in glycosidic units, the peak at 1709 cm^{-1} (C) refers to a shoulder attributed to O-H bond of absorbed water. In according to the literature[71], TEMPO oxidized CNFs shows a prominent peak at 1602 cm^{-1} (D) corresponds to carbonyl groups that make it different from untreated bleached pulp CNFs. Other peaks observed in the range between 1400 cm^{-1} and 1300 cm^{-1} can be attributed to the stretching of C-H₂ and C-H bonds [72]. In particular at $1410\text{--}1420\text{ cm}^{-1}$ (E) there are -CH₂ scissoring motion in cellulose, $1369\text{--}1373\text{ cm}^{-1}$ (F) corresponds to C-H bending, $\sim 1317\text{ cm}^{-1}$ (G) represents CH₂ wagging. The peaks in the region of $1154\text{--}1159\text{ cm}^{-1}$ (H) shows C-C ring stretching band. Peaks at 1052 cm^{-1} (J) shows C-O-C skeletal vibrations. Furthermore, at 900 cm^{-1} (K) there is a peak of improved sharpness associated with cellulosic β glycosidic linkages.

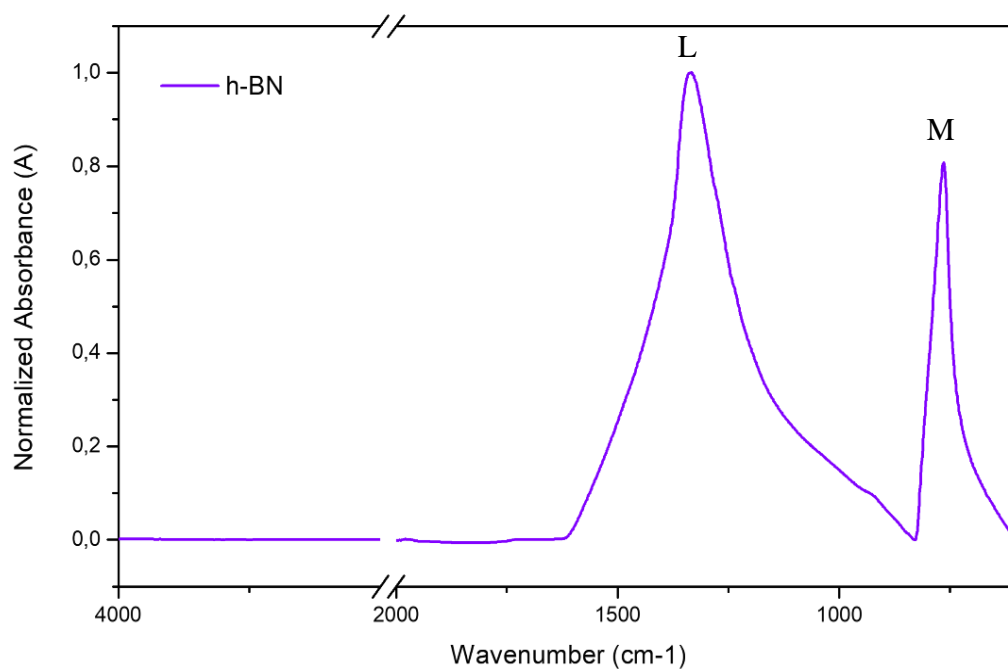


Figure 4.3 – ATR-IR normalized spectrum of h-BN powders

The FT-IR spectrum of the h-BN powders exhibits distinct active phonon modes at 776 cm^{-1} (M) and 1335 cm^{-1} (L), corresponding to the vibrations of the B-N bond. More specifically, the wide band observed at 1335 cm^{-1} is attributed to the in-plane stretching vibration of B-N bonds, while the less-broad band at 764 cm^{-1} corresponds to the out-of-plane bending vibration of B-N-B, as indicated by the characteristic peaks of h-BN in literature [73][74].

Table 4.1 – Bands description of Tempo oxidated cellulose nanofibers (TOCN) and h-BN powders

	Signal	Wavenumbers [cm ⁻¹]	Bands description
CNF	A	3335	(O-H) Stretching
	B	2900	(C-H) Stretching
	C	1709	(O-H) Absorbed water
	D	1602	(COO ⁻) of TOCN
	E	1410-1420	(-CH ₂) scissoring motion in cellulose
	F	1369-1373	(C-H) bending
	G	~ 1317	(CH ₂) wagging
	H	1154-1159	(C-C) ring stretching band
	J	1052	(C-O-C) skeletal vibrations
	K	900	sharpness β glycosidic linkage.
h-BN	L	1335	(B-N) in-plane stretching vibration
	M	764	(B-N-N) out-of-plane bending vibration

To better understand how the chemical bonds vary with increasing boron nitride percentage, FTIR spectra were obtained and are shown in **Figure 4.4**, depicting h-BN/CNF at 20%, 40%, 60%, and 80%. CNF spectrum has used as reference.

As seen from the normalized spectra, taking the TOCN spectrum as a reference, the addition of h-BN at different percentages reveals the appearance of new peaks characteristic of boron nitride at 764 cm⁻¹ (M) and 1335 cm⁻¹ (L) wavelengths. This indicates that h-BN and CNF were mixed together.

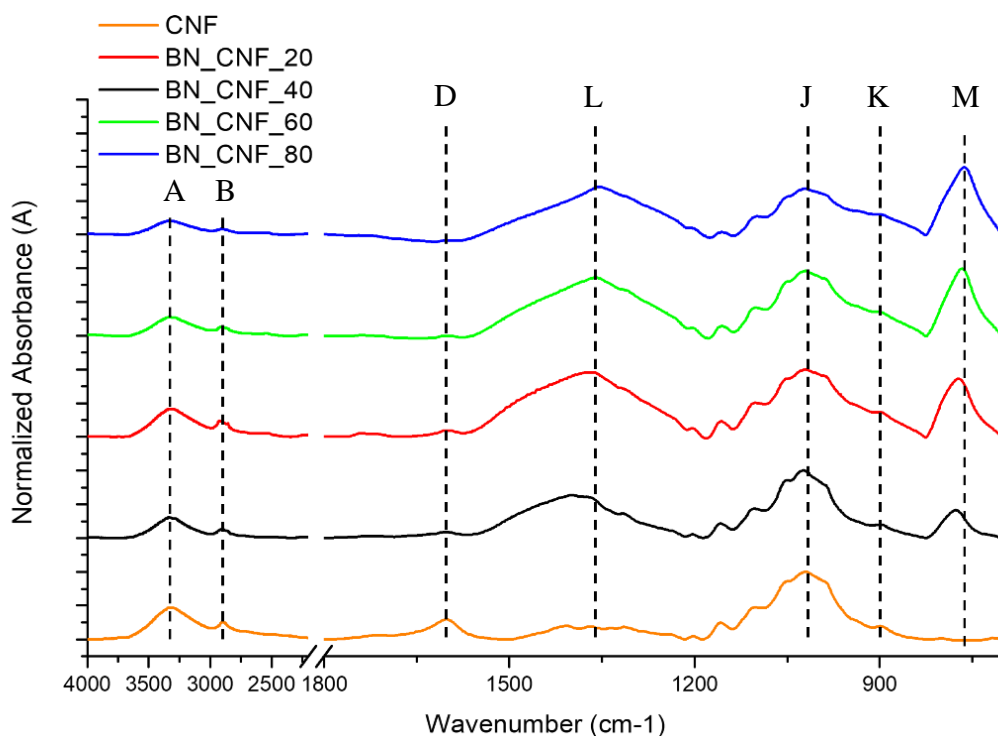


Figure 4.4 – ATR-IR normalized spectrum of h-BN/CNF nanocomposite films with CNF normalized spectrum as reference

The characteristic peaks of TEMPO-treated nanocellulose at 3335 cm^{-1} (A), 2900 cm^{-1} (B), 1602 cm^{-1} (D), $\sim 1317\text{ cm}^{-1}$ (G), and 900 cm^{-1} (K) remain nearly unchanged. However, a reduction in peak signal proportional to the increase in boron nitride concentration from 20% wt to 80% wt can be observed.

On the other hand, there is an increase in the intensity of the characteristic h-BN peaks at 1335 cm^{-1} (L) and 764 cm^{-1} (M), also due to the increase in h-BN concentration.

This could be caused by various factors, such as:

- Signal overlap: The signals of carbon (C) from TOCN may overlap with those of nitrogen (N) and boron (B) from h-BN, making it difficult to distinguish between them.
- Poor dispersion of h-BN: If the h-BN is not well dispersed within the CNF matrix, it may lead to uneven distribution and contribute to the observed changes in the spectra.
- Changes in composition: The reduction in the weight percentage of CNF and the increase in the weight percentage of h-BN can also contribute to the observed changes in the spectra.

Through TGA analysis, it will be possible to gain a more comprehensive understanding of the chemical composition, thermal behavior, and interaction of the materials under consideration.

4.1.3 Morphological and chemical analysis

Scanning Electron microscopy coupled with energy-dispersive X-ray spectroscopy (EDS) were employed in order to characterize surface of h-BN/CNF films and to have information about chemical composition. The surfaces of the samples appear microscopically flat at 500 X magnification as a shown in **Figure 4.5**. The 60% h-BN sample appears to exhibit a layered effect, which could be attributed to various factors such as sample preparation or a region richer in cellulose has been investigated.

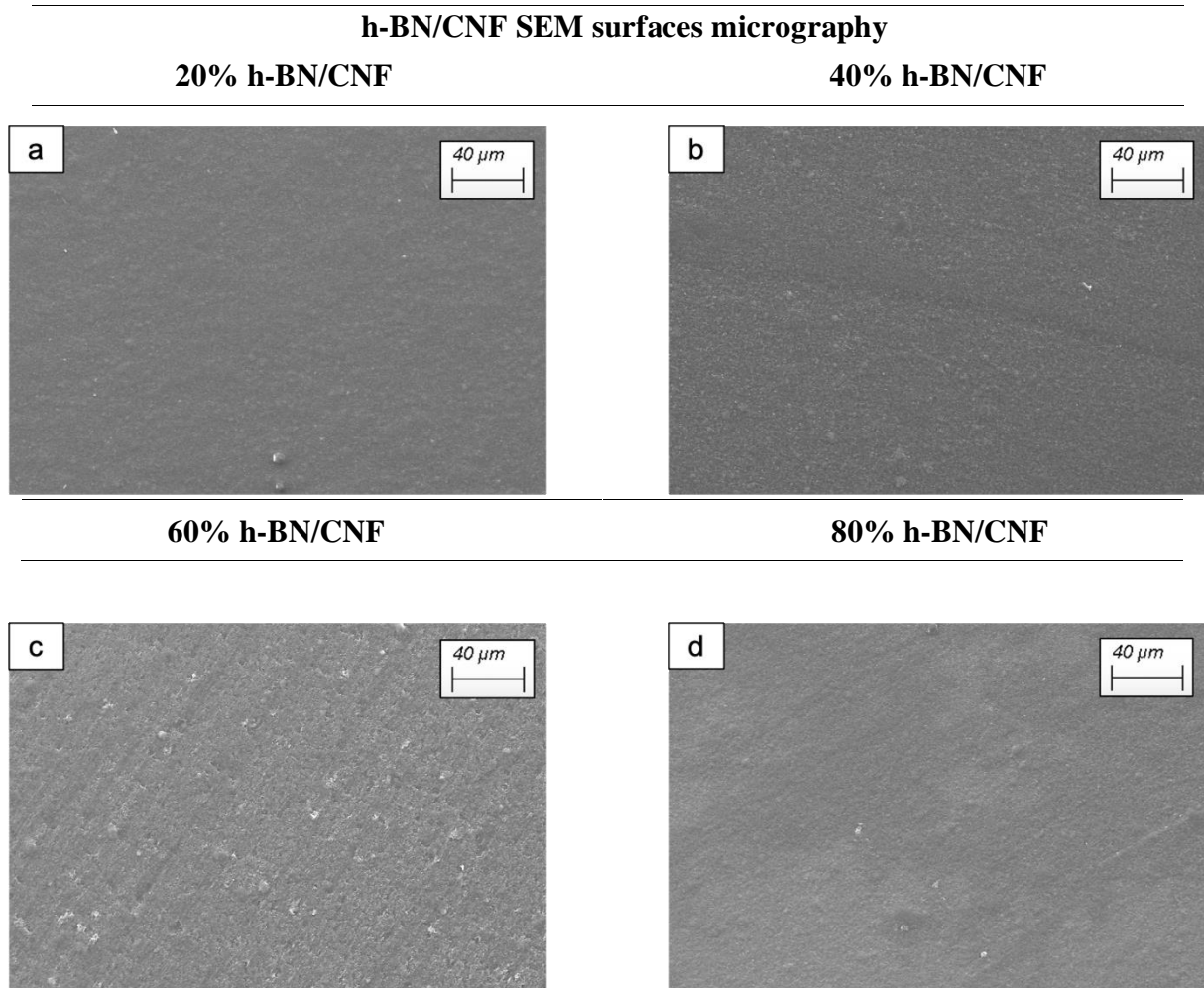


Figure 4.5 – SEM surface images of h-BN/CNF nanocomposites at different compositions: 20% wt (a), 40% wt (b), 60% wt (c), 80% wt (d) at 40 μm scale (500 X)

Instead, a significantly inhomogeneities were observed in the samples at higher magnification, specifically at 20.00 KX and at 50.00 KX. In **Figure 4.6** are reported the cross-sectional micrographs of studied h-BN/CNF samples, in which in red are collected zoomed images in detail at 300-400 nm of the films at different compositions.

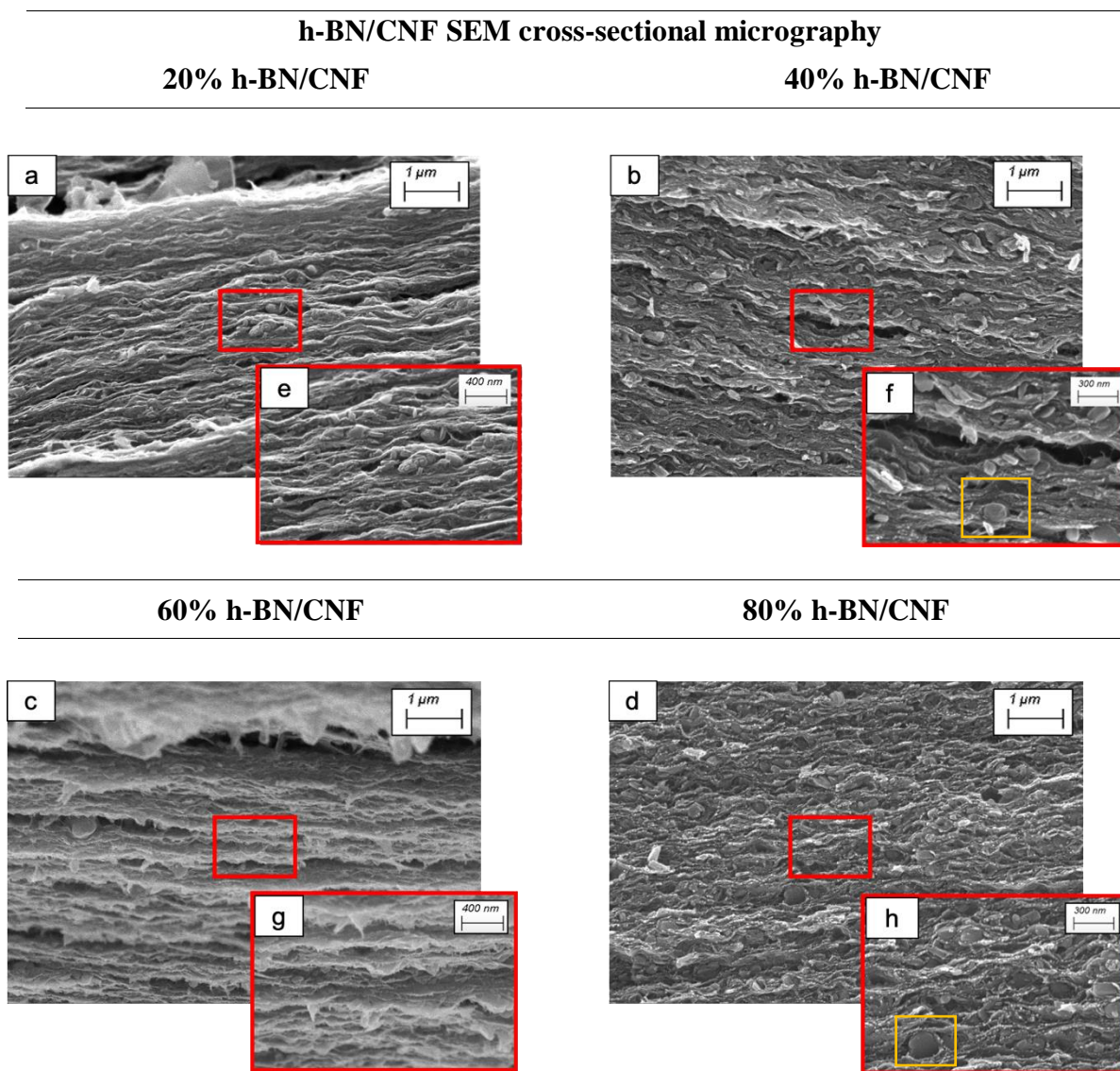


Figure 4.6 – SEM cross-sectional images of h-BN/CNF nanocomposites at different compositions: 20% (a, e), 40% (b, f), 60% (c, g), 80% (d, h) zoomed in details at lower scale (20.00 – 50.00 KX)

After ultrasonication the CNF fibers are fragmented and as we can see at 1 μm and better at 300/400 nm scale, it is indeed challenging to distinguish hexagonal boron nitride from TEMPO nanocellulose fibers. As observed from the SEM images, there is a directional alignment of nanocellulose fibers along the plane, typical of net TOCN films produced with this procedure [75]. Otherwise, at 300 nm scale of 40% h-BN/CNF (**Figure 4.6 – b, f**) and 80% h-BN/CNF (**Figure 4.6 – d, h**) we can see probably h-BN circular particles inside of CNF matrix (yellow square).

In addition, as better shown in 20% h-BN/CNF (**Figure 4.6 – a, e**) there are thin fibers intertwining with each other, forming a three-dimensional fibrous structure. Furthermore, as we can see in **Figure 4.6 – c, g**, a porous surface with holes and fissures of different sizes

can be observed, which can be visualized as dark spots in SEM microscopy, typical of net TOCN cluster pull-out [75]. Furthermore, the holes that can be seen, especially in h-BN/CNF samples, are the result of fracture along different planes, leaving protrusions on the opposite side.

Globally, all h-BN/CNF samples exhibit a good distribution of h-BN in the CNF matrix volume and there is no h-BN layering present. On the other hand, as can be observed more clearly in **Figure 4.6 - a, e**, the dispersion of boron nitride nanoparticles is not optimal, as agglomerates of macro-sized particles have been observed. This can be attributed to the poor affinity of boron nitride particles with water.

To further investigate the presence of h-BN, EDS analysis has been performed (as shown in **Figure 4.7**). It is important to specify that EDS analysis is a qualitative analysis. It is not possible to make exact estimations, but it is still useful to understand if, by increasing the concentration, there is a qualitative increase in the actual content of B and N.

The signals of the elements B, N, and C are overlapping due to their similar characteristics. The 20% and 40% samples show qualitatively the same composition analysis (as shown in **Table 4.2**). The 80% and 60% samples have the same amount of nitrogen (N), while there is a low increase in boron (B) from 40% to 80%. The concentration increases but is not proportional to the theoretical concentration because h-BN tends to precipitate at the bottom due to its poor affinity with the aqueous solvent. The presence of Na could be attributed to the TEMPO oxidation process of native pulp cellulose.

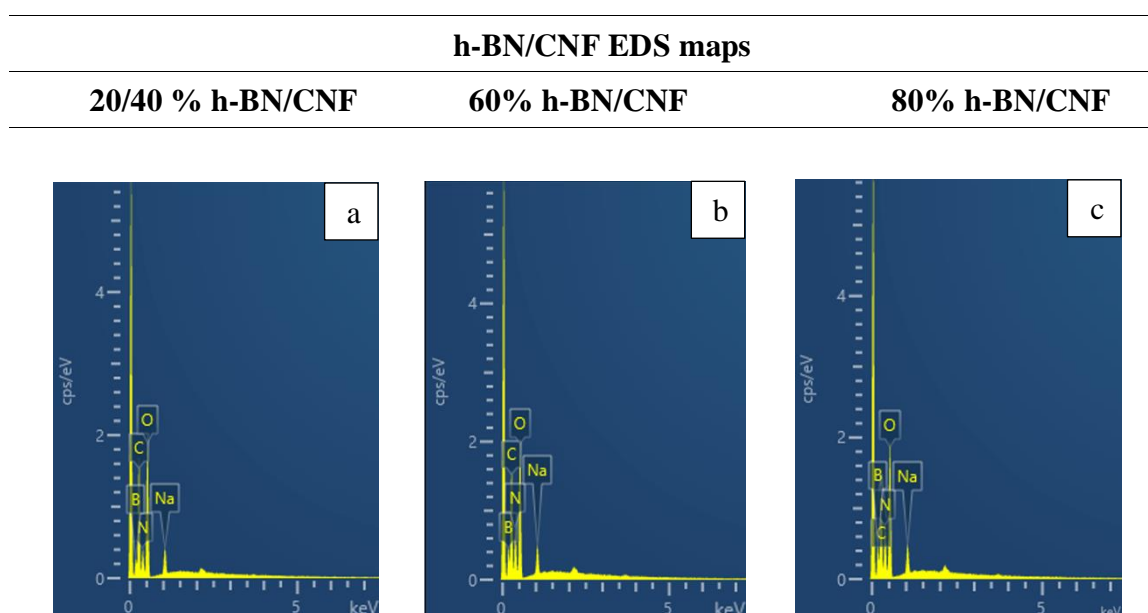


Figure 4.7 – EDS maps of h-BN/CNF nanocomposite films at different composition: 20-40 % (a), 60% (b), 80 % (c)

Table 4.2 – EDS analysis of h-BN/CNF nanocomposite films at different composition: 20-40 % (a), 60% (b), 80 % (c)

Samples	C [wt%]	O [wt%]	N [wt%]	B [wt%]	Na [wt%]
20% BN/CNF	35.7	32.1	16.5	14	1.7
40% BN/CNF	35.7	32.1	16.5	14	1.7
60% BN/CNF	31.1	27.4	22.4	17.8	1.4
80% BN/CNF	31.4	26.6	22.4	18.3	1.4

4.1.4 Thermal conductivity analysis

Due to the poor affinity of h-BN with water, boron nitride probably agglomerated in macroparticles within the TOCN matrix due to weak van der Waals interactions. This was observed in the SEM images analyzed in the previous section 4.1.2, related to morphological characterization. This phenomenon resulted in poor thermal conductivity because the particles were not close enough to create a continuous percolation pathway, hindering thermal conductivity. Preliminary thermal conductivity tests did not yield conclusive results.

4.1.5 Thermal gravimetric analysis

The thermal stability of h-BN/CNF nanocomposite films was characterized under the same operating conditions in both nitrogen and air environments, between 100°C and 700°C in order to determine the decomposition profile of h-BN and CNF films. The thermal stability of h-BN powders and TEMPO-CNF film is represented in **Figure 4.8**.

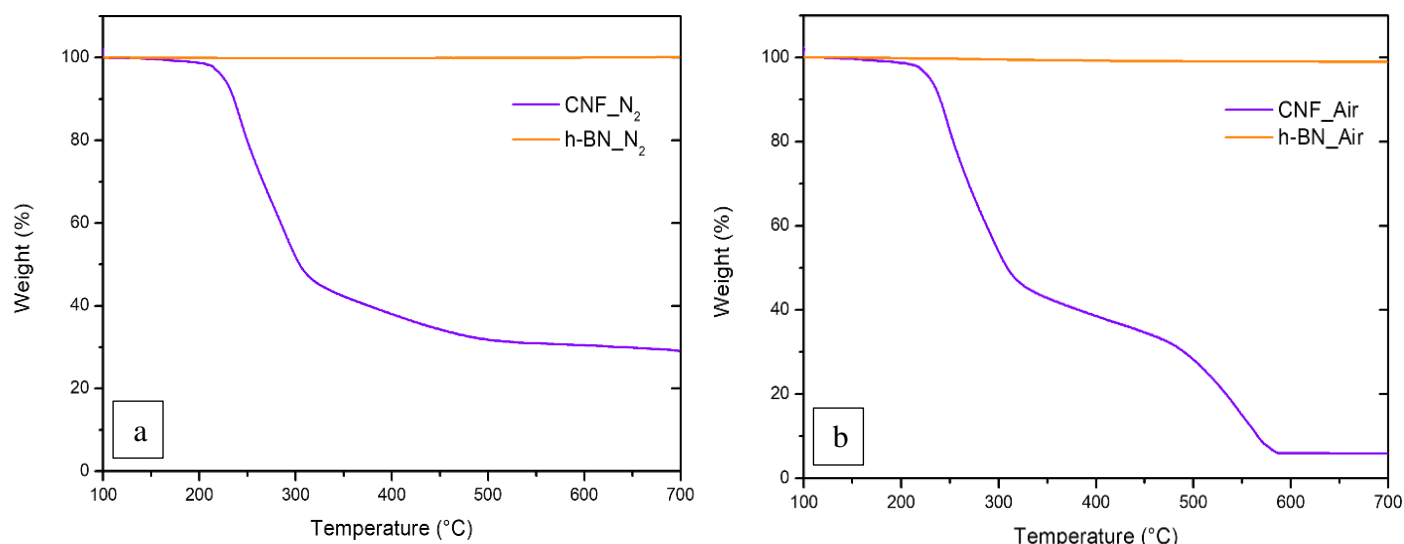


Figure 4.8 – Thermogravimetry curves of CNF film and h-BN powders in N₂ (a) and Air (b) conditions

Before 100 °C, the evaporation of absorbed and intermolecular H-bonded water occurs in both TEMPO-CNF and h-BN in both environment conditions.

In an inert atmosphere (**Figure 4.8 - a**), it has been observed that the decomposition process for TEMPO-CNF occurs in one step between 200°C and 340°C, with a maximum decomposition rate around 300°C. This decomposition phase can be attributed to two competing processes [76]: depolymerization and decomposition of glycosidic units. Depolymerization occurs through the cleavage of acetal bonds between the glycosidic units, resulting in the formation of volatile levoglucosan. On the other hand, decomposition takes place through intramolecular and intermolecular elimination of water, leading to the formation of a thermally stable aliphatic structure, which is further converted into aromatic carbon, releasing CO₂, CO, H₂O, and CH₄ beyond 350°C. The CNF films produced a char residue of 29.12% at a temperature of 700°C. In the same atmosphere, the mass of boron nitride remains almost stable as the temperature increases within the measured range up to 700°C.

In air (**Figure 4.8 – b**), the decomposition process of CNF unfolds in two steps. The first decomposition phase occurs around 300°C and results in a weight loss of 60% that represent a relatively low thermal stability. This phenomenon is attributed to the degradation of glycosidic compounds. The second phase, caused by the decomposition of pyranic structures, begins around 450°C and leads to an overall weight loss of 90%. The residual mass of CNF in air was 5.84%. The mass of boron nitride remains constant in this case as well within the studied annealing range of 100-700°C. According to the literature [77], the resistance to oxidation of h-BN appears to be correlated with the degree of crystallinity and specific surface area of BN. High crystallinity, coupled with a small specific surface area, results in fewer reactive sites for oxidation and, consequently, a reduced mass loss. h-BN begins to oxidize at a higher temperature (1200°C). At this temperature, the oxidation of

boron nitride into B_2O_3 occurs, releasing N_2 . Additionally, an increase in mass is observed at this temperature due to the formation of boron oxide on the surface.

The thermogravimetric curves of h-BN/CNF films at different composition and atmosphere conditions are showed in **Figure 4.9**.

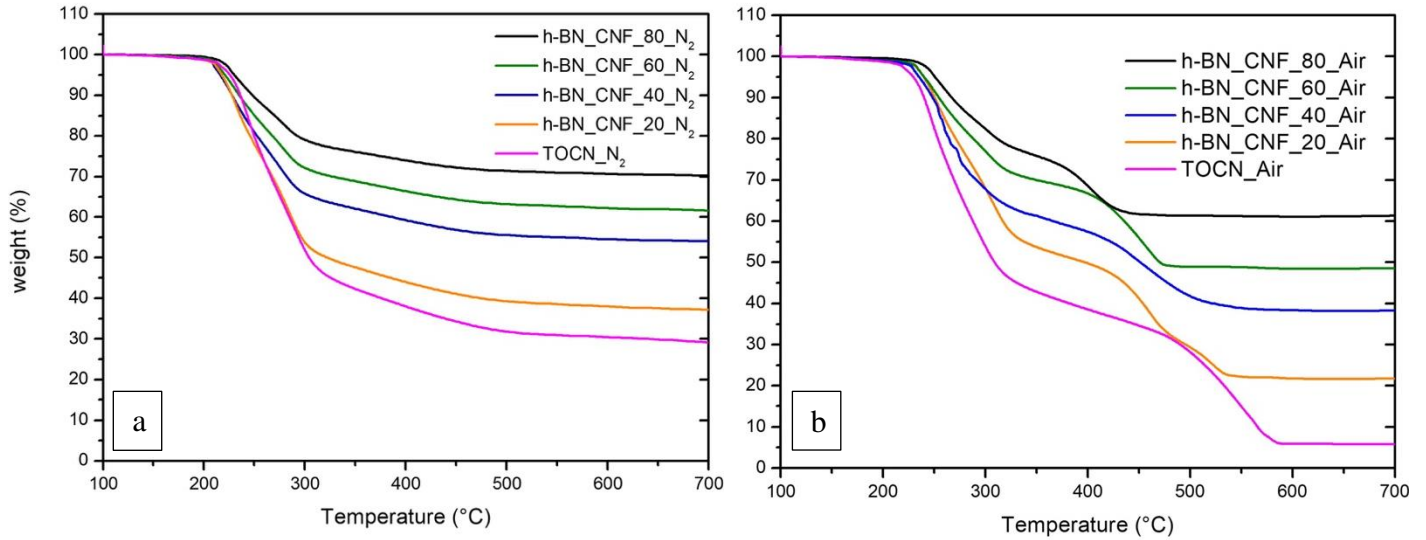


Figure 4.9 – Thermogravimetry curves of h-BN/CNF films at different compositions in N_2 (a) and Air (b) conditions

h-BN do not change the decomposition behavior of TOCN in inert atmosphere because it occurs in one step (**Figure 4.9 – a**) as TOCN film curve. The production of char can be used as an indicator of good fire reaction behavior. As the percentage of added boron nitride increases during the sample preparation, the obtained residue also increases in both environment conditions according to the h-BN theoretically added, as seen in **Figure 4.9 - a, b**. The residue is mainly attributed to the contribution of inorganic boron nitride. Therefore, the residual mass of the samples is determined by the sum of the percentage of added boron nitride and the contribution of organic TOCN char. In many cases, a high residual mass can be associated with better flame-retardant performance. This further analysis was conducted in the present thesis study and will be discussed in the subsequent paragraphs.

In oxidative environment (**Figure 4.9 – b**) the decomposition behavior of these nanocomposites occurs in two steps because the h-BN powders failed to suppress the second weight loss step failing to form an oxygen diffusion barrier. The reason is probably the lower aspect ratio and the poor dispersion of h-BN inside the matrix, as we can see in the SEM images. In this case as well, the contribution of the residue increases with the increasing percentage of h-BN. Nanocellulose matrix in nitrogen already has a good capacity to produce char as show in figure. In air, the residue at 700 °C is basically due to h-BN. Compared with the theoretically added amount, after 40%, the target amount of 60% and 80%. cannot be achieved, as can be seen in the figure. **Table 4.3** displays the residues of TOCN, h-BN, and h-BN/CNF films at different compositions and atmosphere.

Table 4.3 – Residue of h-BN/CNF nanocomposite films at different compositions and environment conditions

Samples	N ₂ Residue [% wt]	Air Residue [% wt]
Net TOCN	29.12	5.84
h-BN	99.7	98.83
20% h-BN/CNF	36.5	21.70
40% h-BN/CNF	53.6	38.22
60% h-BN/CNF	60.9	48.52
80% h-BN/CNF	69.2	61.23

4.1.6 Stress-strain behavior and mechanical properties

By conducting tensile tests, it was possible to obtain stress-strain curves and consequently gather information about the mechanical properties of h-BN/CNF nanocomposite films. Stress - strain curves are shown in **Figure 4.10** and mechanical properties are summarized in **Table 4.3**.

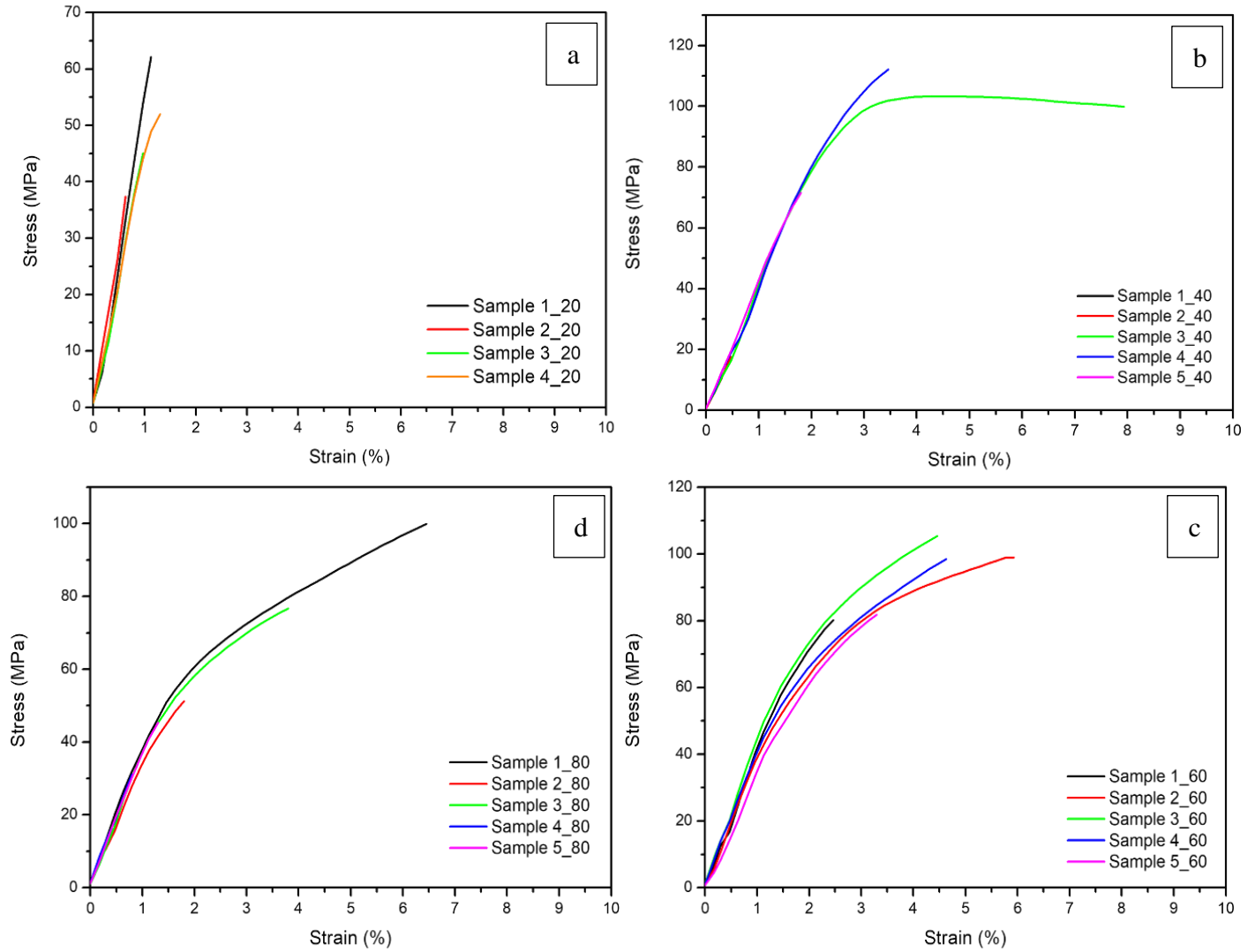


Figure 4.10 – Tensile test curves of h-BN/CNF films at different compositions: 20% h-BN (a), 40% h-BN (b), 60% h-BN (c), 80% h-BN(d)

According to the literature [68], TOCN films produced using the same production process exhibit significantly higher properties compared to h-BN/CNF nanocomposites. The Young's modulus of TOCN films is approximately 14 GPa, and the stress at break is around 310 MPa. In addition, plastic yielding followed by linear strain - hardening and ultimate fracture are observed. This is mainly attributed to the random in-plane orientations of the nanofibrils and minimal porosity in the films.

On the other hand, h-BN/CNF films, due to the poor affinity of boron nitride with water, exhibit poor dispersion of nanoparticles in the TOCN matrix, likely resulting in a drastic reduction in mechanical properties and brittle behavior as shown in **Table 4.3**. The Young's modulus does not exceed 4 ± 1 GPa and the stress at break do not exceed 93 ± 11 MPa. These samples primarily undergo brittle fracture. The standard deviation is very high due to poor particle dispersion. The presence of aggregates of varying sizes negatively affects the elastic modulus.

When the h-BN content is 20 wt%, the h-BN/CNF nanocomposites show the highest average Young's modulus (4124.4 ± 1070 MPa) likely because the TOCN matrix predominates over the h-BN, exhibiting behavior closer to that of net TOCN films.

At high h-BN content (40, 60 wt%), an increase in average strength at break (σ_{mb}) is observed, except for the sample with h-BN content of 80 wt%. The samples with h-BN content of 60 wt% exhibit the highest average strength (2.8 ± 3.1 %) and strain at break (93 ± 11 MPa). It could be due to the improved level of dispersion achieved for the samples with 60% h-BN.

Furthermore, an increase in ductility pointed out by increased ϵ_{mb} is detected, probably for h-BN lubricant properties that improve the sliding of cellulose fibrils. Finally, there is a non-linear reduction in the average Young's modulus with increasing h-BN content, likely related to the agglomerated nanostructure that reduces reinforcement effects and stress transfer.

Different behavior compared to boron nitride has been reported in the literature [68], where various nanoclay compositions with different aspect ratios (montmorillonite (MTM), mica, and saponite (SPN)) have been used. In particular, MTM/CNF achieved the highest Young's modulus, reaching up to 30-40 GPa at 80% clay content. At high clay content, SPN/CNF samples have also exhibited a transition from brittle to ductile behavior, exceeding 250 MPa for 40% volume of clay. This is attributed to the fact that SPN has a lower aspect ratio and good dispersion of clay platelets than h-BN powders.

Table 4.3 – Properties of h-BN/CNF nanocomposite films at different compositions

Samples	Properties		
	E_m [MPa]	ϵ_{mb} [%]	σ_{mb} [MPa]
CNF [68]	≈ 14000	/	≈ 310
20% BN/CNF	4124 ± 1070	1.0 ± 0.3	49 ± 10
40% BN/CNF	3450 ± 332	2.8 ± 3.1	62 ± 46
60% BN/CNF	3521 ± 1005	4.2 ± 1.3	93 ± 11
80% BN/CNF	3727 ± 437	2.8 ± 2.3	61 ± 27

4.1.7 Flammability tests

One of the main objectives of this research is to understand if the specimens produced can exhibit fire properties without using toxic flame-retardant additives and consequently find application in places where high fire safety is required.

Horizontal flammability tests using UL-94 have been conducted to determine the propensity of h-BN/CNF nanocomposites to ignite when exposed to a small methane blue flame. As reported in the literature [68], neat TOCN exhibits rapid fire ignition, followed by self-extinguishing behavior and an afterglow phenomenon (oxidation in the absence of flame) until complete sample consumption.

On the other hand, h-BN/CNF composites have shown excellent flame-retardant and properties, thus guarantee a high level of fire safety. During the test once the flame is removed, the analyzed samples show self-extinguish behavior (as shown in **Figure 4.11**). During exposure to the flame, the compounds released from the decomposition of TOCN are trapped within the boron nitride particles, leading to an increase in the thickness of the nanocomposite.

The boron nitride powder dispersed within the TOCN matrix hinders oxygen diffusion, reduces oxidation rates, and delays the evaporation of volatile compounds. Due to the consumption of the nanocellulose matrix, the BNNS are exposed in the surface. These particles form a hybrid layer made up of carbon from the TOCN and h-BN decomposition. The char acts as a barrier to heat and oxygen, protecting the underlying material from further decomposition and promoting self-extinguishment.

The flame-retardant properties increase with the h-BN content, indeed as can be seen in the samples at the end of the test in **Figure 4.11**, there are a varying length of burned sample. The useful length after extinguishment increases with the increasing addition of h-BN content, except for the 80% wt h-BN nanocomposite that exhibits a more pronounced burned section (and therefore a shorter remaining length). This is due to the poor dispersion of boron nitride nanoparticles. Indeed, a high percentage, many nanoscale aggregates are formed, which significantly increase the flame propagation.

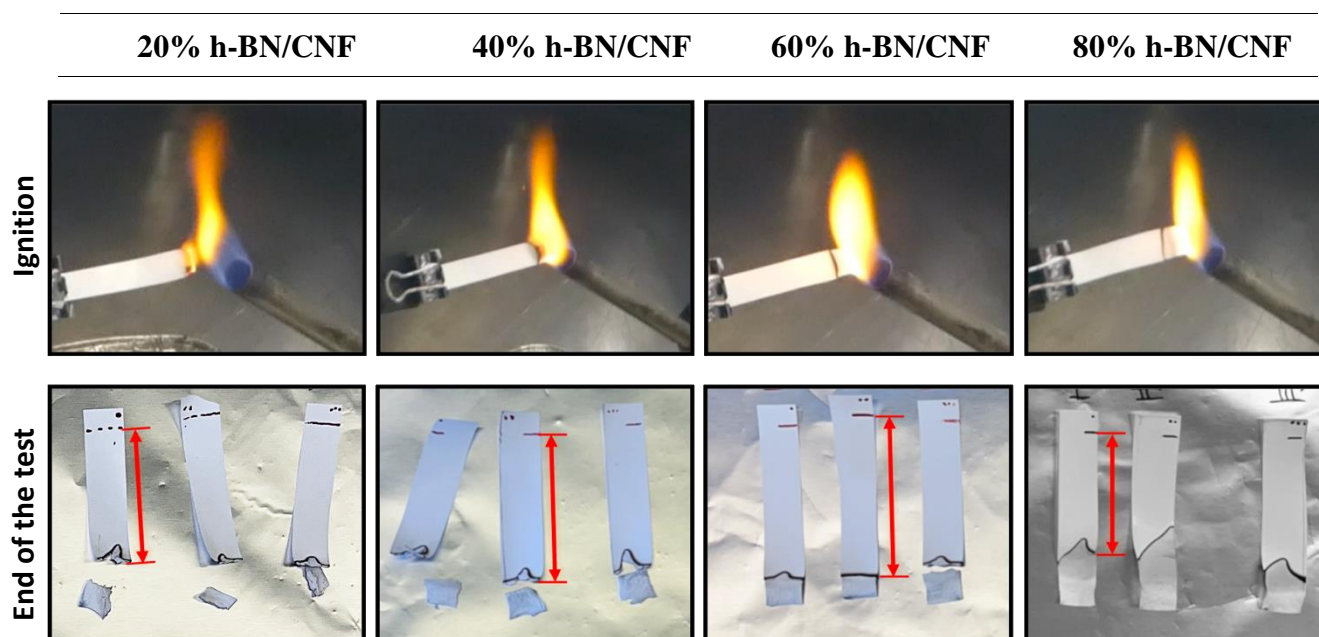


Figure 4.11 – UL-94 test on the h-BN/CNF nanocomposite films at different compositions

Furthermore, the afterglow phenomenon has been detected also for all composites. The analyzed samples exhibit different afterglow times (heat persistence after flame application). In particular, the 40% h-BN/CNF samples show the highest afterglow time of all (9.3 seconds). On the other hand, the 60% h-BN/CNF samples demonstrate the best fire safety performance, exhibiting the lowest afterglow time of all (4 seconds) and the widest remaining length. The afterglow times and the length of the samples at the end of the test are summarized in **Table 4.4**.

The test has been successfully passed by all samples with different percentages of h-BN, as they exhibited self-extinguishing behavior before reaching 1/5 of the useful length of the specimens.

Table 4.4 – Analyzed parameters after UL-94 test on h-BN/CNF nanocomposites films

Parameters	20% h-BN/CNF	40% h-BN/CNF	60% h-BN/CNF	80% h-BN/CNF
Afterglow Time [s]	8.3	9.3	4	7.3
Final length [mm]	32.5	35.8	38.9	29.1

4.1.8 Flame penetration analysis

Figure 4.12 reports flame penetration test performed on all h-BN/CNF samples at different compositions, which reports the temperature profile collected during flame penetration tests for all the tested samples. The application of a flame torch impinging directly on the surface of the sample was sufficient to penetrate and immediately destroy all the h-BN/CNF samples. The reasons can always be attributed to the poor distribution of boron nitride achieved with the technique used for sample preparation, as boron nitride exhibits low affinity with water.

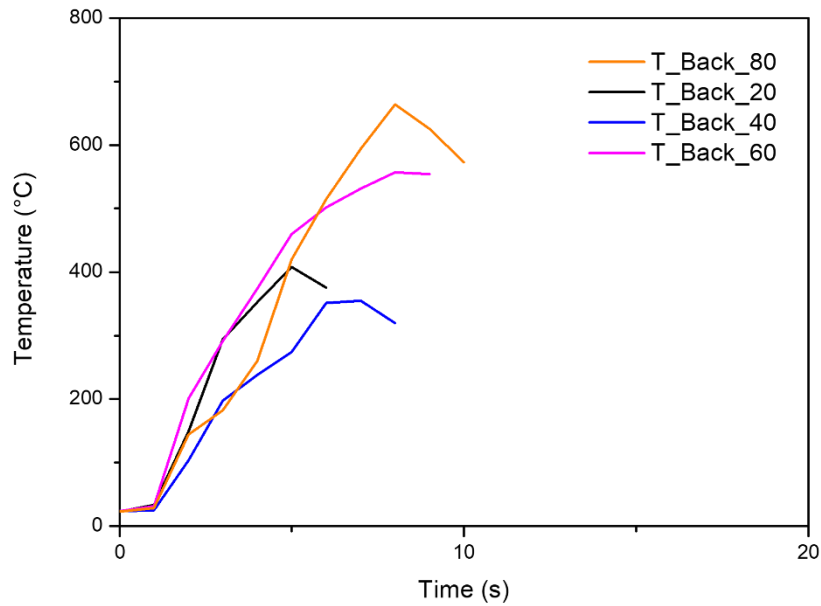


Figure 4.12 – Flame penetration tests: Front and back side temperatures as a function of time for h-BN/CNF films at different compositions: 20% h-BN (T_Back_20), 40% h-BN (T_Back_40), 60% h-BN (T_Back_60), 80% h-BN (T_Back_80)

The curves in the graph represent the back temperatures of the samples at different concentrations. The 20% h-BN/CNF, 40% h-BN/CNF, 60% h-BN/CNF, and 80% h-BN/CNF samples did not show a flame penetration resistance and there are perforated, and the test only lasts for few seconds. For this reason, as we can see in the graph, the front temperature was not taken as a reference.

To better understand the nanocomposites behavior has been used a thermos-camera as support analysis. Snapshots of the penetration test supported by thermographic images are shown in **Figure 4.13**.

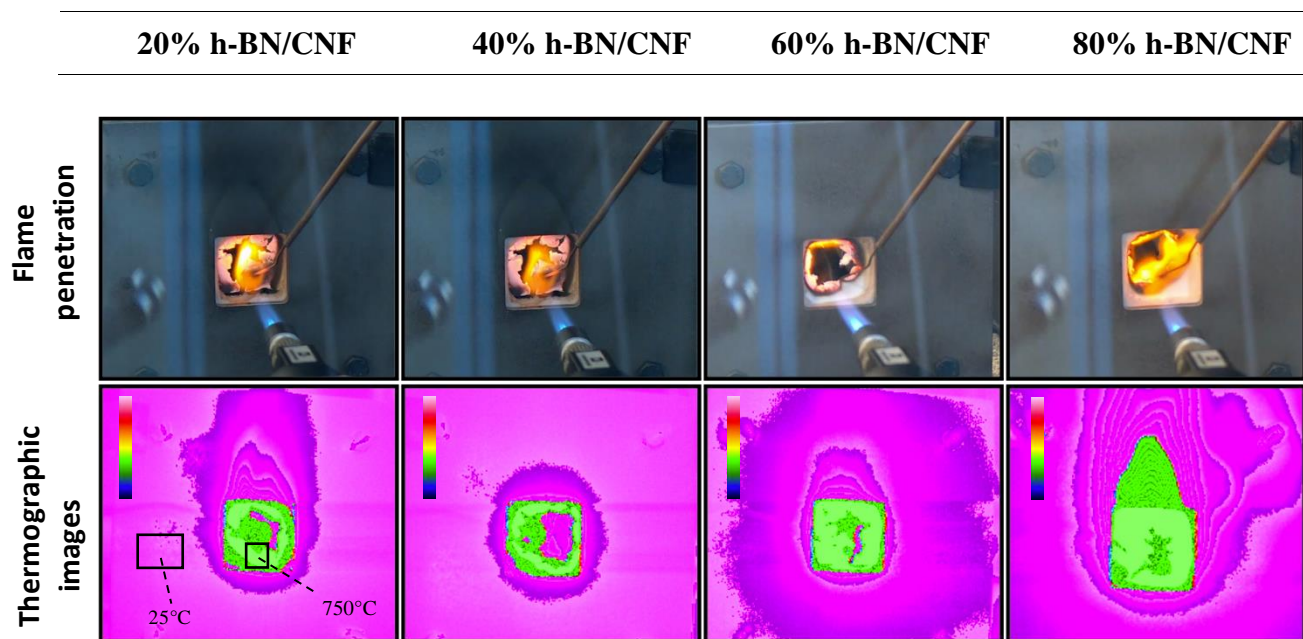


Figure 4.13 – Flame penetration tests: pictures of h-BN/CNF films front surface during the test and thermographic images of back side surface of the samples

4.2 Conclusions and future perspectives

The main objective of this thesis was to investigate whether the presence of hexagonal boron nitride (h-BN) within nanocomposites based on nanocellulose could improve the properties of the composite, particularly its flame retardancy compared to neat nanocellulose. For this reason, h-BN/CNF films with a thickness of around 50 micrometres were produced using vacuum-assisted filtration, starting with the production of TOCN from cellulose pulp.

It was found that the films produced using this technique did not exhibit a good dispersion of boron nitride particles within the nanocellulose matrix due to the poor affinity of h-BN with water. However, they did show a random distribution of particles within the structure thus producing a micro composite.

Thanks to the presence of boron nitride, these nanocomposites exhibited improved fire performance because the char layer formed by nanocellulose with h-BN tended to reach the surface, creating a weak nano-barrier to heat and oxygen, protecting the material from flame-induced degradation and reducing the heat release rate but it fails to prevent afterglow because it is probably made with h-BN aggregates and therefore oxygen can pass through. This analysis was further supported by TGA analysis, which showed a proportional increase in residue with the increasing concentration of added boron nitride in both nitrogen and oxidative environments. In air, the residue at 700°C is basically due to h-BN. Compared with the theoretically added amount, after 40%, the target amount of 60% and 80%. cannot

be achieved. The composites with 60% wt of h-BN demonstrated the best compromise between distribution and dispersion.

On the other hand, the poor dispersion of nanoparticles caused multiple issues for the realized samples. In particular, it resulted in poor flame penetration resistance, as the samples at all compositions perforated within a few seconds. Furthermore, a low thermal conductivity was observed due to the poor dispersion, which did not create a continuous percolation pathway. The poor dispersion also led to a drastic reduction in mechanical properties compared to neat nanocellulose films, with a loss of almost 75% in elastic modulus and tensile strength for the most performant 60% h-BN/CNF film.

In conclusion, the objective of the thesis was partially achieved considering the improvement in fire behaviour. Future developments could involve exploring alternative preparation techniques for this type of films, considering the poor affinity of boron nitride with water, in order to enhance particle dispersion. This could lead to improved flame retardancy while maintaining excellent mechanical and thermal conductivity properties.

References

- [1] S. Spierling, V. Venkatachalam, M. Mudersbach, N. Becker, C. Herrmann, and H.-J. Endres, “End-of-Life Options for Bio-Based Plastics in a Circular Economy—Status Quo and Potential from a Life Cycle Assessment Perspective,” *Resources*, vol. 9, no. 7, p. 90, Jul. 2020, doi: 10.3390/resources9070090.
- [2] C. R. Álvarez-Chávez, S. Edwards, R. Moure-Eraso, and K. Geiser, “Sustainability of bio-based plastics: general comparative analysis and recommendations for improvement,” *J Clean Prod*, vol. 23, no. 1, pp. 47–56, Mar. 2012, doi: 10.1016/j.jclepro.2011.10.003.
- [3] S. Dahiya, R. Katakjwala, S. Ramakrishna, and S. V. Mohan, “Biobased Products and Life Cycle Assessment in the Context of Circular Economy and Sustainability,” *Materials Circular Economy*, vol. 2, no. 1, p. 7, Dec. 2020, doi: 10.1007/s42824-020-00007-x.
- [4] M. C. D. de G. H. K. R. C. J. R. W. B. and A. R. Pia Skoczinski, *Bio-based Building Blocks and Polymers – Global Capacities, Production and Trends 2020 – 2025*. 2021.
- [5] European Bioplastics, “What are bioplastics?,” 2018.
- [6] S. J. Eichhorn et al., “Review: current international research into cellulose nanofibres and nanocomposites,” *J Mater Sci*, vol. 45, no. 1, pp. 1–33, Jan. 2010, doi: 10.1007/s10853-009-3874-0.
- [7] D. Klemm, B. Heublein, H.P. Fink, and A. Bohn, “Cellulose: Fascinating Biopolymer and Sustainable Raw Material,” *Polymer Healthcare*, vol. 44, no. 22, pp. 3358–3393, 2005.
- [8] P. Kumar Gupta et al., “An Update on Overview of Cellulose, Its Structure and Applications,” in *Cellulose*, IntechOpen, 2019. doi: 10.5772/intechopen.84727.
- [9] G. Siqueira, J. Bras, and A. Dufresne, “Cellulosic bionanocomposites: a review of preparation, properties and applications,” *Polymers (Basel)*, vol. 2, no. 4, pp. 728–765, 2010.
- [10] S. Mondal, “Preparation, properties and applications of nanocellulosic materials,” *Carbohydr Polym*, vol. 163, pp. 301–316, 2017.
- [11] D. Klemm, D. Schumann, U. Udhardt, and S. Marsch, “Bacterial synthesized cellulose—artificial blood vessels for microsurgery ,” *Prog Polym Sci*, vol. 26, no. 9, pp. 1561–1603, 2001.
- [12] A. Operamolla, “Recent Advances on Renewable and Biodegradable Cellulose Nanopaper Substrates for Transparent Light-Harvesting Devices: Interaction with

- Humid Environment,” *International Journal of Photoenergy*, vol. 2019, pp. 1–16, Jun. 2019, doi: 10.1155/2019/3057929.
- [13] Y. Habibi, “Key advances in the chemical modification of nanocelluloses,” *Chem Soc Rev*, vol. 43.5, pp. 1519–1542, 2014.
 - [14] Anna J. Svagan, M. Samir, and L.A. Berglund, “Biomimetic Polysaccharide Nanocomposites of High Cellulose Content and High Toughness,” *Biomacromolecules*, vol. 8, pp. 2556–2563, 2007.
 - [15] Y. Habibi, H. Chanzy, and M. R. Vignon, “TEMPO-mediated surface oxidation of cellulose whiskers,” *Cellulose*, vol. 13, no. 6, pp. 679–687, Dec. 2006, doi: 10.1007/s10570-006-9075-y.
 - [16] S. R. Levis and P. B. Deasy, “Production and evaluation of size reduced grades of microcrystalline cellulose,” *Int J Pharm*, vol. 213, no. 1–2, pp. 13–24, Feb. 2001, doi: 10.1016/S0378-5173(00)00652-9.
 - [17] T. Zhang, Q. Cheng, D. Ye, and C. Chang, “Tunicate cellulose nanocrystals reinforced nanocomposite hydrogels comprised by hybrid cross-linked networks,” *Carbohydr Polym*, vol. 169, pp. 139–148, Aug. 2017, doi: 10.1016/j.carbpol.2017.04.007.
 - [18] M. L. Cacicedo et al., “Progress in bacterial cellulose matrices for biotechnological applications,” *Bioresour Technol*, vol. 213, pp. 172–180, Aug. 2016, doi: 10.1016/j.biortech.2016.02.071.
 - [19] X. Du, Z. Zhang, W. Liu, and Y. Deng, “Nanocellulose-based conductive materials and their emerging applications in energy devices - A review,” *Nano Energy*, vol. 35, pp. 299–320, May 2017, doi: 10.1016/j.nanoen.2017.04.001.
 - [20] T. D. O. Gadim et al., “Protonic conductivity and fuel cell tests of nanocomposite membranes based on bacterial cellulose,” *Electrochim Acta*, vol. 233, pp. 52–61, Apr. 2017, doi: 10.1016/j.electacta.2017.02.145.
 - [21] H. M. C. Azeredo, M. F. Rosa, and L. H. C. Mattoso, “Nanocellulose in bio-based food packaging applications,” *Ind Crops Prod*, vol. 97, pp. 664–671, Mar. 2017, doi: 10.1016/j.indcrop.2016.03.013.
 - [22] N. Mahfoudhi and S. Boufi, “Nanocellulose as a novel nanostructured adsorbent for environmental remediation: a review,” *Cellulose*, vol. 24, no. 3, pp. 1171–1197, Mar. 2017, doi: 10.1007/s10570-017-1194-0.
 - [23] T. Lu et al., “Cellulose Nanocrystals/Polyacrylamide Composites of High Sensitivity and Cycling Performance To Gauge Humidity,” *ACS Appl Mater Interfaces*, vol. 9, no. 21, pp. 18231–18237, May 2017, doi: 10.1021/acsami.7b04590.

- [24] I. Siró and D. Plackett, "Microfibrillated cellulose and new nanocomposite materials: a review," *Cellulose*, vol. 17, no. 3, pp. 459–494, Jun. 2010, doi: 10.1007/s10570-010-9405-y.
- [25] Q. Q. Wang, J. Y. Zhu, R. Gleisner, T. A. Kuster, U. Baxa, and S. E. McNeil, "Morphological development of cellulose fibrils of a bleached eucalyptus pulp by mechanical fibrillation," *Cellulose*, vol. 19, no. 5, pp. 1631–1643, Oct. 2012, doi: 10.1007/s10570-012-9745-x.
- [26] W. Stelte and A. R. Sanadi, "Preparation and Characterization of Cellulose Nanofibers from Two Commercial Hardwood and Softwood Pulps," *Ind Eng Chem Res*, vol. 48, no. 24, pp. 11211–11219, Dec. 2009, doi: 10.1021/ie9011672.
- [27] F.W. Herrick, R.L. Casebier, J.K. Hamilton, and K.R. Sandberg, "Microfibrillated cellulose: morphology and accessibility," *J Appl Polym Sci Symp*, vol. 37, pp. 797–813, 1983.
- [28] H. P. S. Abdul Khalil et al., "Production and modification of nanofibrillated cellulose using various mechanical processes: A review," *Carbohydr Polym*, vol. 99, pp. 649–665, Jan. 2014, doi: 10.1016/j.carbpol.2013.08.069.
- [29] A. Blanco, M. C. Monte, C. Campano, A. Balea, N. Merayo, and C. Negro, "Nanocellulose for Industrial Use," in *Handbook of Nanomaterials for Industrial Applications*, Elsevier, 2018, pp. 74–126. doi: 10.1016/B978-0-12-813351-4.00005-5.
- [30] H. M. C. de Azeredo, "Nanocomposites for food packaging applications," *Food Research International*, vol. 42, no. 9, pp. 1240–1253, Nov. 2009, doi: 10.1016/j.foodres.2009.03.019.
- [31] D. R. Paul and L. M. Robeson, "Polymer nanotechnology: Nanocomposites," *Polymer (Guildf)*, vol. 49, no. 15, pp. 3187–3204, Jul. 2008, doi: 10.1016/j.polymer.2008.04.017.
- [32] L. S. S. P. V. B. Pulickel M. Ajayan, *Nanocomposite Science and Technology*. Wiley, 2003. doi: 10.1002/3527602127.
- [33] Md. N. Sakib and A. Asif Iqba, "Epoxy Based Nanocomposite Material for Automotive Application- A Short Review," *International Journal of Automotive and Mechanical Engineering*, vol. 18, no. 3, Oct. 2021, doi: 10.15282/ijame.18.3.2021.24.0701.
- [34] A. Usuki et al., "Synthesis of nylon 6-clay hybrid," *J Mater Res*, vol. 8, no. 5, pp. 1179–1184, May 1993, doi: 10.1557/JMR.1993.1179.

- [35] A. Okada and A. Usuki, "Twenty Years of Polymer-Clay Nanocomposites," *Macromol Mater Eng*, vol. 291, no. 12, pp. 1449–1476, Dec. 2006, doi: 10.1002/mame.200600260.
- [36] N. Basavegowda and K.-H. Baek, "Advances in Functional Biopolymer-Based Nanocomposites for Active Food Packaging Applications," *Polymers (Basel)*, vol. 13, no. 23, p. 4198, Nov. 2021, doi: 10.3390/polym13234198.
- [37] Q. Zhang, L. Zhang, W. Wu, and H. Xiao, "Methods and applications of nanocellulose loaded with inorganic nanomaterials: A review," *Carbohydr Polym*, vol. 229, p. 115454, Feb. 2020, doi: 10.1016/j.carbpol.2019.115454.
- [38] S.-L. Cao, H. Xu, X.-H. Li, W.-Y. Lou, and M.-H. Zong, "Papain@Magnetic Nanocrystalline Cellulose Nanobiocatalyst: A Highly Efficient Biocatalyst for Dipeptide Biosynthesis in Deep Eutectic Solvents," *ACS Sustain Chem Eng*, vol. 3, no. 7, pp. 1589–1599, Jul. 2015, doi: 10.1021/acssuschemeng.5b00290.
- [39] J. Hu et al., "Polymer Composite with Improved Thermal Conductivity by Constructing a Hierarchically Ordered Three-Dimensional Interconnected Network of BN," *ACS Appl Mater Interfaces*, vol. 9, no. 15, pp. 13544–13553, Apr. 2017, doi: 10.1021/acsami.7b02410.
- [40] D. Pan et al., "Highly thermal conductive epoxy nanocomposites filled with 3D BN/C spatial network prepared by salt template assisted method," *Compos B Eng*, vol. 209, p. 108609, Mar. 2021, doi: 10.1016/j.compositesb.2021.108609.
- [41] K. Zhang, Y. Feng, F. Wang, Z. Yang, and J. Wang, "Two dimensional hexagonal boron nitride (2D-hBN): synthesis, properties and applications," *J Mater Chem C Mater*, vol. 5, no. 46, pp. 11992–12022, 2017, doi: 10.1039/C7TC04300G.
- [42] K. Wattanakul, H. Manuspiya, and N. Yanumet, "Thermal conductivity and mechanical properties of BN-filled epoxy composite: effects of filler content, mixing conditions, and BN agglomerate size," *J Compos Mater*, vol. 45, no. 19, pp. 1967–1980, Sep. 2011, doi: 10.1177/0021998310393297.
- [43] Y. K. Shin, W. S. Lee, M. J. Yoo, and E. S. Kim, "Effect of BN filler on thermal properties of HDPE matrix composites," *Ceram Int*, vol. 39, pp. S569–S573, May 2013, doi: 10.1016/j.ceramint.2012.10.137.
- [44] H. Ishida and S. Rimdusit, "Very high thermal conductivity obtained by boron nitride-filled polybenzoxazine," *Thermochim Acta*, vol. 320, no. 1–2, pp. 177–186, Nov. 1998, doi: 10.1016/S0040-6031(98)00463-8.
- [45] K. C. Yung and H. Liem, "Enhanced thermal conductivity of boron nitride epoxy-matrix composite through multi-modal particle size mixing," *J Appl Polym Sci*, vol. 106, no. 6, pp. 3587–3591, Dec. 2007, doi: 10.1002/app.27027.

- [46] X. Li et al., “Highly thermally conductive flame retardant epoxy nanocomposites with multifunctional ionic liquid flame retardant-functionalized boron nitride nanosheets,” *J Mater Chem A Mater*, vol. 6, no. 41, pp. 20500–20512, 2018, doi: 10.1039/C8TA08008A.
- [47] M. Sattanathan, S. Subramani, K. Mohamed, M. Devarajan, and R. M. Nasir, “Synthesis and characterization of hexagonal boron nitride coating on polyethylene terephthalate,” *Iranian Polymer Journal*, vol. 28, no. 11, pp. 969–976, Nov. 2019, doi: 10.1007/s13726-019-00757-9.
- [48] S. Roy et al., “Structure, Properties and Applications of Two-Dimensional Hexagonal Boron Nitride,” *Advanced Materials*, vol. 33, no. 44, p. 2101589, Nov. 2021, doi: 10.1002/adma.202101589.
- [49] S. Dai et al., “Subdiffractional focusing and guiding of polaritonic rays in a natural hyperbolic material,” *Nat Commun*, vol. 6, no. 1, p. 6963, Apr. 2015, doi: 10.1038/ncomms7963.
- [50] S. Dai et al., “Tunable Phonon Polaritons in Atomically Thin van der Waals Crystals of Boron Nitride,” *Science* (1979), vol. 343, no. 6175, pp. 1125–1129, Mar. 2014, doi: 10.1126/science.1246833.
- [51] T. T. Tran, K. Bray, M. J. Ford, M. Toth, and I. Aharonovich, “Quantum emission from hexagonal boron nitride monolayers,” *Nat Nanotechnol*, vol. 11, no. 1, pp. 37–41, Jan. 2016, doi: 10.1038/nnano.2015.242.
- [52] J. Li, S. Majety, R. Dahal, W. P. Zhao, J. Y. Lin, and H. X. Jiang, “Dielectric strength, optical absorption, and deep ultraviolet detectors of hexagonal boron nitride epilayers,” *Appl Phys Lett*, vol. 101, no. 17, p. 171112, Oct. 2012, doi: 10.1063/1.4764533.
- [53] I. N. Volkov et al., “Extended UV detection bandwidth: h-BN/Al powder nanocomposites photodetectors sensitive in a middle UV region due to localized surface plasmon resonance effect,” *Europhys Lett*, vol. 133, no. 2, p. 28002, Jan. 2021, doi: 10.1209/0295-5075/133/28002.
- [54] J. Qiu et al., “Piezoelectricity of Janus Sb₂Se₂Te monolayers: A first-principles study,” *J Appl Phys*, vol. 129, no. 12, p. 125109, Mar. 2021, doi: 10.1063/5.0039605.
- [55] J. Chen, X. Huang, Y. Zhu, and P. Jiang, “Cellulose Nanofiber Supported 3D Interconnected BN Nanosheets for Epoxy Nanocomposites with Ultrahigh Thermal Management Capability,” *Adv Funct Mater*, vol. 27, no. 5, p. 1604754, Feb. 2017, doi: 10.1002/adfm.201604754.

- [56] N. Yang et al., “Preparation and properties of thermally conductive polyimide/boron nitride composites,” *RSC Adv*, vol. 6, no. 22, pp. 18279–18287, 2016, doi: 10.1039/C6RA01084A.
- [57] S.-W. Jin et al., “Eco-friendly preparation and characterization of highly thermally conductive polyimide/boron nitride composites,” *Compos Part A Appl Sci Manuf*, vol. 166, p. 107396, Mar. 2023, doi: 10.1016/j.compositesa.2022.107396.
- [58] D. Gonzalez-Ortiz, C. Salameh, M. Bechelany, and P. Miele, “Nanostructured boron nitride-based materials: synthesis and applications,” *Mater Today Adv*, vol. 8, p. 100107, Dec. 2020, doi: 10.1016/j.mtadv.2020.100107.
- [59] C. Fu et al., “Improving thermal conductivity of polymer composites by reducing interfacial thermal resistance between boron nitride nanotubes,” *Compos Sci Technol*, vol. 165, pp. 322–330, Sep. 2018, doi: 10.1016/j.compscitech.2018.07.010.
- [60] G. U. Siddiqui, M. M. Rehman, Y.-J. Yang, and K. H. Choi, “A two-dimensional hexagonal boron nitride/polymer nanocomposite for flexible resistive switching devices,” *J Mater Chem C Mater*, vol. 5, no. 4, pp. 862–871, 2017, doi: 10.1039/C6TC04345C.
- [61] S.-W. Jin et al., “Eco-friendly preparation and characterization of highly thermally conductive polyimide/boron nitride composites,” *Compos Part A Appl Sci Manuf*, vol. 166, p. 107396, Mar. 2023, doi: 10.1016/j.compositesa.2022.107396.
- [62] C. Gautam and S. Chelliah, “Methods of hexagonal boron nitride exfoliation and its functionalization: covalent and non-covalent approaches,” *RSC Adv*, vol. 11, no. 50, pp. 31284–31327, 2021, doi: 10.1039/D1RA05727H.
- [63] X.-X. Liu, Y.-Z. Huang, and Z.-X. Huang, “Compatibilizing and functionalizing polypropylene/polyethylene by in-situ exfoliating hexagonal boron nitride at interface,” *Compos Sci Technol*, vol. 221, p. 109354, Apr. 2022, doi: 10.1016/j.compscitech.2022.109354.
- [64] A. Walther et al., “Large-Area, Lightweight and Thick Biomimetic Composites with Superior Material Properties via Fast, Economic, and Green Pathways,” *Nano Lett*, vol. 10, no. 8, pp. 2742–2748, Aug. 2010, doi: 10.1021/nl1003224.
- [65] F. Carosio, F. Cuttica, L. Medina, and L. A. Berglund, “Clay nanopaper as multifunctional brick and mortar fire protection coating—Wood case study,” *Mater Des*, vol. 93, pp. 357–363, Mar. 2016, doi: 10.1016/j.matdes.2015.12.140.
- [66] X. Zeng et al., “Artificial nacre-like papers based on noncovalent functionalized boron nitride nanosheets with excellent mechanical and thermally conductive properties,” *Nanoscale*, vol. 7, no. 15, pp. 6774–6781, 2015, doi: 10.1039/C5NR00228A.

- [67] L. Li, L. Maddalena, Y. Nishiyama, F. Carosio, Y. Ogawa, and L. A. Berglund, "Recyclable nanocomposites of well-dispersed 2D layered silicates in cellulose nanofibril (CNF) matrix," *Carbohydr Polym*, vol. 279, p. 119004, Mar. 2022, doi: 10.1016/j.carbpol.2021.119004.
- [68] A. Isogai, T. Saito, and H. Fukuzumi, "TEMPO-oxidized cellulose nanofibers," *Nanoscale*, vol. 3, no. 1, pp. 71–85, 2011, doi: 10.1039/C0NR00583E.
- [69] B. Soni, E. B. Hassan, and B. Mahmoud, "Chemical isolation and characterization of different cellulose nanofibers from cotton stalks," *Carbohydr Polym*, vol. 134, pp. 581–589, Dec. 2015, doi: 10.1016/j.carbpol.2015.08.031.
- [70] B. Soni, E. B. Hassan, and B. Mahmoud, "Chemical isolation and characterization of different cellulose nanofibers from cotton stalks," *Carbohydr Polym*, vol. 134, pp. 581–589, Dec. 2015, doi: 10.1016/j.carbpol.2015.08.031.
- [71] L. A. Calderón-Vergara, S. A. Ovalle-Serrano, C. Blanco-Tirado, and M. Y. Combariza, "Influence of post-oxidation reactions on the physicochemical properties of TEMPO-oxidized cellulose nanofibers before and after amidation," *Cellulose*, vol. 27, no. 3, pp. 1273–1288, Feb. 2020, doi: 10.1007/s10570-019-02849-4.
- [72] S. Jäger, K. Bewilogua, and C.-P. Klages, "Infrared spectroscopic investigations on h-BN and mixed h/c-BN thin films," *Thin Solid Films*, vol. 245, no. 1–2, pp. 50–54, Jun. 1994, doi: 10.1016/0040-6090(94)90876-1.
- [73] M. I. Baraton, T. Merle, P. Quintard, and V. Lorenzelli, "Surface activity of a boron nitride powder: a vibrational study," *Langmuir*, vol. 9, no. 6, pp. 1486–1491, Jun. 1993, doi: 10.1021/la00030a011.
- [74] Z. A. Al-Ahmed, A. A. Hassan, S. M. El-Khouly, and S. E. El-Shafey, "TEMPO-oxidized cellulose nanofibers/TiO₂ nanocomposite as new adsorbent for Brilliant Blue dye removal," *Polymer Bulletin*, vol. 77, no. 12, pp. 6213–6226, Dec. 2020, doi: 10.1007/s00289-019-03068-4.
- [75] W. Guo, Y. Hu, X. Wang, P. Zhang, L. Song, and W. Xing, "Exceptional flame-retardant cellulosic foams modified with phosphorus-hybridized graphene nanosheets," *Cellulose*, vol. 26, no. 2, pp. 1247–1260, Jan. 2019, doi: 10.1007/s10570-018-2127-2.
- [76] N. Kostoglou, K. Polychronopoulou, and C. Rebholz, "Thermal and chemical stability of hexagonal boron nitride (h-BN) nanoplatelets," *Vacuum*, vol. 112, pp. 42–45, Feb. 2015, doi: 10.1016/j.vacuum.2014.11.009.
- [77] D. Fengel, "Ideas on the ultrastructural organization of the cell wall components," *Journal of Polymer Science Part C: Polymer Symposia*, vol. 36, no. 1, pp. 383–392, 1971, doi: 10.1002/polc.5070360127.

Acknowledgements

The acknowledgments mark the end of a journey of studies, making you truly realize how quickly time flies and how hard it is to keep up with it. The Politecnico di Torino has been a great life experience for me, both professionally and, above all, personally. I have learned what it means to have the courage to face new challenges, new sacrifices far from my homeland, which made me understand how few things are truly important in life: love and family. This journey has also allowed me to live a unique experience in Stockholm, more than 3000 km away from my home, studying and interacting with people of different nationalities and lifestyles at one of the most renowned engineering universities in Europe, the KTH Royal Institute of Technology.

I want to thank all the people who have made all of this possible. First and foremost, I want to express a special thanks to my supervisor, Federico Carosio. His expertise and professionalism, and no less important, his trust and advice, have been crucial to the success of this thesis.

I cannot fail to thank Professor Lars Berglund and Yuanyuan Li from the Royal Institute of Technology in Stockholm for giving me the opportunity to have a thesis experience abroad at their university. The opportunity to visit a foreign university, meet new people, and discover new approaches to study and science has been a source of personal and professional enrichment.

A special thanks goes to my co-supervisor Lengwan Li, for his support during my time abroad, for his comforting words in moments of difficulty, and for his great availability he has shown me. Thanks also to Sara Sadatifard for the collaboration and friendship that developed during this experience.

I would also like to thank Dr. Lorenza Maddalena, who supported me during the laboratory experiences at the Politecnico di Torino in Alessandria campus. Thank you for the advice and words of comfort during difficult moments throughout these months. A special thanks goes to all the doctors and staff of the laboratories at the Alessandria campus; you made me feel at home.

In addition to the people directly involved in my work, I would also like to dedicate a thought to the important people in my life.

First and foremost, I would like to thank my parents. Thank you for the sacrifices made during all these years, for supporting me even in difficult times, and for never ceasing to believe in me. You are my role models. I hope this day fills you with joy.

Thanks to my brother Angelo, even though life has taken us to two different places in the world, you have always been there. I'm glad you have embarked on this new university path. Never stop believing in yourself and putting yourself out there. I love you.

A special thanks goes to my girlfriend, Martina. Without you, this journey wouldn't have been the same. Thank you for your love, your laughter, and for being patient with me during all these years when I was locked in the "mad and desperate study tunnel." You have pushed me to always give my best, even when I thought I couldn't do it. You are my point of reference, I love you.

I cannot go without mentioning my university friends, those who have accompanied and supported me from the bachelor's degree to the master's degree. Thank you especially to my dearest colleague, Luana. Thank you for these years of studying together and for sharing with me all the anxieties, sacrifices, and above all, the joys since the beginning of our university career. I wish you all the best in achieving your dreams.

Thank you, Gianmarco, Adriana, Jessica, and Alvaro; without you, I wouldn't have made it this far. Your strength, energy, and laughter have been a fundamental driving force.

Enjoy reading.

Ringraziamenti

I ringraziamenti segnano la fine di un percorso di studi, realizzi davvero quanto veloce scorra il tempo e quanto non si riesca a stargli dietro. Il Politecnico di Torino ha rappresentato per me una grande esperienza di vita, a livello professionale ma soprattutto umano. Ho imparato cos'è il coraggio di affrontato nuove sfide, nuovi sacrifici lontano dalla mia terra, che mi hanno fatto capire quanto siano poche le cose importanti nella vita: l'amore e la famiglia. Questo percorso mi ha permesso ancora di vivere un'esperienza unica a Stoccolma, distante più di 3000 km da casa mia, di studiare e interfacciarmi con persone di diverse nazionalità e stili di vita in una delle Università più rinomate in Europa per l'Ingegneria, il *KTH Royal Institute of Technology*.

Voglio ringraziare tutte le persone che hanno permesso di realizzare tutto questo. Prima di tutti voglio fare un ringraziamento speciale al mio relatore Federico Carosio. La sua competenza e professionalità, ma non meno importanti, la fiducia e i suoi consigli sono stati fondamentali per la riuscita di questo lavoro di tesi.

Non posso non ringraziare il professore Lars Berglund e Yuanyuan Li, del Royal Institute of Technology di Stoccolma per avermi dato l'opportunità di vivere un'esperienza di tesi all'estero presso la sua università. L'opportunità di visitare un'università straniera, conoscere nuove persone e scoprire nuovi approcci allo studio e alla scienza è stata fonte di arricchimento personale e professionale.

Un ringraziamento particolare va al mio co-relatore Lengwan Li per il suo supporto durante il mio periodo all'estero, per le parole di conforto nei momenti di difficoltà e per la grande disponibilità che mi ha dimostrato. Grazie anche a Sara Sadatifard per la collaborazione e amicizia che si è creata durante questa esperienza.

Vorrei anche ringraziare la Dottoressa Lorenza Maddalena che mi ha supportato durante le esperienze di laboratorio al Politecnico di Torino in Alessandria. Grazie per i consigli e le parole di conforto nei momenti di difficoltà durante questi mesi. Un grazie speciale va a tutti i dottori, dottoresse e personale dei laboratori del campus di Alessandria, mi avete fatto sentire a casa.

Oltre alle persone strettamente legate al lavoro, vorrei dedicare un pensiero anche alle persone che hanno un ruolo importante nella mia vita.

Prima di tutto vorrei ringraziare i miei genitori, grazie per i sacrifici compiuti durante tutti questi anni, per avermi sostenuto anche nei momenti difficili e per non aver mai smesso di credere in me. Siete il mio esempio da seguire. Spero che questo giorno vi riempia di gioia.

Grazie a mio fratello Angelo, anche se la vita ci ha portati in due posti diversi nel mondo, ci sei sempre stato. Sono contento che hai intrapreso questo nuovo percorso universitario, non smettere mai di crederci e di metterti in gioco, ti voglio bene.

Un ringraziamento speciale va alla mia ragazza, Martina. Senza di te questo viaggio non sarebbe stato lo stesso, grazie per il tuo amore, le tue risate e per aver avuto pazienza in tutti questi anni in cui ero rinchiuso nel “tunnel dello studio matto e disperato”. Mi hai spinto a dare sempre il massimo, anche quando credevo di non farcela. Sei il mio punto di riferimento.

Non posso non dedicare qualche riga agli amici universitari, quelli che dalla triennale alla specialistica mi hanno accompagnato e sostenuto: grazie soprattutto alla mia collega del cuore Luana, grazie per questi anni di studio insieme e per aver condiviso con me tutte le ansie, i sacrifici e soprattutto le gioie dall’inizio della nostra carriera universitaria. Ti auguro di poter realizzare tutti i tuoi sogni, ti voglio bene.

Grazie Gianmarco, Adriana, Jessica e Alvaro; senza di voi non sarei arrivato fino a questo punto, la vostra forza, l’energia e le risate sono state un motore fondamentale.

Buona lettura.

